

AMERICAN UNIVERSITY OF BEIRUT

Context Inference, Localization and Mapping in  
Indoor Environments using MMWaves

by  
Ali Hussein Yassin

A dissertation  
submitted in partial fulfillment of the requirements  
for the degree of Doctor of Philosophy of Engineering  
to the Department of Electrical and Computer Engineering  
of the Faculty of Engineering and Architecture  
at the American University of Beirut

Beirut, Lebanon  
December 2018

# AMERICAN UNIVERSITY OF BEIRUT

## Context Inference, Localization and Mapping in Indoor Environments using MMWave


by  
Ali Hussein Yassin

Approved by:

\_\_\_\_\_  
Dr. Karim Kabalan, Professor  
Electrical and Computer Engineering

  
Chairman of Committee

\_\_\_\_\_  
Dr. Mariette Awad, Associate Professor  
Electrical and Computer Engineering

  
Advisor

\_\_\_\_\_  
Dr. Youssef Nasser, Senior Lecturer  
Electrical and Computer Engineering

  
Co-Advisor

\_\_\_\_\_  
Dr. Ali Chehab, Professor  
Electrical and Computer Engineering

  
Member of Committee

Dr. Ibrahim Abu Faycal, Professor  
Electrical and Computer Engineering

  
Member of Committee

---

Dr. David Dardari, Professor  
Electrical and Computer Engineering

  
Member of Committee

---

Dr. Ahmad Al-Dubai, Professor  
Electrical and Computer Engineering

  
Member of Committee

---

Dr. Yves Lostanlen, Professor  
Electrical and Computer Engineering

  
Member of Committee

Date of dissertation defense: December 11, 2018





# Acknowledgements

I would like to thank my advisor Professor Mariette Awad and my co-advisor Professor Youssef Nasser for being a tremendous mentor for me. A special thanks and appreciation for encouraging my research and for allowing me to grow as a research scientist. Your advice on both research as well as on my career have been priceless. I would also like to thank the chairman of my committee Professor Karim Kabalan and my committee members, Professor Ali Chehab, Professor Ibrahim Abu Faycal, Professor David Dardari, Professor Ahmad Al-Dubai and Professor Yves Lostanlen for serving as my committee members even at hardship. I also want to thank you for letting my defense be an enjoyable moment, and for your brilliant comments and suggestions, thanks to you. I would especially like to thank and acknowledge the support of Siradel in this work. All of you have been there to support me in finalizing the dissertation of my Ph.D.

A special thanks and appreciation to my family. Words cannot express how grateful I am to my father and mother for all of the sacrifices that you have made on my behalf. Your prayer for me was what sustained me thus far. I would also like to thank my brothers, sister and all of my friends who supported me in earning my Ph.D. degree and fortified me to strive towards my goal. At the end I would like again to express my sincere appreciation to Professor Youssef Nasser who was always my support in the moments when there was no one to answer my queries.

# An Abstract of the Dissertation of

Ali Hussein Yassin for Doctor of Philosophy of Engineering  
Major: Electrical and Computer Engineering

Title: Context Inference, Localization and Mapping in Indoor Environments using MMWaves

Nowadays, the availability of the location information becomes a key factor in today's communications systems for allowing new location based services. In outdoor scenarios, the Mobile Terminal (MT) position is obtained with high accuracy thanks to the Global Positioning System (GPS) or to the standalone cellular systems. However, the main problem of GPS or cellular systems resides in the indoor environment and in scenarios with deep shadowing effect where the satellite or cellular signals are broken. Moreover, the availability of single transmitter in an indoor environment is a main challenge for not only localization but also mapping. Hence, we adopt millimeter wave (MMW) to make use of its propagation characteristics offering solutions for localization in known environments and solutions for Simultaneous Localization and Mapping (SLAM) and context inference in unknown environments with single anchor node located in a random position with respect to the unknown receiver using the concept of virtual anchor nodes and virtual receiver tackling single bounce and double bounce. Furthermore, we tackle mobility whereby we enhance localization and mapping using family of Kalman filters and the concept of learning. In summary, the thesis is divided into six main chapters. In the first chapter, we survey different technologies and methodologies for indoor and outdoor localization with an emphasis on indoor methodologies and concepts. Additionally, we discuss in this chapter different localization-based applications, where the location information is critical to estimate. Finally, a comprehensive discussion of the challenges in terms of accuracy, cost, complexity, security, scalability, etc. is given. The aim of this chapter is to provide a comprehensive overview of existing efforts as well as auspicious and anticipated dimensions for future work in indoor localization techniques and applications. Then, we introduce in the second chapter an introduction to local-

ization and mapping using MMW. In this chapter, we introduce four approaches for indoor localization using single-anchor and MMW propagation characteristics are introduced. More precisely, we introduce the Triangulation (TL), Angle-Difference-of-Arrival (ADoA), Received Signal Strength (RSS) and Time Difference of Arrival (TDoA) techniques to do position estimation for the receiver. Then, we introduce a hybrid localization technique to enhance the localization accuracy of the receiver. We assess the performance of each technique via cumulative distribution function (CDF) for the location estimation root mean square error (RMSE). Simulations confirm that localization of the receiver relying on a single anchor in MMW achieve a few centimeters accuracy. MOSAIC is then proposed in chapter three whereby simultaneous localization and environment mapping is performed using mmWave without a-priori knowledge. In MOSAIC, the positions of virtual anchor nodes (VANs), known as mirrors of the real anchor with respect to obstacle, are estimated using the proposed TL technique, TDoA and RSS. Then it is followed by estimating the obstacle position and its dimensions. Finally, we compare the performance of the proposed techniques according to the Cramer-Rao Lower Bound (CRLB) with  $N$  anchor nodes. Furthermore, we introduce in chapter four an extension to 3D localization and mapping using mmWave. In this chapter, we performed 3D localization and mapping in outdoor vehicular and indoor environments. Mobile environment is then assessed in terms of localization and mapping in chapter five. In this chapter, Extended Kalman Filter (EKF) and Unscented Kalman Filter (UKF) based Probability Density Function (PDF) are used to enhance the estimation of the point of reflections (PoRs). Finally, conclusion is drawn in chapter six.

# Contents

Acknowledgements	v
Abstract	vi
<b>1 Recent Advances In Indoor Localization: State-of-the-Art, Approaches and Applications</b>	<b>1</b>
1.1 Introduction	1
1.2 Fundamental Limits of Localization in Indoor Environments	3
1.3 Basic Positioning Techniques in Indoor Environments	4
1.3.1 Time of Arrival (ToA)	5
1.3.2 Time Difference of Arrival (TDoA)	5
1.3.3 RSS based Fingerprinting	5
1.3.4 Angle of Arrival (AoA)	7
1.3.5 Hybrid Techniques	7
1.3.6 Common Pitfalls in stand-alone positioning techniques	8
1.4 System based Localization in Indoor Environments	9
1.4.1 Ultra-Wideband (UWB) based Localization	10
1.4.2 WLAN- based Localization	10
1.4.3 Sensors Based Localization	11
1.4.4 Signals of opportunities (SoOPs)	12
1.4.5 Challenges and Pitfalls	13
1.4.5.1 Challenges in UWB-based localization system	13
1.4.5.2 Challenges in WLAN-based localization system	13
1.4.5.3 Challenges in Sensors-based localization system	14
1.4.5.4 Common Pitfalls in SoOps	14
1.4.5.5 Energy Efficiency: A common challenge	14
1.5 Cooperative Localization and Hybrid Data Fusion	15
1.5.1 Hybrid Data Fusion (HDF)	15
1.5.1.1 Conventional HDF Techniques	16
1.5.1.2 HDF Techniques including maps and fingerprinting	17
1.5.1.3 Fuse with inertial information	18
1.5.1.4 Fuse with Camera information	19
1.5.1.5 Fuse with other information	19

1.5.2	Cooperative Localization in SLAM . . . . .	19
1.5.3	Common Pitfalls to avoid . . . . .	20
1.6	Learning Algorithms for Localization . . . . .	21
1.6.1	Learning and environment mapping . . . . .	21
1.6.2	Game Theory to improve Localization . . . . .	22
1.6.2.1	Game Theory in localization . . . . .	22
1.6.2.2	Coalition Games for positioning purposes . . . . .	22
1.6.3	Open challenges in localization based learning . . . . .	25
1.7	Applications . . . . .	25
1.7.1	Robotics . . . . .	26
1.7.2	Ambient Assisted Living and Health Applications . . . . .	26
1.7.3	Location-based Services . . . . .	28
1.7.4	5G Networks . . . . .	28
1.8	Comparative Study . . . . .	29
1.9	Perspective and Challenges . . . . .	30
1.9.1	Constructing radio fingerprinting map with less human participation . . . . .	30
1.9.2	Combining various non-radio techniques . . . . .	31
1.9.3	Integrating various wireless positioning solutions . . . . .	31
1.9.4	Security and Privacy . . . . .	31
1.9.5	Scalability . . . . .	31
1.9.6	Complexity . . . . .	32
1.9.7	Accuracy vs. Cost-effective . . . . .	32
1.9.8	Applications and Accuracy . . . . .	33
<b>2</b>	<b>Localization In Known Environment</b> . . . . .	<b>34</b>
2.1	Introduction . . . . .	34
2.2	Characteristics of MmWave Communications . . . . .	35
2.2.1	Wireless Channel Measurement . . . . .	35
2.2.2	Directivity . . . . .	36
2.2.3	Sensitivity to Blockage . . . . .	36
2.3	Localization Techniques . . . . .	37
2.3.1	Virtual Anchors . . . . .	38
2.3.2	The Triangulation (TL) algorithm . . . . .	38
2.3.2.1	Cramer-Rao Lower Bound (CRLB) . . . . .	41
2.3.3	The Angle Differences-of-Arrival (ADoA) Technique . . . . .	42
2.3.3.1	Simulation Results for TL and ADoA . . . . .	43
2.3.4	Received Signal Strength (RSS) Approach . . . . .	45
2.3.4.1	Weighted-Least Square (WLS) Estimator . . . . .	45
2.3.4.2	Maximum Likelihood (ML) Estimator . . . . .	47
2.3.4.3	Cramer-Rao Lower Bound (CRLB) . . . . .	48
2.3.4.4	Simulation Results . . . . .	48
2.3.5	Time Difference of Arrival (TDoA) . . . . .	49

2.3.5.1	Weighted Least Square (WLS) Estimator . . . . .	49
2.3.5.2	Maximum Likelihood (ML) Estimator . . . . .	52
2.3.5.3	Cramer-Rao Lower Bound (CRLB) . . . . .	53
2.3.5.4	Simulation Results . . . . .	53
2.3.6	Hybrid Localization . . . . .	55
2.3.6.1	Simulation Results . . . . .	55
2.4	Conclusion . . . . .	56

### **3 Simultaneous Localization and Environment Mapping without a-priori Knowledge 57**

3.1	Introduction . . . . .	57
3.2	MOSAIC: System Model and Environment . . . . .	59
3.2.1	System Environment . . . . .	59
3.3	Localization using mmWaves . . . . .	60
3.3.1	The Triangulation (TL) Algorithm in Known Environment: an AoA based Approach . . . . .	61
3.3.2	Rx Localization in unknown environment . . . . .	62
3.4	Context Inference and Obstacle Mapping in MOSAIC . . . . .	63
3.4.1	Estimation of VANs positions . . . . .	64
3.4.1.1	Algorithm 1- TL for Estimating VANs . . . . .	64
3.4.1.2	Algorithm 2- TDoA for Estimating VANs . . . . .	65
3.4.1.3	RSS for Estimating VANs using LS Solution . . . . .	67
3.4.1.4	Estimating VANs using RSS-WLS solution . . . . .	69
3.4.2	Obstacle Detection . . . . .	70
3.4.3	Obstacle Dimensioning: Finding the Obstacle Limits . . . . .	71
3.4.4	Clustering the Cloud of Vertices Points . . . . .	72
3.4.5	Discussion on MOSAIC . . . . .	72
3.5	Optimal Number of ANs . . . . .	73
3.5.1	CRLB Derivations with $N$ ANs . . . . .	73
3.5.1.1	CRLB for Algorithm 1 (The TL Approach) . . . . .	73
3.5.1.2	CRLB for Algorithm 2 (TDoA Metric) . . . . .	75
3.5.1.3	CRLB for Algorithm 3 (RSS Approach) . . . . .	76
3.5.2	Discussion . . . . .	76
3.6	Simulation Results . . . . .	77
3.6.1	Parameters and Environment Settings . . . . .	77
3.6.2	Performance of the Rx Localization Algorithm in unknown Environment . . . . .	77
3.6.3	Optimal Number of ANs . . . . .	78
3.6.4	Obstacle Mapping . . . . .	79
3.6.5	Analysis and Conclusions on the Simulations Results . . . . .	80
3.7	Conclusion . . . . .	82

<b>4</b>	<b>Extension to 3D Localization and Mapping</b>	<b>84</b>
4.1	Introduction . . . . .	84
4.2	System Model using Millimeter Wave . . . . .	86
4.2.1	Environment Settings . . . . .	86
4.2.2	Virtual Anchors . . . . .	86
4.3	Localization of the Receiver in an unknown environment: The Proposed Algorithm . . . . .	87
4.3.1	Filtering the Received Rays . . . . .	87
4.3.2	Estimating the Rx Position . . . . .	87
4.3.2.1	RSS . . . . .	88
4.3.2.2	ToA . . . . .	88
4.4	Obstacle Mapping in Single Bounce Scenario . . . . .	89
4.4.1	Estimation of the VAN Positions . . . . .	89
4.4.1.1	Single Bounce Scenario . . . . .	89
4.4.2	Obstacle Detection through Points of Reflection . . . . .	90
4.4.3	Estimation of the Reflection Coefficient . . . . .	91
4.5	Obstacle Detection for double-bounce scenario . . . . .	91
4.5.1	Estimation of the VAN and VRx Positions . . . . .	91
4.5.2	Estimation of the Reflection Points . . . . .	92
4.5.3	Correction of the Estimated Positions of PoR . . . . .	93
4.6	Simulation Results . . . . .	94
4.6.1	Simulation Environment . . . . .	94
4.6.2	Outdoor Vehicular Environment . . . . .	96
4.6.3	Indoor Environment . . . . .	96
4.7	Conclusion . . . . .	98
<b>5</b>	<b>Localization and Mapping in Mobile Environment</b>	<b>99</b>
5.1	Introduction . . . . .	99
5.2	Enhancing the Geometric SLAM Approach using EKF . . . . .	100
5.2.1	Localization of the Receiver . . . . .	100
5.2.2	Estimation of the VANs positions . . . . .	101
5.2.3	Obstacle Mapping through the CoRP . . . . .	102
5.2.4	Points of Reflection in Presence of Metric Estimation Bias . . . . .	102
5.2.4.1	PoR Estimation in Presence of AoA Bias . . . . .	103
5.2.4.2	PoR Estimation in Presence of TDoA Error . . . . .	103
5.2.5	Extended Kalman Filter in Tracking the PoRs . . . . .	105
5.3	Improvement by Neural Network: UKF filter with MEC . . . . .	106
5.3.1	Basic Concepts . . . . .	108
5.3.1.1	Probability Density Function . . . . .	108
5.3.1.2	Renyi's Entropy and Minimum Entropy Criterion . . . . .	109
5.3.2	UKF based PDF Filter with MEC . . . . .	110
5.3.2.1	System Model . . . . .	110
5.3.2.2	RBF and Weights . . . . .	111

5.3.2.3	Pseudo Innovation . . . . .	112
5.3.3	Entropy Based Non-Linear Filtering . . . . .	113
5.3.4	Algorithm Summary . . . . .	114
5.4	Simulation Results . . . . .	114
5.4.1	EKF-SLAM Results . . . . .	114
5.4.2	UKF based PDF Results . . . . .	117
5.5	Conclusion . . . . .	121
<b>6</b>	<b>Conclusion and Future Work</b>	<b>122</b>
	<b>Bibliography</b>	<b>124</b>



# List of Figures

1.1	Heterogeneous Scenario (AP: stands for access point, BS stands for Base Station) . . . . .	2
1.2	Classification of localization methods . . . . .	6
1.3	ToA Ranging . . . . .	6
1.4	TDoA . . . . .	7
1.5	RSS for distance estimation . . . . .	7
1.6	RSS based Fingerprinting Approach . . . . .	8
1.7	AoA Measurements . . . . .	9
1.8	Combination of ToA, AoA and RSS fingerprints . . . . .	9
1.9	Iterative Multilateration . . . . .	18
1.10	Coalition Games . . . . .	23
1.11	List of various wireless-based positioning systems [11] . . . . .	30
2.1	VANs related to first and second order of reflections . . . . .	39
2.2	Triangle formed between $\mathbf{pV}_i$ and $\mathbf{pR}_k$ . . . . .	40
2.3	The geometry of ADoA localization Technique . . . . .	42
2.4	Localization error CDF for TL and ADoA for different values of $\sigma$ (rad) . . . . .	44
2.5	Localization error CDF for TL and ADoA for different values of $\sigma$ (rad) . . . . .	45
2.6	RMSE versus $\sigma_{RSS}$ for estimating receiver using WLS for RSS localization for different values of $\eta$ . . . . .	49
2.7	RMSE versus $\sigma_{RSS}$ for estimating receiver using ML and WLS for different values $\eta$ . . . . .	50
2.8	Localization error CDF for TDoA using WLS for different values of $\sigma_{TDoA}$ (ns) . . . . .	54
2.9	RMSE for receiver localization based on TDoA using WLS and ML versus $\sigma_{TDoA}$ (ns) . . . . .	54
2.10	RMSE for receiver localization using TL, ADoA, TDoA and RSS . . . . .	55
3.1	Steps needed in MOSAIC . . . . .	59
3.2	VANs related to first ( $RRC_1$ ) and second order ( $RRC_2$ ) of reflections . . . . .	61
3.3	Estimated VANs by moving the receiver from $\mathbf{pR}_k$ to $\mathbf{pR}_{k+1}$ . . . . .	65
3.4	Region of possible reflections . . . . .	71

3.5	Indoor scenario for CoRPs' Estimation using AoA with static transmitter and moving Receiver . . . . .	72
3.6	Simulation Results of the Hybrid Approach . . . . .	78
3.7	Estimation error of localizing VANs based on TDoA approach using LS and ML versus $\sigma_{TDOA}$ . . . . .	79
3.8	CRLB of localization accuracy using AoA under LoS/NLoS conditions for various number of ANs . . . . .	79
3.9	CRLB of localization accuracy versus number of ANs using TDoA and RSS . . . . .	80
3.10	RMSE versus $\sigma_{AoA}$ for estimating receiver under LoS/NLoS channel	81
3.11	Obstacle (triangle) mapping using the TL approach to estimate the VANs . . . . .	81
3.12	Obstacle (hexagon and Square) mapping using TDoA . . . . .	82
4.1	The process of localization, context inference and mapping using geometric approach . . . . .	85
4.2	VANs related to first order of reflection . . . . .	89
4.3	VAN and VRx related to first and second order of reflection . . . . .	90
4.4	Vehicular Outdoor Environment, with PoR. The right top corner shows the PoRs without the environment . . . . .	95
4.5	Another Vehicular Outdoor Environment showing estimated PoR	95
4.6	RMSE measurements for the PoR, Distance AN-PoR-Rx, Distance AN-PoR, Outdoor Vehicular Environment . . . . .	97
4.7	Indoor Environment . . . . .	97
4.8	RMSE measurements for the PoR, Distance AN-PoR-Rx, Distance AN-PoR, Indoor Environment . . . . .	98
5.1	Virtual Anchor Node as a mirror to Tx . . . . .	101
5.2	Exact positions of PoRs . . . . .	102
5.3	Estimated positions of PoR with AoA bias at $\sigma = 5^\circ$ . . . . .	104
5.4	Estimated positions of PoR with ToA bias at $\sigma = 1$ ns . . . . .	104
5.5	<b>schematic of UKF based PDF filter</b> . . . . .	107
5.6	The cloud of reflection points with static transmitter and moving receiver: without ToA bias (top) and with ToA bias (bottom) . . . . .	115
5.7	Indoor scenario for CoRPs' Estimation . . . . .	115
5.8	RMSE for estimating Point of Reflections versus $\sigma_t$ and $\sigma_\theta$ . . . . .	116
5.9	MSE ( $m^2$ ) vs $\sigma$ of ToA ( <i>ns</i> ), EKF with 1 iteration . . . . .	116
5.10	MSE ( $m^2$ ) vs $\sigma$ of ToA ( <i>ns</i> ), EKF with 10 iterations . . . . .	117
5.11	The cloud of reflection points with static transmitter and moving receiver: without AoA bias (top) and with AoA bias (bottom) . . . . .	118
5.12	MSE ( $m^2$ ) vs $\sigma$ of AoA ( <i>rad</i> ), EKF with 1 iteration . . . . .	119
5.13	MSE ( $m^2$ ) vs $\sigma$ of AoA ( <i>rad</i> ), EKF with 5 iterations . . . . .	119
5.14	Output error(innovation) in function of k . . . . .	120

5.15	Probability density function of innovation with UKF and UKF+PDF	120
5.16	Estimation of PoR using EKF and UKF based PDF . . . . .	121

# List of Tables

1.1	Comparisons of positioning techniques . . . . .	29
-----	---	----

# Chapter 1

## Recent Advances In Indoor Localization: State-of-the-Art, Approaches and Applications

### 1.1 Introduction

Modern communications systems aim at providing high data rates with ubiquitous service coverage. Nowadays, the availability of the Mobile Terminal or Unlocated Device (UD) location information at the base stations, i.e. its knowledge by the operators, has become a key factor in enabling communications systems to provide new location based services [1]. Practical localization techniques are based on Time of Arrival (ToA), Time Difference of Arrival (TDoA), Received Signal Strength (RSS) and Angle of Arrival (AoA). In outdoor scenarios, the UD position can be obtained with high accuracy from Global Navigation Satellite Systems (GNSS), such as the Global Positioning System (GPS), or from the standalone cellular systems. However, these positioning systems are severely degraded or may fail altogether in indoor environments where the satellite or cellular signals are interrupted, and in scenarios with deep shadowing effects[2]. Various approaches and methodologies have been proposed to deal with these problems. Hybrid positioning is a well-known approach for positioning that exhibits sufficient accuracy and coverage [3]. In this respect, combined localization approaches are extensively proposed in the literature to solve the hearability problem in indoor scenarios. Another potential candidate for critical scenarios consists of the class of heterogeneous approaches that combine different radio access technologies (such as cellular systems like 3G and 4G, WLAN, and WiMAX), as shown in Figure 1.1. Indeed, techniques based on combinations of cellular and WLAN networks have recently received increasing interests from both the localization and communication communities[4][5]. This is not only due to the request made by Federal Communication Commission (FCC) regarding the accu-

rate localization of the UDs, but also because of the many applications that are location sensitive such as billing, fleet management, and mobile yellow pages[6]. Although any positioning techniques could be exploited in indoor scenarios and homogeneous networks, there are practical limits on the combination of these techniques as well as on the minimal number of anchor nodes (AN) that can be used in such scenarios[7]. For instance, in many cases, only one or two ANs are able to communicate with the UD. Hence, new techniques based on hybrid data fusion and/or heterogeneous access are proposed and analyzed in this case. In this chapter, we provide a review on recent techniques and concepts used to

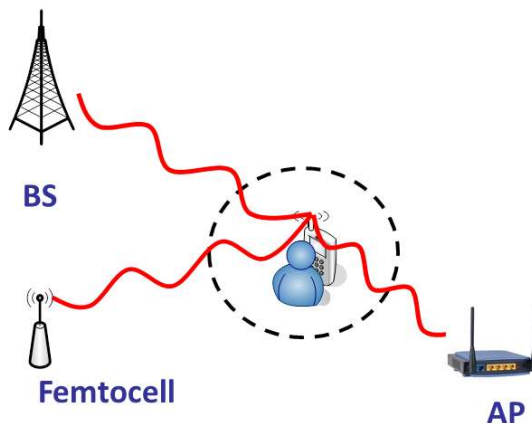


Figure 1.1: Heterogeneous Scenario (AP: stands for access point, BS stands for Base Station)

improve localization with their fundamental limits, challenges and applications with a particular focus on indoor environments. Although reviews on localization techniques are available in the literature [8]-[15], these are either narrow in focus or have been overtaken by significant technological advances. Thus, the survey in [12] is somewhat outdated, whereas the authors of [8] focus only on ultrasonic positioning systems. The work in [10] describes relatively recent localization techniques but does not explore the future trends, challenges, and applications. The works of [13] and [14] review various technologies, such as WLAN, used for indoor positioning in addition to different positioning technique with the metrics used to assess the performance, such as the estimation accuracy of positioning. However, they do not discuss positioning neither from the perspective of energy efficiency nor from the perspective of a requirement in recent applications, such as ambient assisted and health living applications. Additionally, they do not explore advanced methodologies used to enhance localization, such as cooperative localization and data fusion techniques. The survey in [15] provides remarkable classification of different fingerprint-based outdoor localization approaches, discussing how each method works. So, we aim to present a

survey that is restricted neither for fingerprinting-based techniques nor for outdoor localization. As well, the rapid evolution of methodologies and technologies in this domain and the need for a comprehensive and up-to-date survey of the approaches, applications and future trends, provide the motivation for this chapter. To summarize, a number of aspects differentiate this chapter from existing works; first, we review advanced localization techniques and positioning systems for indoor and outdoor environments. Second, we discuss recent methodologies such as data fusion and cooperative techniques used to enhance the accuracy of localization. Third, we present an overview of machine learning techniques that have recently been adopted for localization purposes. Fourth, we describe various localization-based applications from different fields. Finally, we present a comprehensive list of localization challenges foreseen in the future mainly in next generation 5G networks.

The rest of the chapter is organized as follows. In section 1.2 we discuss the fundamental limits of localization in indoor environments and describe the basic localization techniques in section 1.3. Also, we discuss the state-of-the-art system-based localization techniques with the challenges in terms of energy consumption and positioning accuracy in section 1.4. Then, we review cooperative localization and hybrid data fusion techniques in section 1.5. In section 1.6 we turn our attention to the use of game theory generally and coalition games for localization. In section 1.7, we explore various localization-based applications. We present in section 1.8 a comparative study on the accuracy, range and techniques used for different localization systems. Finally, perspectives and challenges of recent advancements in indoor localization are discussed in section 1.9.

## 1.2 Fundamental Limits of Localization in Indoor Environments

Position information is usually provided by global navigation satellite systems, such as GPS or the European satellite navigation system Galileo. However, the accuracy of positioning is affected by the environment, especially in indoor scenarios or dense urban areas where localization using GNSS can be inaccurate or even impossible due to the interruption of the connection with the required satellites. Hence, alternative localization algorithms have to be used to estimate UD position with high accuracy. This has been primarily achieved using radio signals offered by terrestrial radio access networks. Typically, these positioning strategies comprise a two-stage positioning system consisting of a ranging phase where nodes use distance dependent signal relation, such as RSS, ToA, AoA, etc. to estimate their own position. Then, in the second phase, the nodes utilize the position of the known anchors and the information obtained in the ranging phase to compute their own coordinates. The Cramer Rao Lower bound (CRLB) then

defines the fundamental limit on the positioning accuracy of the nodes by modelling the impact of the noisy ToA, AoA, or RSS measurements on the ranging quality. Other bounds on accuracy, such as the Bayesian Cramer Rao bounds, the WeissWeinstein bound and the extended ZikZakai bound can be tighter and more informative than the CRLB when the localization system is map-aware. These bounds indicate that an accuracy of 2m could be reached if a map-based priori knowledge and map-aware localization is used [16][17]. For instance, in [17], RSS based algorithms were evaluated using trace-driven analysis and shown to benefit from the addition of more resources up to a point beyond which their performance degraded. This effect was then mitigated by cleaning the data to remove low quality landmark where the quality is defined in terms of the fit of the distance to RSS model. Hence, the performance is enhanced by cleaning the data. The accuracies in order of 0.2 m are possible when utilizing commodity hardware. Additionally, the maximum error achieved in the worst case scenario can be decreased to reach 1.6 m. However, basic localization techniques have their limitations. ToA/TDoA is limited by the requirement of at least 3 base stations (or ANs) to generate 2-D fix. AoA requires at least two base stations. The performance of AoA techniques is highly dependent on the range giving significant position estimation errors from relatively small error in the AoA measurements. They are restricted by the carrier frequency, and the size of the array. Thus, they are used only for localization in applications with requirement of low accuracy or in combination with other measurements. Also, AoA systems are sensitive to angular multipath, a major effect in indoor environment. Consequently, ToA techniques are preferred in urban areas due to multipath effect whereas AoA are preferred in open areas. Looking at the different access technologies for localization purposes, we can also note various limitations. For instance, empirical analysis of the appropriateness of WLAN localization showed that significant errors always occur, even though reasonable accuracy may be achieved [18]. Errors are mainly due to the presence of different locations with similar radio signatures, such as fingerprints or received signal strength, caused by the dynamic propagation of radio signals [15]. Thus, this is considered as a fundamental limit of pure WLAN-based techniques where large errors in range of 6 to 8m occur. To give more insights about these aspects and limits, we will describe with the necessary details the stand-alone localization techniques used for indoor scenarios.

### 1.3 Basic Positioning Techniques in Indoor Environments

Localization methods are based on the estimation of distance to anchor nodes with known positions and on internode measurements. Node cooperation enhances position estimation and is mostly beneficial when traditional localization



techniques fail to produce accurate estimation, as is the case in indoor scenarios. Linear least squares (LLS) lateration is a simple method for position estimation. Ideally, the unknown node would be located at the intersection of at least three circles with centers at the anchor nodes and radii equal to the distance to each of these anchor nodes. However, as it is highly unlikely that a single point of intersection is obtained, least squares (LS) optimization is used to minimize the sum of squared residuals. Consequently, the problem becomes a nonlinear optimization that needs proper initial estimates [19]. Since nonlinear optimization is computationally expensive, alternative methods, such as linearized expressions, are used to estimate the position using LLS. Although this is not an optimal solution for position estimation, it nevertheless achieves roughly good accuracy with low complexity [19]. In the following, we briefly describe basic standalone positioning techniques used in the context of homogeneous networks with the possibility of hybridization.

### 1.3.1 Time of Arrival (ToA)

The ToA approach includes the calculation of the time needed by the signal to travel from the UD to the ANs. The UD is localized to a circle centered on the AN with a radius  $d$  estimated through the ToA. Hence, to detect the exact location of the UD, at least three ANs are required. In this case, the estimated position of the UD is simply within the region of intersection (if it exists) of the three circles, as shown in Figure 1.3. The actual estimated position could then be easily obtained through any filtering technique such as LS or Weighted Least Square (WLS) [20][21].

### 1.3.2 Time Difference of Arrival (TDoA)

TDoA examines the time difference at which the signal arrives at many measuring units. The transmitter must lie on a hyperboloid for each TDoA measurement with a constant range difference between the two measuring units. Such measurements are taken between multiple pairs of reference points with known locations. Also, relative time measurements are used at each receiving node in place of absolute time measurements. No synchronized time source is needed by TDoA to perform localization; however, synchronization is only needed at the receivers. The location to be estimated is the intersection of many hyperbolic curves, as shown in Figure 1.4. This technique is referred to as multilateration.

### 1.3.3 RSS based Fingerprinting

The RSS approach includes two main methods: the path loss lognormal shadowing model to deduce a trilateration, and the RSS fingerprinting [7]. The first approach is used to estimate the distance between the serving BS and the UD

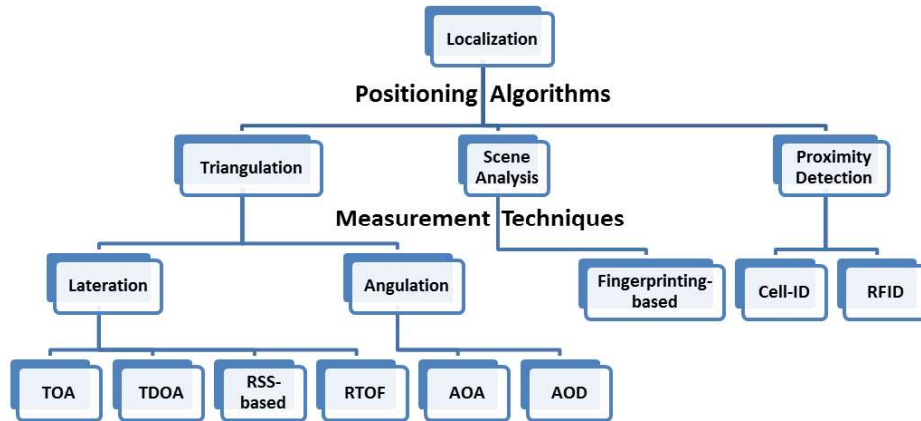


Figure 1.2: Classification of localization methods

based on a path loss lognormal shadowing model, as shown in Figure 1.5. Then, trilateration is used to estimate the location of the UD using at least 3 serving BSs. On the other hand, the RSS-based fingerprinting firstly collects RSS fingerprints of a scene, as shown in Figure 1.6, and then estimates the location of the UD by matching on-line measurements with the closest possible location that corresponds to measurements in a database [4]. Therefore for each possible location, ambiguity points could exist leading to high estimation errors in standalone positioning scenarios.

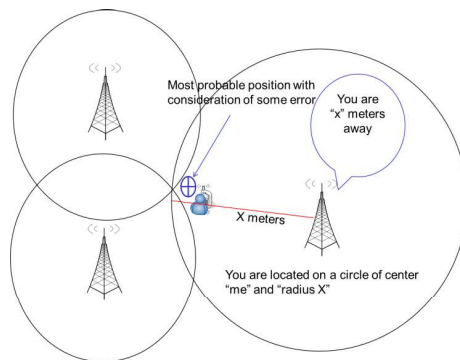


Figure 1.3: ToA Ranging

### 1.3.4 Angle of Arrival (AoA)

This technique includes the calculation of the angle at which the signal arrives from the UD to the ANs. Then, the region where the UD could exist can be drawn, as shown in Figure 1.7. Basically, this region is a line having a certain angle with the ANs. Although at least two ANs are needed to estimate the location of the UD, the position estimation error could be large if a small error occurs in the AoA estimation. Therefore, the AoA based technique is of limited interest for positioning purposes, unless it is used with large antenna arrays.

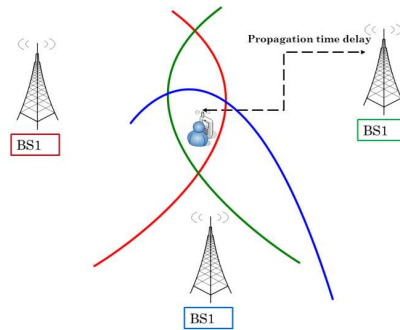


Figure 1.4: TDoA

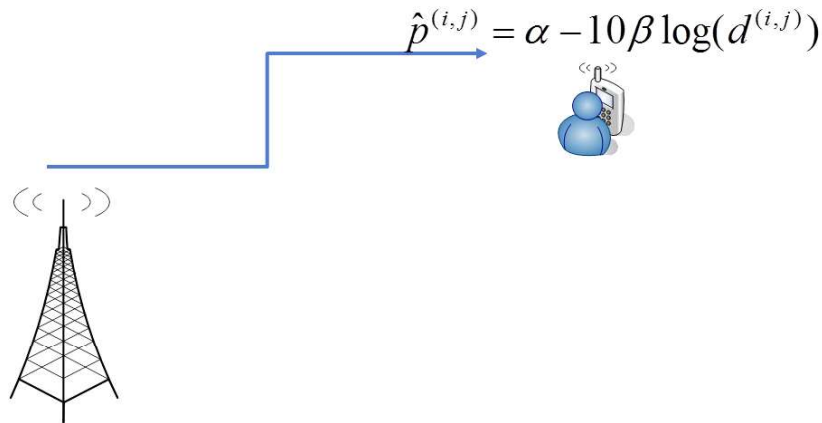


Figure 1.5: RSS for distance estimation

### 1.3.5 Hybrid Techniques

Recently, hybrid and cooperative mobile positioning has emerged as a new stream of wireless location; the core idea of cooperative positioning relies on the utilization of trustworthy short-range measurements to enhance the accuracy of the

location estimation of a wireless system.

Different combinations of the basic standalone positioning techniques (RSS, ToA, TDoA, AoA, etc) have been implemented to enhance the accuracy of location estimation. For instance, a combination of ToA, AoA and RSS based fingerprint approach, as shown in Figure 1.8, provides initial estimation of UDs [22]-[24]. The hybrid ToA/TDoA and RSS proposed in [25] achieves further enhancement in terms of location estimation accuracy when compared to the use ToA or TDoA alone.

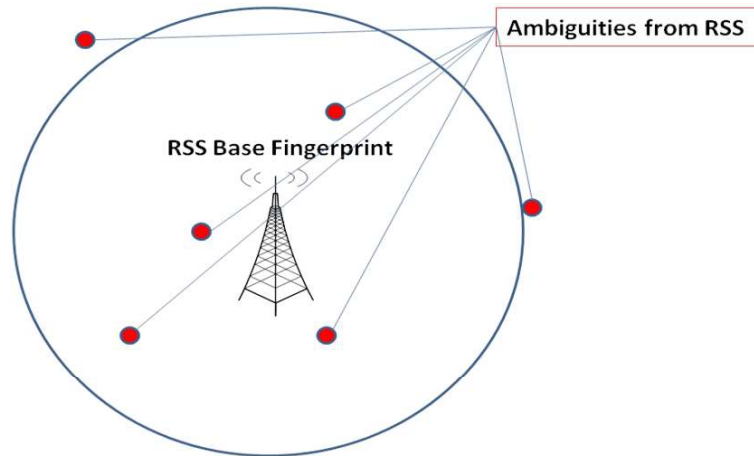


Figure 1.6: RSS based Fingerprinting Approach

### 1.3.6 Common Pitfalls in stand-alone positioning techniques

Generally, stand-alone positioning techniques suffer from drawbacks affecting the localization accuracy. For instance, the ToA technique requires accurate timing reference at the UD and synchronization between this reference and the clock at the anchor. Obviously, it is highly challenging to achieve this task; if it is achieved, it will cause an increase in the cost and dimensions of the mobile device. Besides, a remarkable change in the software of the mobile device is needed by the TDoA approach along with further hardware installations. TDoA requires having the processing done at the UD and sending the estimated location to the system on the reverse link. Hence, the bulk and the costs of the handset will be increased in order to satisfy the estimation and synchronization needs. As well, the RSS technique has drawbacks in terms of difficulty to have a LOS between transmitter and receiver in indoor scenarios. Hence, localization accuracy is affected by the multipath effect induced in indoor environments. Above and beyond, pathloss models are used also to perform localization. However, shadowing and multipath

fading effects deteriorate the accuracy of such models. The accuracy in this case can be improved by using pre-measured RSS contours centered at the receiver, or using many measurements taken at several BSs. Also, the enhancement of the localization accuracy can be achieved by using RSS measurement based on a fuzzy logic algorithm. As well, the AoA technique suffers from drawbacks such as complexity in terms of hardware requirements and reduction in the localization accuracy as the UD moves away from the measuring units.

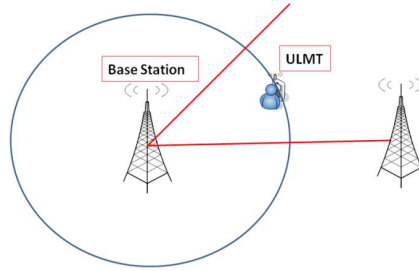


Figure 1.7: AoA Measurements

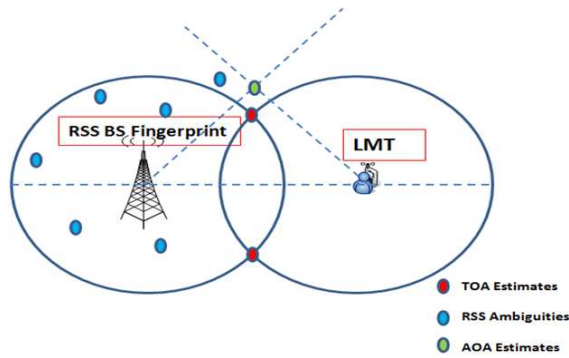


Figure 1.8: Combination of ToA, AoA and RSS fingerprints

## 1.4 System based Localization in Indoor Environments

Despite the fact that hybridization of basic positioning techniques provides improvement in the localization accuracy, there is always a need nowadays for better methodologies that achieve enhancements in energy consumption and further improvements in accuracy. In the literature, different localizations techniques have been proposed that can be classified into the categories shown in Figure 1.2. In all these categories, research has been focused on advanced techniques

based on new metrics and signals such as energy driven, signals of opportunity (SoOP), Ultra-Wide Band (UWB) in addition to the conventional systems such as WLAN, WSN, etc. So, we will discuss more intelligent positioning techniques; specifically, the UWB based localization, WLAN-based localization, and Sensors-based localization. Finally, we will discuss in this section the use of SoOPs as emerging technology to improve localization followed by the challenges of the system-based localization techniques in terms of energy and accuracy.

#### 1.4.1 Ultra-Wideband (UWB) based Localization

UWB technology is based on transmitting ultrashort pulses less than 1 ns, with a low duty cycle from 1 to 1000. The transmitted signal in UWB is sent over multiple frequencies band. UWB then allows accurate localization and tracking of mobile nodes in indoor environments. UWB technology is commonly used by researchers and industry in various fields such as indoor positioning in order to present enhancements in terms of achieving high range measurement resolution and accuracy, low probability of interception, multipath immunity, and the ability to combine positioning and data communication in one system. Additionally, UWB technology is highly scalable and can be used at low cost with a low energy consumption [26]. The position is estimated in UWB-based applications from the radio signals traveling between target node and reference nodes whose positions are well known. This procedure is done using ToA, AoA, RSS, TDoA, and hybrid technique as stated in Section 1.3. Localization systems based on UWB technology achieve an accuracy of centimeters. With three-dimensional positioning based on ToA or TDoA, an accuracy of 15 cm in indoor scenario has been achieved [27]. Indeed, multipath signal components are decomposed by UWB receivers because they possess high bandwidth. In scenarios satisfying Line Of Sight (LOS) conditions, the first path that refers to the LOS component is the robust path used for localization purposes. Nevertheless, more complex techniques are needed if this is not the case in order to perform accurate estimation of the initial delay. Furthermore, the time-based positioning techniques offer higher localization accuracy compared to RSS technique in UWB-based positioning applications since the high bandwidth of UWB is not efficiently used by RSS technique in terms of enhancing positioning accuracy compared to the time-based techniques. On the other hand, ToA and TDoA make use of the fact that UWB signal has high time resolution to increase the positioning accuracy relative to other techniques [28].

#### 1.4.2 WLAN- based Localization

WLAN is the most known solution for indoor positioning [11][12]. Positioning systems based on WLAN provide better performance compared to some technologies, such as GPS, global system for mobile communications (GSM) and

Bluetooth. This aspect is due to the fact that WLAN positioning systems do not require any additional software or hardware manipulation, but are able to perform localization based on the existing infrastructure. RSS is the most known WLAN localization technique due its easy extraction in 802.11 networks and its ability to run on of-the-shelf WLAN hardware. On the other hand, ToA, TDoA, and AoA are less common to WLAN-based positioning systems since angular and time delay measurements are complex.

Usually, WLAN scanning aims to find available networks for connection. Typically, the scanning can be performed at low rate since the set of available networks changes slowly. When a device aims to estimate its own position while acquiring WLAN signals, recurrent RSS measurements are needed from the APs in order to minimize positioning error. A regular update is needed when a positioning device is moving along a trajectory; hence, scanning for available APs on all relevant channels is performed by each device at rate equivalent to the update rate. As averaging a set of RSS measurements reduces the effect of noise, a device that is concerned about positioning accuracy performs the scanning at a rate higher than the update rate. Alternatively, a slower scanning rate than the update rate leads to reduced power consumption at the expense of positioning accuracy. Hence, balancing the trade-off between power consumption and positioning performance is the main driver for a device in selecting its parameters for scanning in WLAN. Two main approaches are used for indoor WLAN: mono-objective approach and multi-objective approach [29]. Both approaches are based on Variable Neighborhood Search, aiming to reduce the positioning error during WLAN planning process. The combination between WLAN positioning system and sensors embedded on smart devices obtains precise indoor localization for mobile smart devices [30]. The reader may refer to [8]-[12] for more information.

### 1.4.3 Sensors Based Localization

Inertial sensors such as gyroscopes are widely used in localization. Nevertheless, inertial sensors, usually based on low-cost MicroElectroMechanical System (MEMS), suffer from errors which in turn affect the localization accuracy [31][32]. In order to alleviate this problem, the work in [33] employs denoising, which reduces noise from raw sensor signals. This approach enhances the accuracy and performance of the system by avoiding breakdowns induced by excessive noise. The localization in sensor-based technologies can be also divided into two categories: (1) Signature-based and (2) Beacon-based techniques. Signature-based techniques [34] assume non-uniform distribution of the nodes to be used as a signature for estimating location by noticing node neighborhoods. In Beacon-based techniques [35], Beacon nodes should identify their absolute positions using GPS or manual configuration. The location of the remaining nodes is estimated using distance/angle measurements to beacon nodes followed by multilateration or triangulation.

Sensors based localization is an important feature of mobile systems, such as Autonomous navigation, entertainment robots, service robots, and military robots [31][36][37]. In these environments, the localization of mobile nodes can be achieved using dead reckoning-based odometry through, for instance, wheel speed sensors [31],[36][37]. Emergency Sensor Networks (ESN) in contexts such as forest fires, natural calamities (hurricanes, storm), and terrorist attacks [38] are also of great interest. The placement of the sensor nodes in emergency applications is extremely localized for each point at which the size of the node group is based on the intensity of the monitored event at that point.

#### 1.4.4 Signals of opportunities (SoOPs)

Currently, mobile terminals implement a variety of communications standards like GSM, UMTS, LTE or even short range communications like Bluetooth or WLAN. Therefore, such terminals are capable of listening to a broad spectrum of radio signals. The transmitters of such radio signals compare to landmarks in classical navigation. Their position might be known. But if the position of the origin of such SoOP is unknown, their observation can still potentially improve the positioning performance of classical mobile radio positioning using downlink reference signals for instance. Basically, these signals are not specific for navigation. SoOPs are RF signals utilized for communication purposes. SoOP has many advantages in terms of signal space diversity and higher received signal power.

Related work considers digital terrestrial video broadcasting signals for positioning purposes [39] based on signal propagation delay estimation. Here the transmitters are fixed and it is reasonable to assume their positions to be known. Skyhook has developed a positioning system based on WLAN signals [40]. This approach requires a database which must be learned and kept up to date using appropriate self-learning algorithms. So inherently this approach does not assume knowledge about the WLAN transmitter positions from the beginning. TV and WLAN signals are combined to improve positioning [41].

Moreover, different mitigation methods such as assisted GPS and differential GPS were proposed to provide enhancements to achieve robust navigation under critical scenarios. Recent proposed navigation systems use SoOP to enhance the accuracy. For instance, cooperative network is developed to provide accurate localization by using large number of nodes combined with SoOP [42]. The fundamental ability of cooperative network is that each node can produce navigation signals that can be used by other users in the network in addition to receiving SoOP from selected towers. In such case, both local and global positioning is possible. Actually, the known positions of the SoOP provide global positioning. On the other hand, local positioning permits signals produced through the cooperative network. Thus, a SoOP technique can be used for the purpose of localization, such as using timing measurements to perform opportunistic posi-



tioning [43]. Many SoOPs are used for mobile localization without GPS [44][45].

### **1.4.5 Challenges and Pitfalls**

The target of this section is to detail the main challenges and pitfalls of each system.

#### **1.4.5.1 Challenges in UWB-based localization system**

The performance of positioning systems based on UWB technology may face many challenges induced by aspects such as extremely cluttered operational environments causing multipath, NLOS and shadowing artifacts. For instance, in ToA-UWB based schemes and NLOS conditions, the performance degradation is mainly due to the mismatch between the first arriving path and the direct path and the addition of detouring delay. Another big challenge of UWB based localization resides in implementing wideband radio devices for a UWB signal with absolute bandwidth larger than 500 MHz. Here, some efforts have been done in the research community to develop such platforms reaching 10 to 15 cm in positioning accuracy. The reader might refer to [46] for more details.

In UWB-based positioning system, interference with the ultra-wide spectrum may occur because of the misconfiguration. Interference may occur also due to the spread of the UWB signal over the bandwidths containing the frequency of the existing narrowband system. Another challenge resides in the need of, at least three receivers with unblocked direct path to the transmitter for normal ToA positioning algorithm. UWB-based positioning system requires also signal acquisition, tracking, and synchronization to be performed with very high precision in time relative to pulse rate. Currently, researchers are working on such problems. We can notice for instance the work in [47][48] where a novel technique for ToA with two receivers is proposed. Even though this work is very interesting to solve such issues, the door is still open for more solutions as limitations and challenges are still there.

#### **1.4.5.2 Challenges in WLAN-based localization system**

WLAN-based localization system is time consuming for site surveying and is labor intensive. Another challenge is the fact that the multipath of such systems is influenced by the existence of physical objects. Also, WLAN-based localization system may interfere with other applications in the 2.4 GHz ISM. Moreover, the variation of signal strength with respect to time is considered a weakness of such system causing deterioration in the localization accuracy. The variation of signal strength caused by the movement of people, doors, and furniture in offices requires updating simultaneously the signal strength map. Hence, this is considered as a main drawback of WLAN fingerprinting systems.

### 1.4.5.3 Challenges in Sensors-based localization system

In terms of methodologies, anchor-based localization techniques are usually preferred in this environment due to their accuracy. Nevertheless, such techniques have disadvantages, such as the need for proper anchors to be installed in WSN. As the anchors have high cost and energy consumption, the number of required anchors must be minimized. Another weakness of anchor-based localization techniques is that a uniform distribution of anchors is needed knowing that this criterion cannot be satisfied in many environments such as battlefields and natural disasters environment, where sensor nodes are deployed randomly. While localization of unknown nodes in WSN is done using randomly selected anchors, the anchors differ in their impacts on the accuracy of localization due to their characteristics and the uncertainties of wireless communication. To solve this problem, the work in [50] proposed a new anchor-based positioning technique by the creation of a database for optimized anchors. Then, anchors from the created database are used to measure the distance to the unknown node and the new located unknown nodes become new anchors in order to decrease the dependency of localization technique on anchors and to ensure that the anchors are uniformly distributed over the network.

### 1.4.5.4 Common Pitfalls in SoOps

When using SoOP for the purpose of localization, one has to consider significant aspects such as the lack of independent SoOP, 2-D vs. 3-D solutions, SoOP clock errors, signal integrity, and multipath and NLOS signals. The uncertainty in the clock of the signal transmitter due to an offset relative to the clock of the receiver in addition to the unknown transmission time is a challenge against localization. As well, hybrid/fused SoOPs are used in order to alleviate the technical challenges obtained from positioning with SoOP [44].

### 1.4.5.5 Energy Efficiency: A common challenge

In many indoor scenarios, the positioning techniques have to be energy efficient as they are based on devices with limited battery life such as sensors, smartphones, etc. Nevertheless, these positioning techniques have various criteria of energy efficiency, service availability, and accuracy. For instance, the energy used during the idle state by an access point (AP) in WLAN networks is wasted if no user is being served. As stated in [51], more than USD 6 billion is spent for almost 74TWh of electricity consumed for internet related equipment every year in USA. Hence, there is a vast need for energy efficient positioning techniques. Although the WLAN based positioning system service approaches are energy efficient techniques, they are not generally obtainable for users. Hence, the work in [52] proposed to use the current WLAN infrastructure and Access Points (Aps) without pre-deployment calibration and a genetic algorithm for energy-efficient

localization purposes, like WLAN access points (APs). Consequently, this approach is restricted to indoor scenarios.

Another interesting approach resides in power cycling algorithms in smartphones [53]. The duty cycling approach polls the built-in sensors of a smartphone at specific time intervals to identify any mobility and whether to turn the GPS on or off. A Bluetooth-based Position Synchronization (BPS) is another idea of energy efficient positioning technique [53]. The location information is shared among devices using BPS over a Bluetooth connection.

Furthermore, positioning systems based on the combination of different methodologies and techniques are also energy efficient. Here we distinguish the works of [54] which provides location estimates through the utilization of heterogeneous positioning services and the combination of techniques including a received signal strength indicator and a 2D trilateration, and of [55] based on context information and a fusion engine using particle filters. Moreover, we provide the work of [56] which introduced a preliminary analysis of probabilistic localization techniques for power-efficient map-aided localization, developing the green global-greedy position estimation (3GPE), and presenting entropy deduction as a new metric for performance assessment. However, this approach still has many challenges. The first is the determination of the inherent relations between the expected errors, the location precision and the probability of each possible matched fingerprint. The second is the evaluation of the accuracy contribution of each AP using the entropy deduction metric of probabilistic fingerprint [57][58].

When accuracy and energy efficiency are required, more technologies advancement should be achieved. This can be obtained by making use of hybrid data fusion concept and cooperative approach between different localization systems as discussed in section 1.5.

## 1.5 Cooperative Localization and Hybrid Data Fusion

### 1.5.1 Hybrid Data Fusion (HDF)

So far, heterogeneous wireless resources are included in most of wireless environments, such as LTE femto base stations, WLAN APs and WSNs. Also, such environments are characterized by the crowded cooperation over medium or short ranges between multi-standard UDs. Additionally, radiolocation ability is efficient in such scenarios for the sake of enhancing connectivity performance and enabling context-based services or indoor navigation [59].

However, due to the signal attenuation and the multi-path propagation problems caused by reflections of radio signals, the accuracy of wireless-based indoor positioning is severely degrading in uncontrolled environments. Many researchers combine other sources of sensors (e.g. inertial measurement unit (IMU), cameras,

and range finders) to compensate for these problems. Fusing the information from different positioning systems with different physical principles can improve the accuracy and robustness of the overall system.

It is worth noting that various wireless devices, such as Bluetooth, WLAN and radio frequency identification (RFID), provide a localization accuracy ranging from several meters to centimeters inside buildings. So, we will review in this section first the conventional techniques based on HDF. Then, we will discuss the fusion with maps and fingerprinting, fusion with inertial information, fusion with camera information, and fusion with other information such as the spatial structure information of an environment.

### 1.5.1.1 Conventional HDF Techniques

Recently, research work has been focusing on two main approaches in HDF, the centralized and non-centralized approaches. Iterative positioning (e.g. [60],[61],[62]) and cooperative links selection (e.g. [63],[64]) are used with the non-centralized approach. Moreover, such heterogeneous and cooperative environments include complex phenomena such as the conjunction of harmful sparse connectivity, space-time correlations among various radio access technologies and poor Geometric Dilution Of Precision (GDOP) conditions. The authors of [65], however, carried out extensive research that dealt uniquely with cooperation in homogeneous scenarios. As well, a measurement campaign in jointly heterogeneous and cooperative wireless indoor scenarios uses ZigBee devices with RSS measurement abilities [66].

HDF methods estimate reliable position information to the benefit of communications. The work in [67] has introduced the main radio technologies and scenarios for wireless positioning assessed by the Wireless Hybrid Enhanced Mobile Radio Estimators (WHERE) European project. Two novel particle filter based HDF techniques are used to either track the position directly from the received signal or the path dependent parameters. Moreover, new cooperative schemes, based on obtaining proper mathematical representations corresponding to LOS and non-LOS propagation, are used to enhance the performance of mobile communication systems in terms of position accuracy and reliability.

Another interesting set of work resides in the combination between angle-based localization, map filtering, and pedestrian dead reckoning [68] where absolute location estimates are provided by the angle-based localization system. On the other hand, accurate length and shape of the traversed route are obtained from pedestrian dead reckoning (PDR) without absolute location and heading information. The estimates obtained from PDR movement and angle-based location techniques are merged together with a building vector map in a particle filter that is used as the fusion filter in this study. Hence, merging information from different positioning techniques can lead to higher positioning accuracy for several of indoor scenarios.

Hybridization is also used for the purpose of pedestrian tracking [69]. Usually, this hybrid technique merges inertial measurements and RSS information via a Kalman filter. Classic hybrid methods for pedestrian tracking (e.g. [70] and [71]) were based on the utilization of a map-based or fingerprinting RSS localization method. However, this requires a time-consuming calibration step in order to create the radio map of the environment to be utilized for position estimation of mobile node through the matching between map measurements and mobiles measurements. On the other hand, another hybrid localization method [69] uses a channel modeling technique where a propagation channel model serves to give a direct relation between the distance between two nodes and the RSS; then, a positioning technique or triangulation is utilized to estimate node position from a set of distances to some known anchor nodes. Yet, fingerprinting methods provide higher accuracy; however, this approach has minimal calibration cost. Additionally, the fusion between inertial measurements and channel-based localization provides enhancements over fingerprinting methods in terms of positioning accuracy [69].

Generally, techniques based on LS are mainly used in cooperative positioning schemes as in [72]-[75]. On the other hand, statistical approaches such as factor graphs [47] and belief propagation [76] make use of a set of observations and a priori probability distributions of node positions to estimate the maximum a posteriori location.

It is worth mentioning that distributed localization is also used in HDF through the so-called iterative multilateration (see [77] for instance). Once the position is estimated for an unknown node, this node is used as an anchor node whose estimated position is broadcasted to all neighboring nodes. The procedure is shown in Figure 1.9, where the target can do self-localization by making use of not only neighboring anchor nodes, but also virtual anchor nodes that have been localized in earlier iterations. Virtual anchors are localized with different levels of uncertainties. Also, this process is iterated until all nodes with at least three reference nodes achieve estimation for their position. In this case, information is needed only within local neighborhood, thus reducing communication cost at the cost of error propagation. Consequently, it is essential to have careful selection of reference nodes in order to reduce the accumulation of error through considering the uncertainties in estimating reference nodes.

### 1.5.1.2 HDF Techniques including maps and fingerprinting

A number of propagation model-based or fingerprinting-based techniques have been proposed for indoor wireless positioning. RF location fingerprinting [78] uses a set of sensor measurements (i.e. RSS) from WLAN access points, GSM, RFID readers, or other RF-based sensors to represent the locations. On the other hand, propagation model-based approaches [79][80] require an explicit sensor model to predict the propagation of the RF signals. However, their accuracy is affected

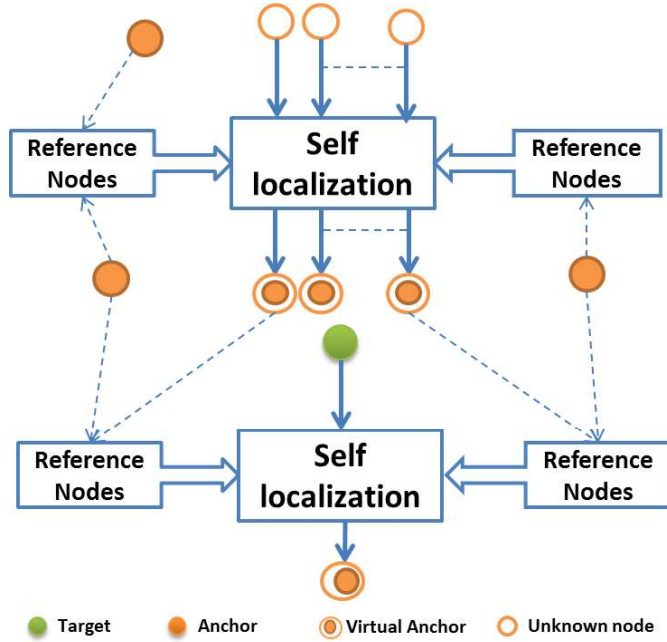


Figure 1.9: Iterative Multilateration

by a large number of environmental factors, since it is almost impossible to find a universal model to characterize the radio signal propagations in indoor environments due to severe multipath and numerous site-specific parameters. This approach does not rely on any explicitly predicted model to characterize the sensors behavior. Instead, an a priori set of fingerprints that expresses the sensors output at sampled locations in the global frame has to be recorded in advance during an offline training phase. In the online localization phase, the location of a node is determined by matching the current observations with the recorded reference fingerprints. Fingerprinting-based approaches are therefore assumed to be more accurate and robust as compared to the model-based approaches with regard to location-specific distortions.

The traditional fingerprinting-based approaches require a time-consuming and laborious site survey phase in order to construct, combine with and update the fingerprinting map. Therefore, some researchers proposed different techniques to reduce the site survey in the traditional fingerprinting-based approaches. Here, we mention the works of [81] exploiting human motions, [82] using smartphone-based crowdsourcing, and [83] adopting ray tracing tool.

### 1.5.1.3 Fuse with inertial information

The movement of a mobile object can be estimated from the IMU and thus can be integrated into indoor positioning systems to improve their performance.

The position estimates can be improved and smoothed by fusing the WLAN and IMU data [84]. Moreover, the orientation information can be retrieved using the movements of the pedestrian, which leads to a more precise WLAN positioning system. The IMU information assists the selection of nearest neighbors for real-time WLAN fingerprinting positioning in order to reduce the positioning error [85]. It is combined also with a region-based fingerprinting using a Kalman Filter to improve the positioning accuracy [86]. The accuracy is further improved through a multisensory system, which combines data from different sensors (RSS, visual features, and built-in accelerometer) in smartphones [87].

#### 1.5.1.4 Fuse with Camera information

A hybrid indoor location estimation system is achieved also by merging the information from WLAN with the build-in camera on a smart-phone for position estimation [88]. This approach utilizes visual markers pre-installed on the floor for the position correction. Visual information is combined also with the radio data to track a person wearing a tag using a mobile robot in indoor environments [89]. The authors of [90] presented a method to integrate range-based sensors and ID sensors (i.e. infrared or ultrasound badge sensors) using a particle filter to track people in a networked sensor environment. As a result, their approach is able to track people and determine their identities owing to the advantages of both sensors.

#### 1.5.1.5 Fuse with other information

The spatial structure information of an environment may be used to improve the localization accuracy. Given a map of an environment, an object can only appear in the free space of the environment. Hence, different kinds of information fusion lead to an improvement in the positioning accuracy, usually at the cost of additional complexity. For instance, data fusion occurs also with different types of RF sensors to improve the localization accuracy since different positioning systems may complement each other [91].

### 1.5.2 Cooperative Localization in SLAM

The Simultaneous Localization And Mapping (SLAM) technique performs localization relative to a map of an unknown environment that is simultaneously acquired by a moving node. While SLAM techniques are used in outdoor environments, their utilization in indoor scenarios is however dominant. SLAM is a localization technique used to build up a map within a known or unknown environment while at the same time tracking the current location. SLAM algorithms are tailored to the available resources, aiming to work with operational compliance and not targeting perfect results. Published approaches are employed

in self-driving cars, unmanned aerial vehicles, autonomous underwater vehicles, robots and even inside the human body. SLAM is mainly used in cases where nodes are not equipped with a GPS sensor. As alternative, incremental egomotion sensors, such as inertial navigation and odometry, are used for localizing the mobile node. Nevertheless, error is accumulated over time by such sensors making accurate map generation a challenging task.

In practice, we have two main methods listed under cooperative SLAM localization. The first one is the centralized approach through which a central system distributes the data to all nodes (such as robots) in the group. The weakness of this system is that any fault in the central unit leads to a failure of the whole localization system, and nodes are limited in mobility in order to keep contact with the central system. On the other hand, the second method is the decentralized approach through which the exchange of the data between nodes is done without the need of a central unit [92][93].

In SLAM, the data, of both the sensor networks and the autonomous nodes or vehicles, is usually merged for enhancing localization techniques [94]. Basically, the one-way cooperative localization scheme is based on the fact that one system is supplementing the other to do localization. The two-way cooperative localization technique is based on the idea of sensors performing their own localization by themselves first and then performing localization of the vehicles (or robots), while the localization of the vehicles will be done by themselves.

SLAM presents critical challenges in robot research community due to the non-linear nature of the problems therein. As discussed by [95], Extended Kalman filter (EKF) is widely utilized for the localization of robot and the incremental development of the environment map in SLAM. Besides, the localization in non-linear SLAM systems is tackled also in EKF literature. Particle filter is also used to denote both possible map configurations and robot poses. Using a new map representation denoted by distributed particle mapping allows an efficient preservation and update of hundreds of robot positions and candidate maps.

Simultaneous Localization and Mapping and Moving Object Tracking (SLAMMOT) represent a normal continuation for the SLAM problem with moving objects. The SLAMMOT technique is used to solve the observability problem as well as enhance the accuracy of localization, mapping, and tracking [96]. Other extensions of SLAM techniques also exist. We notice the Cooperative Simultaneous Localization, Mapping and Target Tracking [97], the distributed strong tracking unscented particle filter which uses distributed particle filter [98]. All these techniques are applicable in indoor environment.

### 1.5.3 Common Pitfalls to avoid

In this section, we handle the pitfalls to avoid while using data fusion techniques in cooperative localization.

Data fusion is highly critical in WSN since it increases the network lifetime and



achieves the objectives of the application, such as target tracking, event detection and decision making. Consequently, applying inappropriate data fusion leads to misleading evaluations and waste of resources. Hence, we must take care of probable limitations of data fusion so that we can prevent blundering cases from occurring. Also, WSN recommends applying data fusion in a distributed fashion in order to increase network lifetime. Nonetheless, we must also take care of the challenges obtained when performing data fusion in a distributed manner. Therefore, a centralized fusion system may provide better performance than the distributed system.

Moreover, the feasibility of data fusion techniques requires the evaluation of process computational cost and the delay presented in the communication. The centralized version is preferred when computational resources are available and the cost of transmission is somehow low.

Statistical data fusion techniques such as probabilistic data association and Kalman techniques have an optimal performance under particular conditions. However, the target cant be assumed to be moving independently and the measurements cant be assumed to have normal distribution around the estimated position. Second, it is difficult to attain a priori probabilities for detection errors and misleading measurements, knowing that statistical methods represent events as probabilities. On the other hand, the complexity of statistical techniques optimizing numerous frames increases exponentially with the number of targets. Hence, such techniques are considered to be computationally intensive. So, it is preferred to assume no interaction between particles and to perform individual tracking.

Challenges are also induced by the data fusion process with distributed data fusion techniques. These challenges include out-of-sequence measurements, temporal and spatial alignments of the information and data correlation. As shown by many researchers [60]-[98], the cooperative and hybrid data fusion approaches enhance significantly the accuracy of localization and navigation of mobile users, despite of the drawbacks listed above. However, the accuracy limit is still not clear and requires further investigation. In philosophy, learning from your past evolves your future. As Leo Buscaglia said, Change is the end result of all true learning.

## **1.6 Learning Algorithms for Localization**

### **1.6.1 Learning and environment mapping**

In localization, both supervised and unsupervised learning approaches have been proposed. For instance, in Self-Organizing Map (SOM), the adopted approach is unsupervised learning [99]. Nevertheless, supervised learning techniques are presented since the relationship from distances information (inputs) to desirable behavior of the node (outputs) to be localized are achievable.

In SLAM, learning techniques are widely combined with environmental mapping. For instance, the standard SLAM is extended into signal-strength-based SLAM with learning approaches through the Gaussian Process Latent Variable Model (GP-LVM) [99]. Combining GP-LVM and a dynamic motion model, a topological graph of the environment is built up from the raw signal strength data. This map is then used for efficient localization by applying Bayesian filtering [100][101]. In indoor environment, learning and radio maps are used to obtain high accuracy. Radio map can be automatically constructed via crowdsourcing and RSS measurements [102]-[104]. However, as RSS measurements are vulnerable to environment dynamics they are more extravagant in indoor environments with severe multipath. Consequently, the location will be estimated with low accuracy. Doing the site survey repetitively and applying appropriate learning approaches solve this problem despite of its complexity in terms of time consumption. Fresh RSS measurements can be taken to adapt the radio map by deploying fixed reference ANs [105]-[108]. Hence, location service is enhanced with high quality when the radio map is always updated through learning. Among others, game theory has gained a lot of research interest in this domain.

## 1.6.2 Game Theory to improve Localization

Game theory originates from the field of applied mathematics to analyze complex interactions between entities. Basically, game theory is a set of analytic tools that perform distributed decision process. Generally, a game is composed of decision makers, i.e. players with different strategies. Each player has a utility (payoff) that represents the level of satisfaction. The aim of each player is to maximize his own expected payoff [109]. Game theory includes coalition formation. The classification of coalition game is done by mapping a network component as a game component, nodes as players, available adaptations as action set, and performance metrics as utility function [110].

### 1.6.2.1 Game Theory in localization

Game theory is very efficient for localization purposes since it permits the formation of optimal coalitions of nodes for localizing a target node. Greedy strategies are usually proposed and used to minimize the error of their localization process and reduce the power consumption. Thus, it is important to study the tradeoffs in selecting an effective strategy for indoor localization.

### 1.6.2.2 Coalition Games for positioning purposes

Game theory has been used in localization, primarily for demonstrating the trade-off between cost and performance and for selection of reference nodes [111], specifically for allocating measurements between reference nodes aiming to localize the

target. In a distributed localization approach, the concept of game theory and utility functions is used to determine the combination of reference (anchor) nodes that lead to the best localization performance [77]. To implement the cooperative localization approach, a coalition game denoted by the pair  $(N, v)$  is adopted, where  $N$  represents a finite set of players and  $v$  denotes its utility function. The players are the element of  $N$  and any non-empty subset  $C \subseteq N$  represents a coalition, as shown in Figure 1.10. Particularly,  $N$  represents the grand coalition. Basically, the coalition value, represented by  $v$ , denotes the value of a coalition in a game. The payoff  $x_i$  of each player  $i \in S$  represents the amount of utility received by each player from the division  $v(S)$ . Hence, the payoff allocation is denoted by  $x \in \mathbb{R}^{|S|}$ , where  $|S|$  is the cardinality of  $S$ . The localization procedure here is demonstrated as a game fitting in the class of weighted-graph games. For such illustration, the players are defined as the vertices, and the value of a coalition can be defined as the summation of the weights of edges connecting pair of vertices in coalition. The main concept is to allocate more measurements to nodes with higher contribution in the localization process. Generally, coalitional

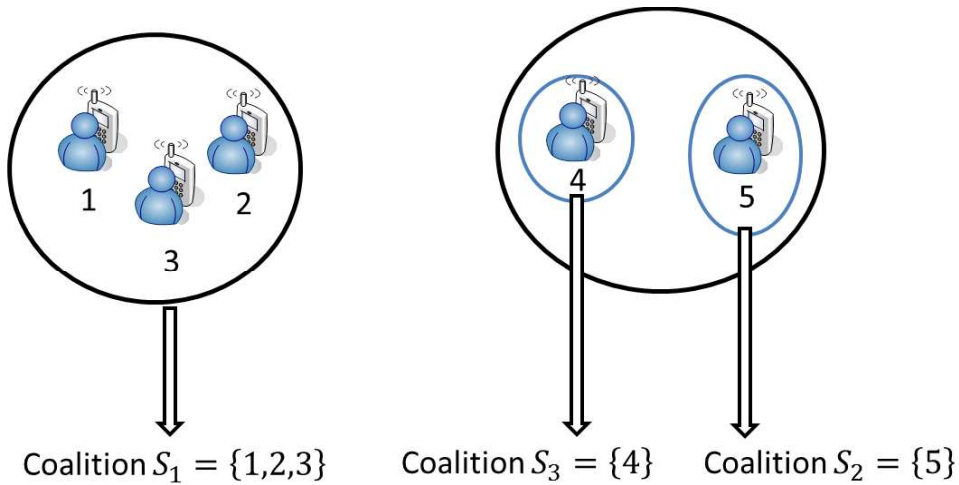


Figure 1.10: Coalition Games

games are categorized into two kinds depending on the distribution of the gain among players in a coalition. The first type is the transferable utility (TU) game where we may have proportionality in the total gain attained between players in a coalition bound by feasibility constraints. A non-transferable utility (NTU) game is the second type. In such game, additional constraints, preventing arbitrary allocation, are imposed on the assigned strategies. Also, the payoff of each player is based on joint actions inside coalition. The localization problem can be also seen as a coalitional formation game within nearby anchors [112], where coalition formation is done through merge and split procedure, to reduce the cost of communications. The localization problem here is a game of NTU nature since the

same position estimate is obtained by all nodes within the locating coalition and the power consumed is determined based on the relative locations of the nodes. To do so, a utility function is defined to model the cost and quality indicator of the localization [77]. In practice the definition of the cost and utility functions depend on the coalition cardinality, the limit of error targeted and the range of distances to be estimated through coalition games. For instance, a good choice is to define a utility function which increases with the distance between the anchor nodes and/or the error between the estimation and real measurement decreases. In such a choice is made, the cost of coalition will be less. In a real scenario with multiple anchor nodes, the following utility function of a node  $x$  could be made:

$$f_x(N) = \alpha \left[ 1 - \frac{1}{N} \sum_{i \in N} \frac{(d'_i - \hat{d}_i)^2}{R^2} \right] - \frac{(1 - \alpha)}{N} \sum_{i \in N} \frac{d_{ih}^2}{R^2} \quad (1.1)$$

where  $0 \leq \alpha \leq 1$  regulates the tradeoff between cost and performance,  $N$  is the number of measurements taken at a given location  $x$ ,  $d'_i$  represents the estimated distance of the  $i$ -th node,  $\hat{d}_i$  represents the distance between the  $i$ -th node and the joint estimated target position,  $h$  is the coalition head index and  $R$  is the coverage range.

One can also define other utility functions determined by locations of all nodes in the coalition with cardinality  $N$  at a given measurement instance by:

$$f(N) = \alpha \left[ 1 - \frac{1}{N} \sum_{i \in N} \frac{(d'_i - \hat{d}_i)^2}{R^2} \right] - \frac{(1 - \alpha)}{N} \sum_{i \in N} \frac{d_{ih}^2}{R^2} \quad (1.2)$$

The interest in each coalition function defined above is different. For instance, the first coalition could be used at each node at different time stamps to reduce the total energy consumption throughout all readings. The second function could be used with spatial correlation of nodes readings. A good example therein is given in [112] where the authors proposed non-super-additive coalition. It is the case when the grand coalition, a coalition that comprises all nodes, is not optimal. Another approach in coalition games would be in considering the coverage area of the target node as a set of correlation regions [113]. The correlation region in this case represents the region where readings reported by nodes are alike. According to the localization performance, it is viable to assume that redundant information is provided by spatially correlated nodes in terms of GDOP or CRLB. Hence, we can represent the coverage area of the target node by set of active nodes acting as anchors. This approach reduces the complexity of the search method because only a subset of anchor nodes is involved in the process of forming coalition. As a common rule of thumb, the localization in indoor environments from the perspective of a game theory deals with mobile devices as players competing

on limited resources to perform position estimation [111]-[113]. This problem is formulated as a standard non-cooperative game, where the players are the mobile devices, the strategies are the scanning parameters and the payoff for each player involves the accuracy level of positioning and the power consumption.

### 1.6.3 Open challenges in localization based learning

In general, many challenges are recognized when using learning techniques for localization in heterogeneous wireless environment. In multi-agent localization, various activities are proposed to handle centralized localization approaches through the utilization of physical tagging. This helps in identifying the single agent position to global positioning systems based on cameras or GPS. However, in practical environments and mainly in indoor scenarios, it is preferred to avoid these centralized multi-agent approaches since they reduce the system autonomy and range of applicability. Based on that, probabilistic and distributed framework solves the problem of mutual localization with unidentified relative position measures [114][115]. This comes at the detriment of centralized failure risk. In game theory based localization, a main challenge is to recognize the players and identify the localization problem as a cooperative or non-cooperative game. The selection of the players and strategies defined by each player with their objectives are vital in identifying the game. Players are assumed to be rational individuals in game theory since the actions taken by each player is based on his best interest. In such scenario, game theory models and explores the competitive or cooperative interaction among nodes (anchors or not) and/or network operators that represent rational decision makers. Another challenge in cooperative games resides in the need of collaboration among users for the sake of maximizing their payoffs, in our case the location information; however, players may refuse cooperation and be selfish in order to preserve limited resources such as energy or optimize their own profit. Hence, incentive mechanisms are preferred to be embraced. Furthermore, the decision process done by the players is considered as a critical feature to consider in game theory in general and in localization particularly. Finally, in indoor wireless environment, defining the utility function as a function of the location is a complicated task due to the vast number of several applications with dissimilar needs.

## 1.7 Applications

In this section, we detail the main applications of localization in indoor environments. Indoor positioning and navigation for mobile devices is a market with expected size of 4 billion dollars in 2018 [116]. A reliable, user-friendly, and accurate solution for indoor positioning and navigation might open the doors to the definition of new applications and the creation of new business opportunities in

countless scenarios [117], and is indeed considered as a cornerstone in the realization of the Internet of Things vision [118][119]. It is worth mentioning that some of these applications could be also applied in outdoor scenarios.

### 1.7.1 Robotics

Robotics is one of the main applications of indoor localization. Many researches and developments have been conducted for implementing mobile multi-robot systems applications. The movement of robots in real large indoor scenarios where cooperation is required between them is a critical topic. For instance, cooperation between robot teams enhances the mission outcomes in applications such as surveillance, unknown zones exploration, guiding, or connectivity maintenance. Ubiquitous Networking Robotics in Urban Settings (URUS) project [120] is an excellent example using localization for evacuation in case of emergency where the robots lead the people to safe area via safe pathways in case of fire. Moreover, obstacle avoidance and dynamic and kinematic constraints are considered in robotics in order to achieve complete navigation system [121][122]. Similarly, the work in [123] used the idea of forces among robots to avoid obstacles. Another application is seen in [124] where a multi-robot navigation system takes into account all robot (dynamic) constraints and calculates one function for all the formation to perform robot navigation with assured collision avoidance. SLAM is also very interesting in robotics. Therein, the tasks performed by a robot are done autonomously without the awareness of its surrounding and own position. SLAM is useful in construction autonomous robots. However, it requires high processing resources to carry out SLAM in real time [125]. Then, C-SLAM [126] solves the problem by constructing the environment map based on the collaboration between multiple robots. A global map is obtained in C-SLAM by merging individual maps obtained by multiple robots. Additionally, accurate navigation of mobile robot in indoor environments is achieved through an UWB navigation system [127]. The navigation system consists of two sub-systems: the robot control system and the localization system. Autonomous robot navigation is achieved in this system through a TDoA-based localization technique, digital implementation of transmitter and receiver and combination of both sub-systems [127]-[129].

### 1.7.2 Ambient Assisted Living and Health Applications

Indoor localization is one of the useful constituent in AAL tools. AAL environments are generated from ambient intelligence which is an advanced tool performing creative machine-human interactions. For instance, AAL tools aim to enhance health status of older adults by making them able to control their healthiness conditions [130][131]. Elderly people make use of such applications for the purpose of monitoring, tracking and other location-based applications. Besides, we real-

ize the significance of such applications in indoor scenarios where GPS signals are useless. Some of indoor localization systems based on AAL applications are Smart floor technology to notice the existence of people [132] and Passive Infrared (PIR) sensors to notice motion of people. Currently, indoor positioning is central in the deployment of seamless emergency response services such as E911 in the US, hindered by the lack of common benchmarks and platforms [133][134]. This has recently pushed different research entities worldwide to propose advanced and beyond state-of-the-art solutions in this domain with applications varying from ambient assisted living, elderly support, emergency cases, etc. Here, we should mention the work of the project SALICE [135][136] which proposed solution based on the heterogeneous combination between satellite-based localization and communications systems to provide emergency services. The project is mainly based on combining delay diversity techniques and maximum ratio combining between satellite and terrestrial sites. The deployment of gap fillers (used as relays) on the border of the emergency area is another proposition of the project to increase the signal diversity by alternating between LOS and NLOS conditions. In parallel, standardization bodies also recognized the fundamental role of location information, and are actively working on standards related to the retrieval of location information, the Location Working Group within the Open Mobile Alliance [137] and the technical specification TS23.271 by the 3GPP [138] being notable examples, as well as the upcoming 18305 standard by International Organization for Standardization and International Electrotechnical Commission, whose joint JTC1/SC31 subcommittee includes a working group on positioning. Last but not least, hardware companies are also pursuing the design of systems and chips for accurate indoor positioning, e.g. based on IEEE 802.11ac or IEEE 802.15.4. Investigations in indoor scenarios on UWB for human body localization are performed via numerical and analytical methods by placing wearable compact sensors on the upper part of the body. This work succeeded in performing 3D localization using such sensors. Also, UWB technology is appropriate for wearable wireless sensor networks, and a 3D localization accuracy of 2 cm to 3 cm is achieved; hence, a system with this accuracy can be applicable for monitoring patient, tracking and applications for capturing motion. Other applications are also based on UWB technology [49][139] where orthopedic computer-aided surgery as well as its integration with smart surgical tools such as wireless probe for real-time bone morphing is implemented [49]. UWB positioning system is proven to achieve a real time 3D dynamic accuracy of 5.24 mm to 6.37 mm. Hence, this dynamic accuracy implies the potential for millimeter accuracy. This accuracy satisfies the requirement of 1 mm to 2 mm 3D accuracy for orthopedic surgical navigation systems.

### 1.7.3 Location-based Services

Location-based Services (LBS) are defined generally as service that outspreads GIS capabilities or spatial information to end users through wireless networks and/or the internet. Yet, LBS applications can offer the context and the connectivity needed to dynamically associate the position of a user to context-sensitive info about current environments; whereas conventional GIS applications are concentrated on geographical information for land planning and management. Hence, high level of personalization is achieved with LBS applications that simplify a capability of making each user the center of his universe. LBS send data dependent on context and accessed by a mobile device by knowing the geographical location. LBS service is required for indoor and outdoor environments. For instance, indoor LBS include applications to obtain safety information or up-to-date data on cinemas, events or concerts in the vicinity. Further applications of this type include a navigation application used to direct a user to the target store in a public building. Moreover, LBS are used for advertisements, billing, and for personal navigation to guide guests of tradeshows to the targeted exposition booth. Also, LBS applications can be used at bus or train stations to navigate to the bus stop. Likewise, LBS are used for notification based on proximity, automated logon/logoff tasks in institutions and the profile matching.

### 1.7.4 5G Networks

Location information can be used to address many challenges in 5G networks [140]. The accuracy of location estimation was improved from hundreds to tens of meters using cell-ID localization in 2G, localization based on timing via synchronization signals in 3G and reference signals dedicated for localization in 4G. As well, localization technologies can be used by numerous devices in 5G to attain an accuracy of location estimation in the range of centimeter. Basically, in 5G networks, it is expected to use precise location estimation through all layers of the communication protocol stack [141]. This fact is due to several aspects [140]. One of these aspects is the inverse-proportionality between SNR and distance due to pathloss; hence, the distance becomes an indicator of the interference level and the received power. So, the best multi-hop path between the source and the destination in a dense network becomes the shortest path in terms of distance when neglecting the shadowing factor. Next, remarkable differences in the localized power are recognized due to shadowing effect. Additionally, nearby terminals can be used to induce local channel information due to the fact that shadowing often reveals decorrelation distances larger than localization uncertainty. So, the use of precise location information by 5G networks over all layers of communication protocol stack is due to the prediction of most of the 5G user terminals in their mobility patterns knowing that these terminals will be either associated with fixed or controllable units or people. Last but not least, local-



Table 1.1: Comparisons of positioning techniques

Wireless Positioning Systems	Localization Technique	Range	Accuracy
Dolphin [145][146]	ToA, trilateration	Room	2 cm
RFID/INS [147]-[152]	RSS/INS	Indoor	2 cm
UWB [153]-[156]	TDoA/ToA, trilateration	15 m	10 cm
RFID/FPM [157]	RSS/INS	Indoor	1.7 m
Land Marc [158][159]	RSS, triangulation	50 m	1-2 m
GPS [160][161]	ToA, trilateration	Global	1-5 m
Radar [162][163]	RSS, triangulation	Room scale	2-3 m
Cricket [164]	ToA, trilateration	10 m	2 cm
Active Bats [165]	ToA, trilateration	50 m	9 cm
Active Badge [166][167]	ToA, trilateration	5 m	7 cm
COMPASS [168][169]	RSS, triangulation	15 m	1.65 m
WhereNet [170][171]	RSS, triangulation	20 m	2-3 m
LiFS [81]	Fingerprinting Database		9 m
Bluetooth [172][173]	RSSI Fingerprinting	Indoor	2-5 m

ization is not only required for location-based services, but also for several jobs in cyber-physical systems, like smart transportation systems and robotics in 5G networks [142][143]. Furthermore, methods for resource allocation based on location awareness [144] can diminish delays and overheads since they can predict the quality of channel further than customary time scales. This is indeed one of the technical targets of the 5G technologies.

## 1.8 Comparative Study

In this section, we will present a comparative study between different localization techniques in terms of range accuracy for different applications. Basically, we present in Table 1.1 a comparison between different positioning systems showing the range, accuracy, and the technique(s) used. All of the positioning systems and the location information are reported from literature and produced in real time (according to the references mentioned). Moreover, we can observe in Figure 1.11 the accuracy achieved by different wireless based positioning systems used for indoor, outdoor and locally urban, and rural and remote areas. It is very clear from this figure that the accuracy requirements depend on the scale of the transmission; hence, it will affect the type of application supported by the corresponding localization technique. So, it is important to notice vitality of localization in current and future wireless systems in any and all applications and scenarios.

## 1.9 Perspective and Challenges

In this section, we summarize the perspectives and challenges in indoor localization. We should mention that many challenges and pitfalls have been addressed in the previous sections. The target of this section is just to summarize on the main ones and provide some details on those which have not been addressed so far.

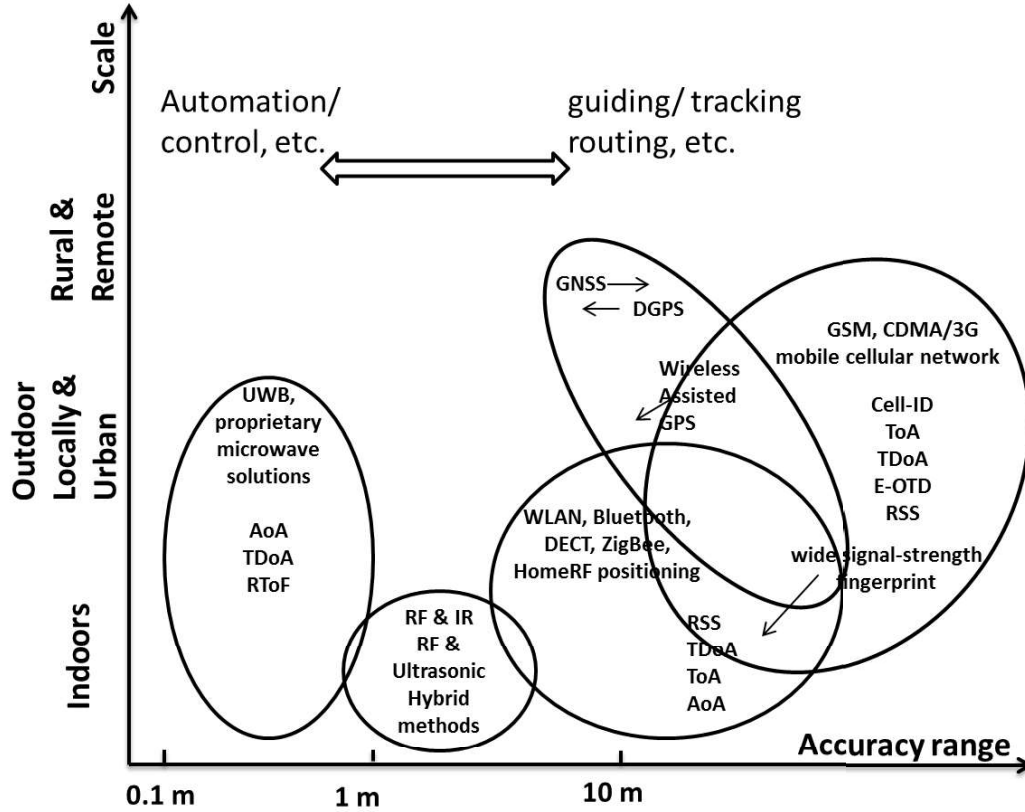


Figure 1.11: List of various wireless-based positioning systems [11]

### 1.9.1 Constructing radio fingerprinting map with less human participation

Although the fingerprinting-based approach provides satisfactory accuracy, one often has to reconstruct or update the fingerprinting map to capture the features of a new environment (for example, when new sensors are installed), which is extremely time-consuming. Moreover, the complexity of the fingerprinting-based approaches is proportional to the number of entities one wants to locate. For

example, in order to locate a laptop and a smart phone, we need to build up a fingerprint map for each of them due to the heterogeneity of these devices. So the main challenge to address here is to have a unified framework for radio fingerprinting maps independently of entitles.

### **1.9.2 Combining various non-radio techniques**

The use of non-radio technologies (IMU, visual sensors) can compensate for the errors from the existing wireless positioning technology. The improved accuracy is achieved by the additional installations of the costly equipment; therefore investigating a cost-effective wireless positioning system is still a promising direction.

### **1.9.3 Integrating various wireless positioning solutions**

A variety of wireless sensors can be used for positioning services. Different sensors are working with different physical principles. Combining the measurements from different positioning systems can improve performance of the overall solution.

### **1.9.4 Security and Privacy**

The security and privacy factors are considered important to discuss with Indoor Positioning Systems (IPSs) within Personal Network [12], where users position people and objects in their home. The user cares if he is being tracked and his activities are being known by someone. Typical IPSs have threats in WLAN-IPS environment. For instance, positioning system based on RSS measurements threaten security since the mobile device collects the measurements of all AP devices and personal data such as AP ID is sent to the IPS server [174]. Additionally, the privacy in IPSs can be enhanced via a controlled access to the information distribution and location information. As well, security and privacy can be improved in IPSs from the software and system architecture perspectives. For instance, position system architecture dealing with self-localization can guarantee high degree of privacy and security for users when the estimation of the position is done at the target device [12]. Hence, the location information cant be accessed by anyone in Personal Networks (PNs) if the target device doesnt provide it to an entity.

### **1.9.5 Scalability**

A scalable positioning system means that it functions properly when its scope gets larger. Usually, the performance of localization reduces with the increase in the distance between the transmitter and receiver. Further, a positioning system may require scaling on 2 axes, density and geography. Geographic scaling represents the coverage of an area or volume, whereas density scaling represents

the number of units positioned per unit geographic space or area per time period. Wireless signal channels may turn out to be congested as more area is covered or the units in such area are crowded; hence, further computation or communication infrastructure may be required to do localization. In addition, the dimension of a system is another metric for scalability. A positioning system may locate objects in 2-D space, 3-D space or in both. So far, most of the proposed techniques are dealing with 2D while the recent recommendations from different standardization committees require 3D information with high accuracy (FCC recommendation for instance). This is then another important aspect to be tackled in the future.

### 1.9.6 Complexity

Positioning systems have complexity in terms of software, hardware, and operation factors. Specifically, software complexity represents the complexity of computations in a positioning algorithm. If a centralized server side handles the computations, location estimation is performed quickly because of the existence of adequate power supply and great processing capability. However, if the computations are performed at the mobile user, complexity becomes evident since mobile users have weak processing power and short battery life; thus, positioning techniques with low complexity are preferred in this case. Additionally, representing complexity of various positioning techniques through a formula analytically is really a difficult task; hence, the time spent for computations should be considered. Also, location rate is used as an indicator for complexity. Oppositely, we have location lag that represents the delay between movement of a mobile user to a new position and the reporting of this new position by the system.

### 1.9.7 Accuracy vs. Cost-effective

Different levels of accuracy are achieved with different positioning systems. For instance, an accuracy of 2 m to 3 m is achieved with RADAR [162]. On the other hand, 2 cm accuracy is achieved with a cricket system that is based on ultrasonic signals [164]. Furthermore, WLAN-based positioning system utilizes the existing WLAN infrastructures for localization; therefore, the positioning accuracy highly depends on the environments and placements of the wireless sensor nodes. Other positioning systems usually require previous installation of the beacons in the environment. Therefore, in practice, it is very challenging to meet accuracy requirement and at the same time keep within minimum number of beacons and mobile device costs. The trade-off between accuracy and cost consists of a capital challenge in indoor scenario since from one side; the accuracy suffers from the existence of obstacles and multi-path transmission while the cost is quite affordable due to the availability of signals (such as WLAN) at reduced cost.

### 1.9.8 Applications and Accuracy

The accuracy of the localization techniques highly depends on the applications. While some techniques are working perfectly in indoor scenarios, for instance, they might not be applicable in medical applications such as in Wireless Body Area Networks due to the precision requirement (in mm). This is a general challenge which should be tackled in any application and environment. Particularly, in mmWave, a promising candidate for 5G networks, the accuracy and means of localization are still open research issues to be solved. Nevertheless, the importance of high accuracy is primordial in this environment.

# Chapter 2

## Localization In Known Environment

### 2.1 Introduction

MilliMeter Wave (MMW) wireless communication systems have recently gained great research interests due to their benefits in terms of spectrum, propagation characteristics, potential applications and services [175][176]. Basically, MMW spectrum ranges between 30 GHz and 300 GHz. A band of these frequencies is said to be unparalleled compared to cellular and Wireless Local Area Network (WLAN) microwave systems operating at frequencies below 6 GHz.

Technically, MMW spectrum can be used for military, radar and cellular services. For instance, the spectrum at 28 GHz, 38 GHz, and 70-80 GHz provides promising channel propagation specifications for the evolving fifth generation (5G) of cellular systems [177][178]. Among the potential services offered by MMW, localization and mapping appears as key factor in enabling new means and tools for communications systems [1]. Moreover, Indoor Positioning Systems (IPSs) are the center of attention for researchers because of the vast technological enhancement in smartphones and tablets, and the evolving technology of Internet of Things (IoT) as a future service in 5G. For instance, localization is critical for detecting products stored in a warehouse, medical equipment and personnel in a hospital, firemen in a building of fire, and police dogs finding explosives in a building. With the evolution of MMW communication systems, IPSs will exploit the infrastructure of future MMW groundwork.

MMW systems are equipped with steerable mechanisms due to the necessity of employing high-gain directive antennas. Furthermore, the small wavelength of MMW systems promotes the use of Multiple-Input Multiple-Output (MIMO) required to achieve time diversity [180]. Further researches showed that MMW channel behaves as the quasi-optical channel; hence, the Line of Sight (LoS) factor is dominant [181]. Thus, MMW channel models take into consideration no more

than double-bounce reflection effect since higher order of bounces for non-Line of Sight (NLoS) paths is deteriorated at mm-wave frequencies [182]. The characteristics of the channel at those frequencies showed that reflections don't generate significant amount of scattering [183], and that the transmitted beam will have the same directivity after reflections with slight scattering [184]. Hence, Snells law holds in terms of the equality between the angles of departure and incidence upon reflection [181]. These propagation characteristics could be then used for localization and mapping. However, the appropriate channel models, localization procedures and mapping approaches should be derived [178][185][186].

In literature, there exist few researches on localization systems operating at 60 GHz. Most of the research work done focused on measuring the delay spread used for systems based on Time-of-Arrival (TOA), Time-Difference-of-Arrival (TDOA) and Angle-of-Arrival (AoA) methods [187], [188]. The benefit behind using the 60 GHz band is achieved within the availability of a very large bandwidth (up to 7 GHz); hence, achieving accurate range measurements.

In this chapter, we propose two localization techniques for estimating the location of the receiver through a single anchor node. Then, we propose to estimate obstacles positions and dimensions in an indoor environment. This is done by creating Virtual Anchor Nodes (VANs) and adopting Triangulation (TL) and Angle-Difference-of-Arrival (ADoA). The proposed methods allow us to develop context inference and mapping of the indoor environment. The proposed techniques achieve very high accuracy reaching sub-meters (few centimeters in some cases). Hence, they could be easily adopted for IoT applications mainly in health, fire and emergency.

## 2.2 Characteristics of MmWave Communications

To take full advantage of mmWave communications, its characteristics should be specified and taken into consideration in design of network architectures and protocol. In the following subsections a summary of these characteristics.

### 2.2.1 Wireless Channel Measurement

At the time signals at lower frequency bands can propagate for many miles and penetrate easily through buildings, millimeter wave signals suffer from huge propagation loss where they can travel only few miles and cannot penetrate solid materials well. Range of mmWave communications is limited by the rain attenuation and atmospheric and molecular absorption characteristics of mmWave propagation. Despite their disadvantages causing problems in communication systems, these characteristics of millimeter wave propagation can allow more densely packed communications links, thus increase security of communication transmissions. Moreover, it is been shown that rain attenuation and atmospheric

absorption do not create significant additional path loss for cell sizes about 200 m. Hence, mmWave communications are mainly used for indoor environments, and small cell access and backhaul with cell sizes about 200 m.

### 2.2.2 Directivity

Millimeter wave links are inherently directional. Communications between two devices are not possible if their beam directions are not pointing towards each other. Hence, to achieve a high gain at a specific direction, the antenna array drives its beam towards this direction electronically by controlling the phase of the signal transmitted by each antenna element. All other directions will offer a very low gain. The directional beam pattern improves the transmission range but it complicates communication protocol designs. For that, efficient protocols and beam training procedures are essential to discover the best beam direction pair between devices and reduce the required beam training time.

### 2.2.3 Sensitivity to Blockage

Diffracting around obstacles whose size is significantly larger than the wavelength is almost limited by electromagnetic waves. Obstacles like humans and furniture can block links because of their so small wavelength at 60 GHz (5 mm). For example, blockage by a human can penalize the link budget by 20-30 dB [10]. Results shows that in presence of human activities, channel in a realistic indoor environment is blocked for about 1% or 2% of the time for one to five persons[11]. Therefore, mmWave links are interrupted by human mobility resulting in a time-varying network topology. Ensuring a reliable connection for delay-sensitive applications such as HDTV is a big challenge for mmWave communications.

Moreover, the relations between index of refraction, speed of light in vacuum and speed of light in medium are valid for light. Hence, having signals with behavior far away from optical behavior would make these equations invalid. That's why we go to mmWave to make use of Snell's law as a good estimator to use for classifying obstacles. So, it is not a matter of a direct relation between frequency and index of refraction; it is related to the behavior of the signal in indoor scenarios if we can apply the concept of snell's law or not. Snells law relates the incident angle  $\theta_i$  and the medium of incidence  $n_i$  to the angle of refraction  $\theta_r$  and medium of refraction  $n_r$  through the following equation:

$$n_i \sin(\theta_i) = n_r \sin(\theta_r) \quad (2.1)$$

We assume obstacles as pure reflectors. Hence, the rays are 100% reflected when they hit the obstacle. This aspect facilitated the process of estimating the VAN and detecting the obstacle limits. On the other hand, assuming that part of the ray will be reflected and part will be refracted with the use of the AoA and



Snells Law allows us to determine the angle of refraction and reflection. Next, we will relate the reflectance obtained from snells law with the reflection coefficient obtained from the RSS at the receiver in order to classify obstacles by estimating the index of refraction of the obstacle.

## 2.3 Localization Techniques

Our proposed MMW localization technique is tested in an indoor environment consisting of a rectangular room bounded by four walls, the ceiling and the floor. We grouped the room boundaries and radio-reflective obstacles in the reflective objects set . Obstacles are described as two-dimensional flat polygonal faces with sharp vertices and straight edges. Each oriented surface  $S$  is denoted by its perpendicular line, written as:

$$y = p_y + \alpha \times (x - p_x) \quad (2.2)$$

where  $\mathbf{p} = [p_x, p_y]$  is a point of intersection between the surface and its perpendicular and  $\alpha$  is the slope of the line orthogonal to the surface  $S$ , represented by the following equation:

$$\alpha = \frac{-1}{\beta} \quad (2.3)$$

Knowing that  $\beta$  is the slope of the surface  $S$ , which can be found as:

$$\beta = \frac{yP1 - yP2}{xP1 - xP2} \quad (2.4)$$

where  $p1 = [xP1, yP1]$  and  $p2 = [xP2, yP2]$  are two points on the surface  $S$ . By assumption, a single MMW Access Point (AP), seen as Anchor Node (AN), is deployed in the room at a location  $\mathbf{pT}$  and is used as anchor node for localization objectives. Additionally, the AP is assumed to broadcast its position and the specifications of the objects in to the node(s) targeted for localization. This assumption holds for devices used for localization with hard energy limitations. The AoA spectrum,  $SP_p(\theta)$ , is a  $2 \times L$  matrix that records the amplitude of each received ray component (RRC) as a function of the azimuth  $\theta$  at a given location  $\mathbf{p}$ , where  $L$  is the number of RRCs. Each RRC can be either due to a LOS link between the transmitter and the receiver or due to NLOS link caused by reflections of one or more surfaces in the obstacle set . In addition,  $SP_p(\theta)$  contains in its first row the amplitude of each RRC sorted in decreasing order and in its second row the azimuth  $\theta$  with respect to reference angle  $\theta_0$ . Hence, each column of  $SP_p(\theta)$  is seen as a vector of polar coordinates that represents the amplitude and the phase of the vector relative to  $\theta_0$ . Moreover, the room geometry is assumed to be known for user(s) to be localized.

### 2.3.1 Virtual Anchors

The concept of VAN is widely used in literature, mainly in ultra-wide band [197] for localizing a receiver using single anchor node with MMW propagation characteristics. In this chapter, concept of VAN is used for the purpose of context inference and mapping of indoor environment through obstacle detection. As introduced also, the first column vector of  $SP_p(\theta)$  represents the LOS path between the transmitter and the receiver to be localized, and the columns 2 :  $L$  represent the NLOS paths. So, we have  $L - 1$  RRCs that correspond to NLOS paths. Each of these paths can be modeled as emitted by a virtual anchor node (VAN) through a virtual LOS path reaching the receiver  $\mathbf{pR}$ . The locations of the VANs, as shown in Figure 2.1 are determined by mirroring the AP  $\mathbf{pT}$  with respect to the surfaces in the obstacle set  $O$  since it is the source of signal reflections. So, the obstacle will be the perpendicular passing through the midpoint of the segment between the transmitter and the VAN. Knowing the slope of the surface  $S$  in the obstacle set  $O$ , we can calculate the slope of the segment between transmitter and the VAN using equation (2.3). Then, the coordinates of the VAN  $(xV_i, yV_i)$ , the mirroring of the transmitter with respect to the obstacle, are calculated using equation (2.4), where  $\beta$  and  $\mathbf{pT} = (pT_x, pT_y)$  are known. We denote  $V = \{pv_0, pv_1, \dots\}$  to be the set of the positions of all possible VANs, and we denote  $\bar{V} = \{V_0, V_1, \dots\}$  to a partition of  $V$ . We let  $V_0 = \mathbf{pT}$ , and each set  $V_i, i = 1, 2, \dots$  represents all VANs that has been mirrored  $i$  times due to reflections caused by any surface in the obstacle set  $O$ . Actually, there is no limit on the number of reflections of the signal transmitted by  $\mathbf{pT}$ . However, a MMW signal fades quickly during its propagation as it reflects off the surfaces. So, we limited the set  $V$  by assuming a maximum reflection order  $\mu$  [196]. So, the set of all VANs will be represented as  $V_\mu = \bigcup_{i=0}^{\mu} V_i$ . As shown in Figure 2.1, the anchors  $V_i$  and  $V_j$  represent first and second order of reflection respectively; hence,  $\mathbf{V}_i \in V_1$  and  $\mathbf{V}_j \in V_2$ .

### 2.3.2 The Triangulation (TL) algorithm

As stated in the introduction, we adopt the concept of triangulate-validate (TV) in [198] and we simplify it to lead what is called here Triangulation (TL). TV is based on coordinate transformation to map the received power and angle of arrival of each RRC into vectors from the position of any anchor. Adopting an initial guess in the localization approach, the TV algorithm proposes a cost function to measure the compatibility between the RRCs and the VANs. However, the TL technique in this chapter is based on solving a system of equations relating the receiver with the anchor nodes using the coordinates of the receiver and the anchor nodes, the distance between them and the angle with respect to the positive x-axis. Contrarily to [198], TL approach does not use a cost function to validate the estimation. It is a simple Least Square followed by averaging. It

is a simple way taking into account all the VANs. It does not eliminate neither scale any of the VANs positions as done with TV, as the target is to estimate the obstacles dimensions and location (not the receiver).

It would be easier to estimate the position of the receiver through a direct triangulation method if we know the association between the VANs in  $V$  and the RRCs in  $SP_p(\theta)$ . However, this association is unknown; hence, we have to estimate the position via set of TL steps that are shown to be less complex than the method of maximum-likelihood (ML) [197]. Moreover, we restrict the set  $V$  to reach a maximum reflection order  $\mu_{max}$ . Actually, a low value of  $\mu$  makes more sense for Triangulation since reflections fade the signal; thus, VANs of high reflection order can be far away from the receiver. As well, the MMW signal is almost seen as a noise after more than two reflections; hence, we set  $\mu_{max} = 2$ . TL steps are based on forming a triangle between the unknown receiver and each anchor node. As shown in Figure 2.2, the following relations are constructed using trigonometric relations in the right triangle formed between the receiver  $\mathbf{pR}_k$  at time  $k$  and VAN  $\mathbf{pV}_i$  as follows:

$$xV_i - xR_k = \rho_{k,i} \cdot \cos \theta_{k,i} \quad (2.5)$$

$$yV_i - yR_k = \rho_{k,i} \cdot \sin \theta_{k,i} \quad (2.6)$$

where  $\mathbf{pV}_i = (xV_i, yV_i)$  and  $\mathbf{pR}_k = (xR_k, yR_k)$  are the VANs and the unknown receiver respectively. Also,  $\theta_{k,i}$  and  $\rho_{k,i}$  are the AoA and the distance of the

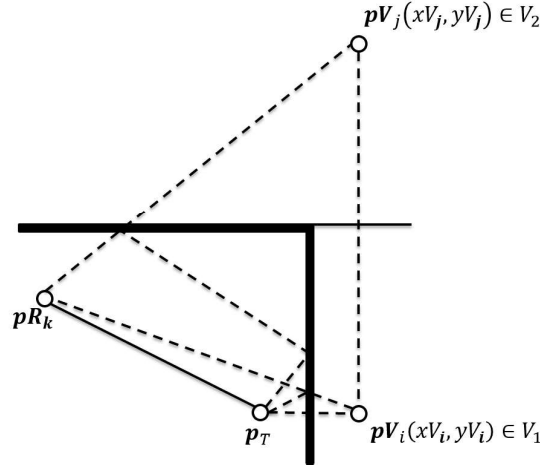


Figure 2.1: VANs related to first and second order of reflections

RRC "transmitted virtually" from the VAN  $\mathbf{pV}_i$  to the receiver at position  $\mathbf{pR}_k$ , respectively. Then for each pair of virtual anchor nodes  $\mathbf{pV}_i$  and  $\mathbf{pV}_j$ , we solve the system of equations in (2.5) and (2.6) corresponding to  $\mathbf{pV}_i$  with those corresponding to  $\mathbf{pV}_j$  to obtain the following system of equations:

$$xV_i - xV_j = \rho_{k,i} \cdot \cos \theta_{k,i} - \rho_{k,j} \cdot \cos \theta_{k,j} \quad (2.7)$$

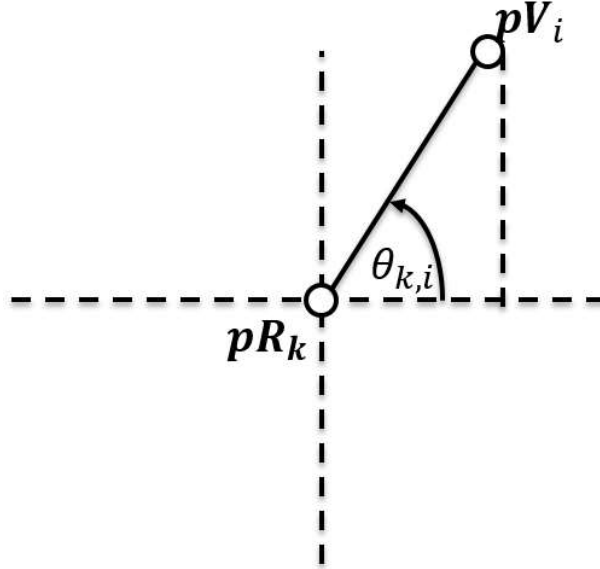


Figure 2.2: Triangle formed between  $\mathbf{pV}_i$  and  $\mathbf{pR}_k$

$$yV_i - yV_j = \rho_{k,i} \cdot \sin \theta_{k,i} - \rho_{k,j} \cdot \sin \theta_{k,j} \quad (2.8)$$

The above system of equation can be written using matrix notation as follows:

$$\mathbf{V}_{i,j} = \mathbf{\Gamma} \cdot \mathbf{P} \quad (2.9)$$

where  $\mathbf{V}_{i,j}$ ,  $\mathbf{\Gamma}$ , and  $\mathbf{P}$  are defined as follows:

$$\mathbf{V}_{i,j} = \begin{bmatrix} xV_i - xV_j \\ yV_i - yV_j \end{bmatrix}$$

$$\mathbf{\Gamma} = \begin{bmatrix} \cos \theta_{k,i} & -\cos \theta_{k,j} \\ \sin \theta_{k,i} & -\sin \theta_{k,j} \end{bmatrix}$$

$$\mathbf{P} = \begin{bmatrix} \rho_{k,i} \\ \rho_{k,j} \end{bmatrix}$$

Solving equation (2.9), we obtain the following:

$$\mathbf{P} = \mathbf{\Gamma}^{-1} \cdot \mathbf{V}_{i,j} \quad (2.10)$$

After solving for  $\mathbf{P}$ , the estimation of the position  $\mathbf{pR}_k$  of the receiver can be done by replacing  $\rho_{k,i}$  in equation (2.7) and equation (2.8). The TL steps are repeated for all possible pairs of  $(\mathbf{pV}_i, \mathbf{pV}_j), i \neq j$  in the set  $V_{max}$ . So, we will obtain  $K$  estimates of the receiver position. The final estimate will be the average of all estimates  $\mathbf{pR}_k, k = 1, 2, \dots, K$ .

### 2.3.2.1 Cramer-Rao Lower Bound (CRLB)

Assuming a wideband multipath model, we estimate the receiver position using the TL and ADoA techniques based on a Gaussian AoA model. This model represents scenarios where there is strong LOS component that could be resolved by the receiver separately from multiple NLOS components due to local scattering. For a single transmitter  $\mathbf{p}T$  with an AoA  $\theta(\mathbf{p}T)$  at the receiver, the Gaussian LOS model with local scattering is defined as follows:

$$p_{LOS}(\hat{\theta}/\mathbf{p}T) = \frac{1}{\sqrt{2\pi}\sigma(1-2Q(\frac{\pi}{2\sigma}))} \exp\left(-\frac{(\hat{\theta}-\theta(\mathbf{p}T))^2}{2\sigma^2}\right) \quad (2.11)$$

where  $\hat{\theta} \in [0, \pi]$  and  $Q(t) = \int_t^\infty \exp(-t^2/2) dt / \sqrt{2\pi}$  and  $\sigma^2$ , the estimation error variance, represents the spatial extent of scattering. Additionally, the remaining AoA measurements due to reflected and scattered NLOS paths are assumed to be virtually in LOS with VANs. Hence, the distribution of these NLOS paths is defined as follows:

$$p_{NLOS}(\hat{\theta}_i/\mathbf{p}\mathbf{V}_i) = \frac{1}{\sqrt{2\pi}\sigma(1-2Q(\frac{\pi}{2\sigma}))} \exp\left(-\frac{(\hat{\theta}_i-\theta(\mathbf{p}\mathbf{V}_i))^2}{2\sigma^2}\right) \quad (2.12)$$

Hence, the AoA estimates are generated for a wideband multipath model based on the following distribution:

$$p_{\text{wideband}}(\hat{\theta}_1, \hat{\theta}_2, \dots, \hat{\theta}_L/\mathbf{p}T) = p_{LOS}(\hat{\theta}_1/\mathbf{p}T) p_{NLOS}(\hat{\theta}_2/\mathbf{p}\mathbf{V}_2) \dots p_{NLOS}(\hat{\theta}_L/\mathbf{p}\mathbf{V}_L) \quad (2.13)$$

where  $L$  is the number of RRCs. Accordingly, the log-likelihood function for the estimates of the AoA for all RRCs is as follows:

$$L(\hat{\theta}_1, \hat{\theta}_2, \dots, \hat{\theta}_L/\mathbf{p}T, V) = -\sum_{i=1}^L \frac{(\hat{\theta}_i - \theta_i(\mathbf{p}\mathbf{V}_i))^2}{\sigma^2} \quad (2.14)$$

where  $\theta_i(\mathbf{V}_i)$  is the true AoA coming from the VAN  $\mathbf{p}\mathbf{V}_i$  to the receiver and  $\mathbf{p}\mathbf{V}_1 = \mathbf{p}T$ .

Then, we construct the Fisher Information Matrix (FIM)  $\mathbf{F}(\{\mathbf{p}T, V\})$  in order to calculate the Cramer-Rao Lower Bound (CRLB), which is  $\mathbf{F}^{-1}(\{\mathbf{p}T, V\})$ . For the Gaussian model in equation (2.13),  $\mathbf{F}(\{\mathbf{p}T, V\})$  is defined as follows:

$$\mathbf{F}(\{\mathbf{p}T, V\}) = \begin{pmatrix} \sum_{i=1}^L \frac{\sin^2(\theta_i)}{\sigma^2 \rho_i^2} & -\sum_{i=1}^L \frac{\cos(\theta_i) \sin(\theta_i)}{\sigma^2 \rho_i^2} \\ -\sum_{i=1}^L \frac{\cos(\theta_i) \sin(\theta_i)}{\sigma^2 \rho_i^2} & \sum_{i=1}^L \frac{\cos^2(\theta_i)}{\sigma^2 \rho_i^2} \end{pmatrix} \quad (2.15)$$

Knowing that the total error of localizing the receiver is the sum of variances along the  $x$  and  $y$ , we define the CRLB for localizing the receiver using the TL technique as follows:

$$\text{CRLB}_{AoA} = \text{Tr}(\mathbf{F}^{-1}(\{\mathbf{pT}, V\})) = \frac{\sum_{i=1}^L \frac{1}{\sigma^2 \rho_i^2}}{\sum_{i=1}^L \sum_{j=i+1}^L \frac{\sin^2(\theta_i - \theta_j)}{\sigma^4 \rho_i^2 \rho_j^2}} \quad (2.16)$$

### 2.3.3 The Angle Differences-of-Arrival (ADoA) Technique

The TL method is based on the azimuth  $\theta$  of all RRCs with respect to reference angle  $\theta_0$ . The knowledge of  $\theta_0$  is assumed to be known; however, this may not be a valid assumption due to the error in the measurement of  $\theta_0$  that may be done using a digital compass of a smartphone. ADoA doesn't require the knowledge of  $\theta_0$  since it will be neglected in the difference between two AoA values. The reader may refer to [198] for more information about ADoA in mmWave. However, we give the main equations for the flow of context inference and obstacle mapping in the next sections. In ADoA, we take all possible triplets of VANs ( $\mathbf{V}_i, \mathbf{V}_j, \mathbf{V}_q$ ),  $i \neq j \neq q$ , and we define the angle of differences as follows:

$$\delta_1 = SP_{p2,j} - SP_{p2,i} \quad (2.17)$$

$$\delta_2 = SP_{p2,q} - SP_{p2,j} \quad (2.18)$$

As shown in Figure 2.3, the trajectory of receiver  $\mathbf{pR}_k$  is a circle where  $\widehat{\mathbf{pV}_i \mathbf{pR}_k \mathbf{pV}_j}$

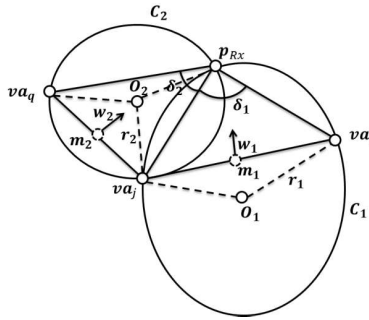


Figure 2.3: The geometry of ADoA localization Technique

is constant and equals to  $\delta_1$ . As well, we assume  $\widehat{\mathbf{pV}_i \mathbf{pR}_k \mathbf{pV}_j} > 0$  if  $\mathbf{pV}_i$  follows  $\mathbf{pV}_j$  in a counterclockwise direction within the semi-circle and  $|\widehat{\mathbf{pV}_i \mathbf{pR}_k \mathbf{pV}_j}| < \pi$ , where  $|\cdot|$  operator generates the absolute value of the measured angle. Consider the circumference  $C_1$  in Figure 2.3; we use the relation between central and vertex angles intercepting the same chord ( $\widehat{\mathbf{pV}_i \mathbf{pV}_j}$ ) in a circle to obtain the following relation:

$$\widehat{\mathbf{pV}_i \mathbf{O}_1 \mathbf{pV}_j} = 2 \cdot \widehat{\mathbf{pV}_i \mathbf{pR}_k \mathbf{pV}_j} = 2 \cdot \delta_1 \quad (2.19)$$

If  $\widehat{\mathbf{pV}_i \mathbf{pR}_k \mathbf{pV}_j} > \pi/2$ , then  $\left| \widehat{\mathbf{pV}_i \mathbf{o}_1 \mathbf{pV}_j} \right| > \pi$ . Thus, we wrap  $\widehat{\mathbf{pV}_i \mathbf{o}_1 \mathbf{pV}_j}$  to the interval  $[-\pi, \pi)$  using the operator  $WP(\cdot)$ . So, the radius  $r_1$  of  $C_1$  is calculated using geometric relation in a circle as follows:

$$r_1 = \frac{\|\mathbf{pV}_i - \mathbf{pV}_j\|}{2 \cdot \sin\left(\left|WP\left(\widehat{\mathbf{pV}_i \mathbf{o}_1 \mathbf{pV}_j}\right)\right|/2\right)} \quad (2.20)$$

As shown in Figure 2.3,  $\vec{w}_1$  is the perpendicular vector to vector  $\widehat{\mathbf{pV}_i \mathbf{pV}_j}$ . Hence, knowing the orientation vector of  $\widehat{\mathbf{pV}_i \mathbf{pV}_j}$  is equal to  $(xV_i - xV_j, yV_i - yV_j)$ , we can define the following perpendicular orientation vector:

$$\vec{w}_1 = (yV_i - yV_j, -(xV_i - xV_j)) \quad (2.21)$$

Hence, the coordinates of center  $\mathbf{o}_1 = (xV_{o_1}, yV_{o_1})$  for  $C_1$  is defined as follows:

$$xV_{o_1} = xV_{m_1} \pm \left( \frac{\vec{w}_1(1)}{\|\vec{w}_1\|} \sqrt{r_1^2 - \left(\frac{\|\mathbf{pV}_i - \mathbf{pV}_j\|}{2}\right)^2} \right) \quad (2.22)$$

$$yV_{o_1} = yV_{m_1} \pm \left( \frac{\vec{w}_1(2)}{\|\vec{w}_1\|} \sqrt{r_1^2 - \left(\frac{\|\mathbf{pV}_i - \mathbf{pV}_j\|}{2}\right)^2} \right) \quad (2.23)$$

where  $m_1 = (xV_{m_1}, yV_{m_1})$  is the midpoint of the chord  $(\widehat{\mathbf{pV}_i \mathbf{pV}_j})$ . Similarly, we can compute the radius  $r_2$  and the center  $\mathbf{o}_2 = (xV_{o_2}, yV_{o_2})$  for the circle  $C_2$ . Then, the intersection between  $C_1$  and  $C_2$  is considered as a proper estimation for the receiver position whenever the intersection point is pointed by the orientation vectors  $\vec{w}_1$  and  $\vec{w}_2$ . As well, we choose the solution that validates the angle of arrival for each RRC. As we did for the TL algorithm, we verify if the position estimation is within the room geometry and doesn't belong to any surface in the obstacle set  $O$ . This algorithm is repeated over all possible triplets of VANs  $(\mathbf{pV}_i, \mathbf{pV}_j, \mathbf{pV}_q), i \neq j \neq q$  that belong to the set  $V_{max}$ . So, we obtain a set of position estimations that represents the intersection between the circumferences  $C_1$  and  $C_2$  determined by the angle differences of arrival  $\delta_1$  and  $\delta_2$  and the chords  $\widehat{\mathbf{pV}_i \mathbf{pV}_j}$  and  $\widehat{\mathbf{pV}_j \mathbf{pV}_k}$ ,  $\mathbf{pV}_i, \mathbf{pV}_j, \mathbf{pV}_q \in V_{max}$ . The final estimation of the receiver position is the average of all possible position estimations obtained from the ADoA technique.

### 2.3.3.1 Simulation Results for TL and ADoA

The room geometry is of rectangular type of size  $8.9 \times 6.3$  m. We take the south-western corner of the room to be the reference of the Cartesian coordinate

system. The angles are measured with respect to the positive part of the x-axis. The transmitter is set at position  $\mathbf{pT} = (0.2, 0.2)$  m. We assume the antenna at the transmitter to be omnidirectional; hence, the transmitted power  $PT(\theta)$  is constant for all  $\theta$ . Instead, antenna array is used at the receiver with a reception beam pattern described as  $P_{Rx}(\theta) = \exp\left(-\frac{\theta^2}{2s^2}\right)$ ,  $s = 0.1$ . The value of parameter  $s$  and the Gaussian shape have been devised empirically. Additionally, all results were implemented for 10000 realizations. The CDF for the localization

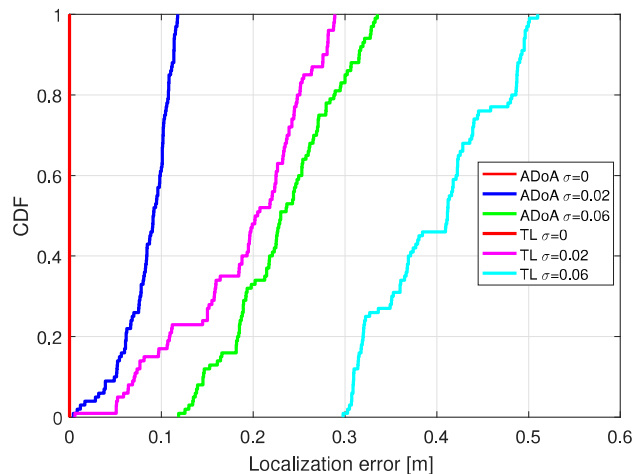


Figure 2.4: Localization error CDF for TL and ADoA for different values of  $\sigma$  ( $rad$ )

error shown in Figure 2.4 shows that for ideal case, where  $\sigma = 0^\circ$ , both the TL and the ADoA techniques localize the receiver with full accuracy. When the value of  $\sigma$  increases, the accuracy of localization achieved using TL and ADOA decreases. For instance, when  $\sigma = 0.02rad = 1.15^\circ$ , the accuracy of localization achieved with TL and ADoA is almost 0.3 m and 0.1 m, respectively. Additional increase in the noise to reach  $\sigma = 0.06rad = 3.44^\circ$ , localization accuracy decreases to reach an error of more than 0.5 m and 0.33 m, respectively, at 90% of the estimates. Moreover, we can observe from Figure 2.4 that TL achieves higher localization accuracy compared to ADoA as we increase  $\sigma$ . Nevertheless, the performance of not only ADoA but also TL is far from the CRLB level. As shown in Figure 2.5, the proposed standalone TL and ADoA localizing techniques dont provide the ultimate estimation accuracy; thus, other localizing techniques, such as RSS and TDoA, can be combined to achieve higher accuracy of localization.



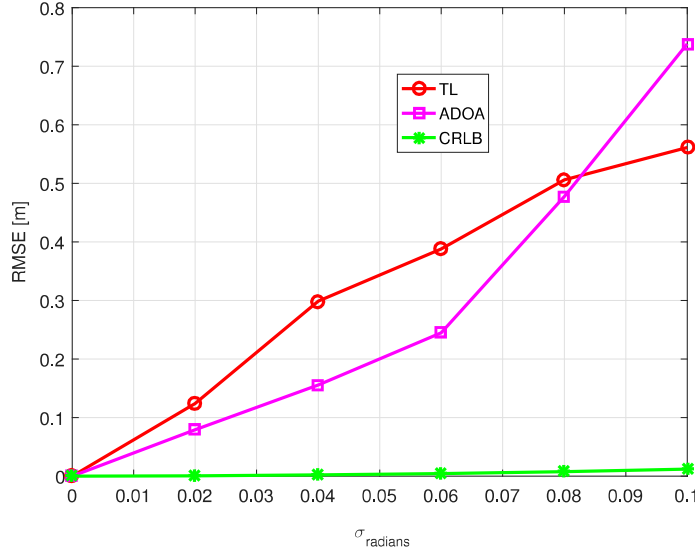


Figure 2.5: Localization error CDF for TL and ADoA for different values of  $\sigma$  (rad)

## 2.3.4 Received Signal Strength (RSS) Approach

### 2.3.4.1 Weighted-Least Square (WLS) Estimator

We modeled the estimation of the receiver position using AoA localization approach via the proposed TL technique and the ADoA algorithm. In this section, we are going to estimate the receiver position using the RSS based localization approach.

The VANs in this approach can be seen as anchor nodes collecting measurements to localize the single AP receiver. The received power at these anchor nodes follows a log-normal shadowing pathloss model in MMW channels [196][197]. The received power,  $P_i$ , is calculated using the following equation:

$$P_i [dBm] = P_0 - 10\eta \log_{10} \frac{d_i}{d_0} + n_i, i = 1, \dots, L \quad (2.24)$$

where  $P_0$  is the power at the reference distance  $d_0$ ,  $\eta$  is the pathloss exponent (PLE),  $d_i$  is the Euclidean distance between the receiver and the  $i$ th VAN,  $L$  is the number of VANs representing the number of RRCs, and  $n_i$  is the zero mean Gaussian random variable measured in dB scale with shadowing fading effect described by the standard deviation  $\sigma_{RSS}$ . The square of the distance  $d_i$  between the VAN  $\mathbf{pV}_i$  and the receiver  $\mathbf{pR}_k$  is represented as follows:

$$d_i^2 = \|\mathbf{pV}_i - \mathbf{pR}_k\|_2^2 = (xV_i - x_{Rx})^2 + (yV_i - y_{Rx})^2 \quad (2.25)$$

Without loss of generality, we assume the transmitter to be the reference. Hence, for  $i > 1$ , we define the following:

$$x_{Rx}d_i^2 - d_1^2 = xV_i^2 - 2x_{Rx} \cdot xV_i + yV_i^2 - 2y_{Rx} \cdot yV_i \quad (2.26)$$

Expressing equation (2.26) in matrix form, we obtain the following equation:

$$\begin{bmatrix} 2xV_2 & 2yV_2 \\ \vdots & \vdots \\ 2xV_L & 2yV_L \end{bmatrix} \cdot \begin{bmatrix} x_{Rx} \\ y_{Rx} \end{bmatrix} = \begin{bmatrix} xV_2^2 - xV_1^2 + yV_2^2 - yV_1^2 + d_1^2 - d_2^2 \\ \vdots \\ xV_L^2 - xV_1^2 + yV_L^2 - yV_1^2 + d_1^2 - d_L^2 \end{bmatrix} \quad (2.27)$$

The real distance  $d_i$  is not known in RSS localization; hence, noisy estimations of the distance,  $\tilde{d}_i$ , obtain from equation (2.24), are related with the unknown position of the receiver  $\mathbf{pR} = [x_{Rx}, y_{Rx}]^T$  as follows:

$$\mathbf{R} \cdot \mathbf{pR} = \mathbf{T} \quad (2.28)$$

where  $\mathbf{R}$  and  $\mathbf{T}$  are defined as follows:

$$\mathbf{R} = \begin{bmatrix} 2(xV_2 - xV_1) & 2(yV_2 - yV_1) \\ \vdots & \vdots \\ 2(xV_L - xV_1) & 2(yV_L - yV_1) \end{bmatrix}$$

$$\mathbf{T} = \begin{bmatrix} xV_2^2 - xV_1^2 + yV_2^2 - yV_1^2 + d_1^2 - d_2^2 \\ \vdots \\ xV_L^2 - xV_1^2 + yV_L^2 - yV_1^2 + d_1^2 - d_L^2 \end{bmatrix}$$

The estimation of  $\mathbf{pR}$  in (2.28) is solved linearly using the weighted least-squares estimator, as shown in the following equation:

$$\hat{\mathbf{pR}} = (\mathbf{R}^T \mathbf{W} \mathbf{R})^{-1} \mathbf{R}^T \mathbf{W} \mathbf{T} \quad (2.29)$$

where the weighting matrix  $\mathbf{W}$  is equal to the inverse of the covariance matrix  $\Sigma_{Rx}$  of the vector  $\mathbf{T}$ .  $\Sigma_{Rx}$  provides a measure of the estimation error variance. Assuming that the measurements of  $\tilde{d}_i$  are independent [201],  $\Sigma_{Rx}$  is calculated from the random vector  $\mathbf{T}$  as shown below:

$$\Sigma_{Rx} = \begin{bmatrix} Var(\tilde{d}_1^2) + Var(\tilde{d}_2^2) & Var(\tilde{d}_1^2) & \dots & Var(\tilde{d}_1^2) \\ Var(\tilde{d}_1^2) & Var(\tilde{d}_1^2) + Var(\tilde{d}_3^2) \dots & \dots & Var(\tilde{d}_1^2) \\ \vdots & \vdots & \ddots & \vdots \\ Var(\tilde{d}_1^2) & Var(\tilde{d}_1^2) & \dots & Var(\tilde{d}_1^2) + Var(\tilde{d}_L^2) \end{bmatrix} \quad (2.30)$$

where  $Var$  represent the variance, and the terms of  $\Sigma_{Rx}$  are computed using the following equation:

$$Var\left(\tilde{d}_i^2\right) = \mathbf{E}\left[\tilde{d}_i^4\right] - \left(\mathbf{E}\left[\tilde{d}_i^2\right]\right)^2 \quad (2.31)$$

In addition, equation (2.24) shows that the measured distance  $\tilde{d}_i$  follows a log-normal random distribution, modeled using the following equation:

$$\tilde{d}_i = d_i \cdot 10^{\frac{N(0, \sigma_{RSS})}{10\eta}} = e^{N\left(\ln d_i, \frac{\sigma_{RSS} \ln 10}{10\eta}\right)} \quad (2.32)$$

where the mean and the standard deviation of the distribution are  $\mu_d = \ln d_i$  and  $\sigma_d = \sigma_{RSS} (\ln 10) / 10\eta$ , respectively. The  $n$ -th moment of a lognormal random variable with mean  $\mu_d$  and standard deviation  $\sigma_d$  is calculated as  $\mu_n = e^{n \cdot \mu_d + (n^2 \sigma_d^2) / 2}$ . Hence, we calculate  $\mathbf{E}\left[\tilde{d}_i^2\right]$  and  $\mathbf{E}\left[\tilde{d}_i^4\right]$  as follows:

$$\mathbf{E}\left[\tilde{d}_i^2\right] = e^{2\mu_d + 2\sigma_d^2} \quad (2.33)$$

$$\mathbf{E}\left[\tilde{d}_i^4\right] = e^{4\mu_d + 8\sigma_d^2} \quad (2.34)$$

Thus, the variance is computed as follows from equation (2.31):

$$Var\left(\tilde{d}_i^2\right) = \mathbf{E}\left[\tilde{d}_i^4\right] - \left(\mathbf{E}\left[\tilde{d}_i^2\right]\right)^2 = e^{4\mu_d} \cdot \left(e^{8\sigma_d^2} - e^{4\sigma_d^2}\right) \quad (2.35)$$

As a result, the RSS localization estimation error is controlled by two factors of MMW communications: the PLE  $\eta$ , and the random shadow fading standard deviation  $\sigma_{RSS}$ . MMW is expected to affect significantly the estimation error because of the high pathloss.

#### 2.3.4.2 Maximum Likelihood (ML) Estimator

We also propose to use the combination between WLS and ML estimators with the RSS approach aiming to localize the receiver with higher accuracy. Given equations (2.24) and (2.32), the density of  $P_i$  is defined as follows:

$$f_p(P_i) = \frac{10 / \log 10}{\sqrt{2\pi\sigma_{RSS}^2}} \frac{1}{P_i} \exp\left[-\frac{\left(\frac{10\eta}{\sigma_{RSS} \log 10}\right)^2}{8} \left(\log \frac{d_i^2}{\tilde{d}_i^2}\right)^2\right] \quad (2.36)$$

Hence using equation (2.36), we calculate the expectation of  $\tilde{d}_i$  as follows:

$$E\left[\tilde{d}_i\right] = \exp\left[\frac{1}{2} \left(\frac{\ln 10 \sigma_{RSS}}{10\eta}\right)^2\right] d_i \quad (2.37)$$

We denote  $\alpha = \exp \left[ \frac{1}{2} \left( \frac{\ln 10 \sigma_{RSS}}{10\eta} \right)^2 \right]$ . After we get the estimation of the receiver position  $\hat{\mathbf{p}}_{Rx:RSS}$  using the WLS estimator for a number of realizations, we select the estimation that satisfies the ML criteria using the following expression:

$$\arg \sum_{\mathbf{p}\hat{\mathbf{R}}_{\min_{i=1}}^L} \left( \ln \frac{\tilde{d}_i^2 / \alpha^2}{\left( \mathbf{p}\hat{\mathbf{R}}(1) - \mathbf{p}\mathbf{V}_i(1) \right)^2 + \left( \mathbf{p}\hat{\mathbf{R}}(2) - \mathbf{p}\mathbf{V}_i(2) \right)^2} \right)^2 \quad \hat{\mathbf{P}}_{ML} = \quad (2.38)$$

### 2.3.4.3 Cramer-Rao Lower Bound (CRLB)

The Cramer-Rao Lower Bound (CRLB) for an unbiased estimator is based on calculating the second partial derivative for the log-likelihood function (LLF) of the probability density function. Consider the RSS approach for localizing the receiver, the LLF of the probability density function of  $P_i$  defined in (2.36) is expressed as follows:

$$\begin{aligned} \log(Pr(\mathbf{P}; \mathbf{d})) &= \log \left( \prod_{i=1}^L \frac{10/\log 10}{\sqrt{2\pi\sigma_{RSS}^2}} \frac{1}{P_i} \exp \left[ -\frac{\left( \frac{10\eta}{\sigma_{RSS} \log 10} \right)^2}{8} \left( \log \frac{d_i^2}{\tilde{d}_i^2} \right)^2 \right] \right) \\ &= L \times \log \left( \frac{10}{\log(10) \sqrt{2\pi\sigma_{RSS}^2}} \right) + \sum_{i=1}^L \left( \log \left( \frac{1}{P_i} \right) - \frac{\left( \frac{10\eta}{\sigma_{RSS} \log 10} \right)^2}{2} \left( \log \left( \frac{d_i}{\tilde{d}_i} \right) \right)^2 \right) \end{aligned} \quad (2.39)$$

Then, the second partial derivative is defined as follows:

$$\frac{\partial^2 (\log(Pr(\mathbf{P}; \mathbf{d})))}{\partial \mathbf{d}^2} = -\frac{\left( \frac{10\eta}{\sigma_{RSS} \log 10} \right)^2}{\ln 10} \sum_{i=1}^L \frac{1}{d_i^2} \left( \frac{1}{\ln 10} - \log \left( \frac{d_i}{\tilde{d}_i} \right) \right) \quad (2.40)$$

Consequently, the CRLB is calculated as follows:

$$CRLB_{RSS} = \frac{\ln 10}{\left( \frac{10\eta}{\sigma_{RSS} \log 10} \right)^2} \frac{1}{\sum_{i=1}^L \frac{1}{d_i^2} \left( \frac{1}{\ln 10} - \log \left( \frac{d_i}{\tilde{d}_i} \right) \right)} \quad (2.41)$$

### 2.3.4.4 Simulation Results

We test the performance of RSS technique for localizing the receiver. Figure 2.6 shows the root mean square error (RMSE) for localizing the receiver using the weighted least square solution of the RSS approach. The figure shows the error for different values of the PLE  $\eta$  versus  $\sigma_{RSS}$ . The error of estimation increases with the increase in  $\sigma_{RSS}$ . However, the estimation error decreases with the

increase in the PLE  $\eta$ . Knowing that the scenario under simulation is based on first and second order of reflection, higher values of  $\eta$  generate less estimation error since it accommodates more precisely for NLOS effect. Additionally, more improvement could be made in order to achieve an accuracy that is closer to the CRLB shown for different values of the PLE  $\eta$  in Figure 2.6. Consequently, we used the ML estimator over set of estimates obtained by the WLS in order to localize the receiver using the RSS approach more accurately. As shown in Figure 2.7, the combination between WLS and ML estimators achieves accurate localization of the receiver with an error less than 5 cm at maximum.

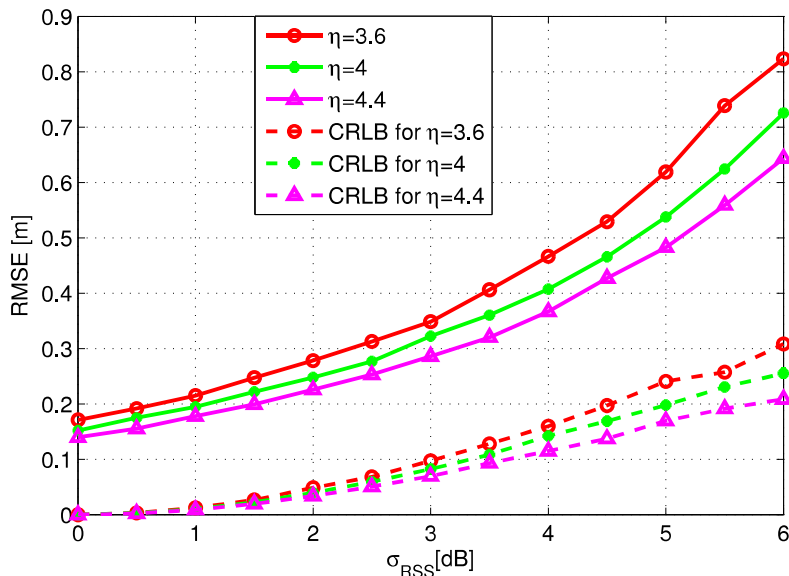


Figure 2.6: RMSE versus  $\sigma_{RSS}$  for estimating receiver using WLS for RSS localization for different values of  $\eta$

## 2.3.5 Time Difference of Arrival (TDoA)

### 2.3.5.1 Weighted Least Square (WLS) Estimator

The receiver position is estimated now using TDoA weighted least square estimator. The distances between the receiver and the  $i$ th VAN in absence of noise is represented as follows:

$$d_{i1} = c \times t_{i,1} = d_i - d_1, i = 1, \dots, L \quad (2.42)$$

where  $t_{i,1}$  is the TDoA of the received signal at the pair of the  $i$ th VAN and the transmitter respectively, and  $c$  is the speed of the signal propagation. As shown in equation (2.42), the estimated TDoAs are converted to range difference

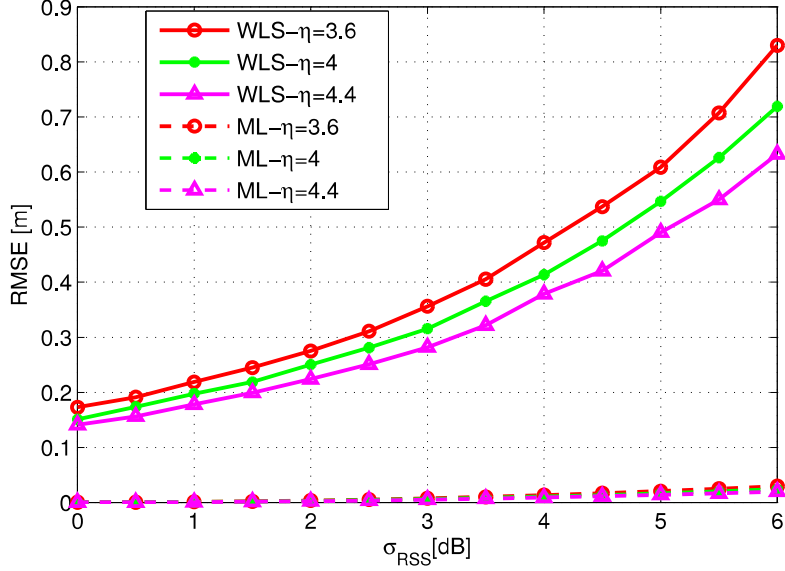


Figure 2.7: RMSE versus  $\sigma_{RSS}$  for estimating receiver using ML and WLS for different values  $\eta$

of arrival (RDoA) measurements creating a set of nonlinear equations describing the hyperbolic range difference. The receiver position can be estimated from the intersection of the resultant hyperboloids. In realistic scenarios, RDoA measurements  $\tilde{d}_{i1}$  are obtained with noise as modeled in the following equation:

$$\tilde{d}_{i1} = d_{i1} + n_{i1} = d_i - d_1 + n_{i1}, i = 1, \dots, L \quad (2.43)$$

where  $n_{i1}$  is the zero mean Gaussian random noise vector of the RDoA measurement with a  $(L - 1) \times (L - 1)$  covariance matrix  $\Sigma_d$  that is expressed as follows:

$$\begin{aligned} \Sigma_d &= E \left\{ \begin{bmatrix} n_{21} \\ \vdots \\ n_L \end{bmatrix} \begin{bmatrix} n_{21} & \dots & n_L \end{bmatrix} \right\} \\ &= c^2 \sigma^{2T} \begin{bmatrix} 1 & 1/2 & \dots & 1/2 \\ 1/2 & \ddots & \ddots & \vdots \\ \vdots & \ddots & \ddots & 1/2 \\ 1/2 & \dots & 1/2 & 1 \end{bmatrix} \end{aligned} \quad (2.44)$$

where  $\sigma^{2T}$  represent the noise of the TDoA measurements. Equation (2.43) can be written as  $\tilde{d}_{i1} + d_1 = d_i + n_{i1}$ . Hence, squaring and substituting with equation

(2.25), we obtain:

$$x_{Rx}(xV_i - xV_1) + y_{Rx}(yV_i - yV_1) + d_1\tilde{d}_{i1} = \frac{1}{2} \left[ (xV_i^2 - xV_1^2) + (yV_i^2 - yV_1^2) - \tilde{d}_{i1}^2 \right] + \frac{1}{2}n_{i1}^2 + d_in_{i1} \quad (2.45)$$

We denote the unknown vector to be  $\mathbf{pR}_{(1)} = [x_{Rx}, y_{Rx}, d_1]^T$ ; hence, the problem now is formulated as follows:

$$\mathbf{R}_1\mathbf{pR}_{(1)} = \mathbf{T}_1 + \epsilon_1 \quad (2.46)$$

where  $\mathbf{R}_1$  and  $\mathbf{T}_1$  are expressed as follows:

$$\mathbf{R}_1 = \begin{bmatrix} (\mathbf{pV}_2 - \mathbf{pV}_1)^T & \tilde{d}_{21} \\ \vdots & \vdots \\ (\mathbf{pV}_L - \mathbf{pV}_1)^T & \tilde{d}_{L1} \end{bmatrix}$$

$$\mathbf{T}_1 = \frac{1}{2} \begin{bmatrix} m_{21} - \tilde{d}_{21}^2 \\ \vdots \\ m_{L1} - \tilde{d}_{L1}^2 \end{bmatrix}$$

and  $m_{21} = \mathbf{pV}_2^T\mathbf{pV}_2 - \mathbf{pV}_1^T\mathbf{pV}_1$ . Knowing that the measurement error  $n_{i1}$  is small, the noise vector  $\epsilon_1$  is approximated as follows:

$$\epsilon_1 \approx [n_{21}d_2, \dots, n_{L1}d_L]^T \quad (2.47)$$

Finally, the solution of equation (2.46) is obtained using weighted-least square estimator as follows:

$$\hat{\mathbf{pR}}_{(1)} = (\mathbf{R}_1^T\mathbf{W}_1\mathbf{R}_1)^{-1}\mathbf{R}_1^T\mathbf{W}_1\mathbf{T}_1 \quad (2.48)$$

where  $\mathbf{W}_1$ , the weighting matrix, is the inverse of the covariance matrix of the noise represented by equation (2.47):

$$\mathbf{W}_1 = (E[\epsilon_1\epsilon_1^T])^{-1} = (\mathbf{F}_1\boldsymbol{\Sigma}_d\mathbf{F}_1^T)^{-1} \quad (2.49)$$

where  $\mathbf{F}_1 = \text{diag}\{d_2, d_3, \dots, d_L\}$ . Additionally,  $\mathbf{pR} = [x_{Rx}, y_{Rx}]$  and  $d_1$  are assumed independent by the weighted least square solution of equation (2.48). Moreover, the estimator in equation (2.48) doesnt provide high accuracy [202]; hence, we enhance the estimation accuracy via the minimization of the weighted least square solution. So, we square the elements of  $\mathbf{pR}_{(1)}$  to get:

$$\mathbf{R}_2\mathbf{pR}_{(2)} = \mathbf{T}_2 + \epsilon_2 \quad (2.50)$$

where  $\mathbf{R}_2$ ,  $\mathbf{pR}_{(2)}$ , and  $\mathbf{T}_2$  are expressed as follows:

$$\mathbf{pR}_{(2)} = \begin{bmatrix} (x_{Rx} - xV_1)^2 \\ (y_{Rx} - yV_1)^2 \end{bmatrix}$$

$$\mathbf{R}_2 = \begin{bmatrix} 1 & 0 \\ 0 & 1 \\ 1 & 1 \end{bmatrix}$$

$$\mathbf{T}_2 = \begin{bmatrix} \left(\hat{\mathbf{pR}}_{(1)}(1) - xV_1\right)^2 \\ \left(\hat{\mathbf{pR}}_{(1)}(2) - yV_1\right)^2 \\ \left(\hat{\mathbf{pR}}_{(1)}(3)\right)^2 \end{bmatrix}$$

and  $\epsilon_2$  represents the error obtained because of the non-zero covariance in  $\hat{\mathbf{pR}}_{(1)}$ . So, we obtain after another weighted least square minimization the following:

$$\hat{\mathbf{pR}}_{(2)} = (\mathbf{R}_2^T \mathbf{W}_2 \mathbf{R}_2)^{-1} \mathbf{R}_2^T \mathbf{W}_2 \mathbf{T}_2 \quad (2.51)$$

where  $\mathbf{W}_2$ , the weighting matrix, is selected based on the estimation error. Finally, the location estimate  $\hat{\mathbf{pR}} = [\hat{x}_{Rx}, \hat{y}_{Rx}]^T$  is defined as follows:

$$\hat{\mathbf{pR}} = P \left[ \sqrt{\hat{\mathbf{pR}}_{(2)}(1)} \quad \sqrt{\hat{\mathbf{pR}}_{(2)}(2)} \right]^T + \mathbf{pV}_1 \quad (2.52)$$

where  $P = \text{diag} \left\{ \text{sgn} \left( \hat{\mathbf{pR}}_{(1)}(1) - xV_1 \right), \text{sgn} \left( \hat{\mathbf{pR}}_{(1)}(2) - yV_1 \right) \right\}$  removes the sign ambiguity due to the square roots in equation (2.52). On the other hand,  $\mathbf{W}_2$  is the inverse of the estimation error that can be expressed as follows:

$$\mathbf{W}_2 = (E [\epsilon_2 \epsilon_2^T])^{-1} = \left( \mathbf{F}_2 \text{cov} \left( \hat{\mathbf{pR}}_{(1)} \right) \mathbf{F}_2^T \right)^{-1} \quad (2.53)$$

where  $\mathbf{F}_2$  and  $\text{cov} \left( \hat{\mathbf{pR}}_{Rx:TDoA(1)} \right)$  are defined as follows:

$$\mathbf{F}_2 = \text{diag} \left\{ \left( \hat{\mathbf{pR}}_{(1)}(1) - xV_1 \right), \left( \hat{\mathbf{pR}}_{(1)}(2) - yV_1 \right), \hat{\mathbf{pR}}_{(1)}(3) \right\} \quad (2.54)$$

$$\text{cov} \left( \hat{\mathbf{pR}}_{(1)} \right) = (\mathbf{R}_1^T \mathbf{W}_1 \mathbf{R}_1)^{-1} \quad (2.55)$$

As a conclusion, the estimation of the receiver position based on TDoA is affected by the channel root mean square (RMS) delay spread,  $\sigma_T$  as shown in equations (2.51) and (2.52). The narrow beams used in MMW reduce the delay spread; hence, the error of estimating the receiver can be reduced in the MMW band.

### 2.3.5.2 Maximum Likelihood (ML) Estimator

We also propose to use the combination between WLS and ML estimators aiming to localize the receiver with higher accuracy. Given equation (2.43), the density of  $\tilde{d}_{i1}$  is defined as follows:

$$f(\tilde{d}_{i1}) = \frac{1}{\sqrt{2\pi c^2 \sigma^{2T}}} \exp \left[ -\frac{\left( \tilde{d}_{i1} - d_{i1} \right)^2}{2c^2 \sigma^{2T}} \right] \quad (2.56)$$



After we get the estimation of the receiver position  $\hat{\mathbf{pR}}$  using the WLS estimator for a number of realizations, we select the estimation that satisfies the ML criteria using the following expression:

$$\hat{\mathbf{p}}_{ML} = \arg \min_{\mathbf{pR}} \sum_{i=1}^L \left( \tilde{d}_{i1} - \sqrt{\left( \hat{\mathbf{pR}}(1) - \mathbf{pV}_i(1) \right)^2 + \left( \hat{\mathbf{pR}}(2) - \mathbf{pV}_i(2) \right)^2} \right) \quad (2.57)$$

### 2.3.5.3 Cramer-Rao Lower Bound (CRLB)

Similar to the calculation of the CRLB for the RSS approach, we calculate the CRLB for estimating the receiver position using TDoA approach. Due to the whiteness of the noise and the property of exponential functions, we calculate the probability density function of  $\tilde{d}_{i1}$  defined in equation (2.44) as follows:

$$\begin{aligned} Pr(\tilde{\mathbf{d}}; \mathbf{d}) &= \prod_{i=1}^L \frac{1}{\sqrt{2\pi c^2 \sigma^{2T}}} \exp \left[ -\frac{(\tilde{d}_{i1} - d_{i1})^2}{2c^2 \sigma^{2T}} \right] \\ &= \frac{1}{(2\pi c^2 \sigma^{2T})^{\frac{L}{2}}} \exp \left[ -\frac{\sum_{i=1}^L (\tilde{d}_{i1} - d_{i1})^2}{2c^2 \sigma^{2T}} \right] \end{aligned} \quad (2.58)$$

Applying the same methodology used for RSS, we calculate the second partial derivative of the LLF for the probability density function defined in equation (2.58) as follows:

$$\frac{\partial^2 \left( \log \left( Pr(\tilde{\mathbf{d}}; \mathbf{d}) \right) \right)}{\partial \mathbf{d}^2} = -\frac{L}{c^2 \sigma^{2T}} \quad (2.59)$$

Consequently, the CRLB for estimating the receiver position using TDoA is as follows:

$$CRLB_{TDoA} = \frac{c^2 \sigma^{2T}}{L} \quad (2.60)$$

### 2.3.5.4 Simulation Results

Using the same scenario used for testing TL, ADoA, and RSS, we tested the performance of TDoA in localizing the receiver. For instance, Figure 2.8 shows the CDF of estimating the receiver using the weighted least square solution of the TDoA approach. We observe that the error of estimation increases with the increase in  $\sigma_{TDoA}$ . For the sake of achieving higher accuracy, we used the ML estimator with the TDoA localization approach. As shown in Figure 2.9, ML estimator achieves estimation accuracy less than 10 cm that is closer to the CRLB compared to the performance of the WLS estimator.

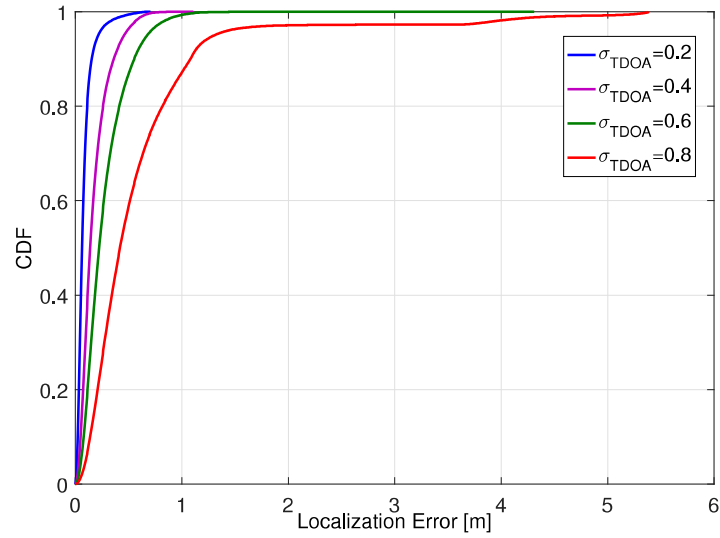


Figure 2.8: Localization error CDF for TDoA using WLS for different values of  $\sigma_{TDOA}$  (ns)

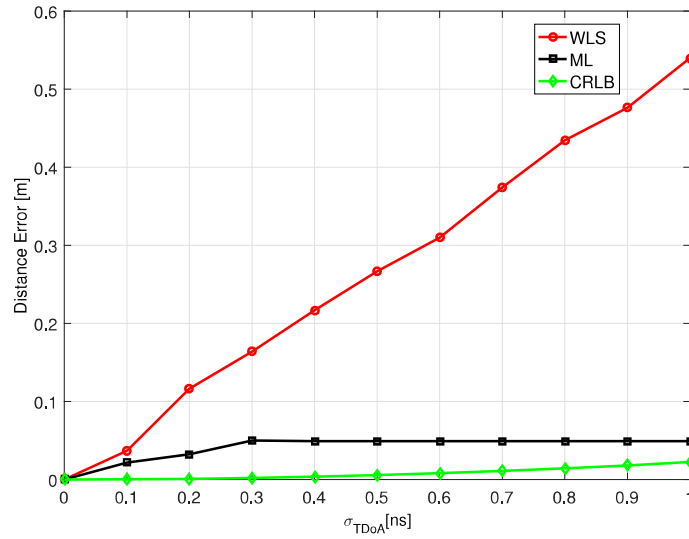


Figure 2.9: RMSE for receiver localization based on TDoA using WLS and ML versus  $\sigma_{TDOA}$  (ns)

### 2.3.6 Hybrid Localization

Recently, hybrid and cooperative mobile positioning has emerged as a new stream of wireless location. The core idea of cooperative positioning relies on the utilization of trustworthy short-range measurements to enhance the accuracy of the location estimation of a wireless system. Different combinations of the basic standalone positioning techniques (RSS, ToA, TDoA, AoA, etc) have been implemented to enhance the accuracy of location estimation. Thus, the combinations between TL and ADoA, TL and RSS, TL and TDoA and TL, TDoA, ADoA and RSS are implemented to show further enhancement compared to the standalone positioning techniques in terms of localization accuracy.

#### 2.3.6.1 Simulation Results

Using the same scenario used for testing TL, ADoA, and RSS, we tested the performance of different combinations of the standalone basic positioning techniques in localizing the receiver. For instance, Figure 2.10 shows the RMSE of estimating the receiver using the TL, ADoA, RSS in combination with TL, and ADoA in combination with TL, TL in combination with TDoA, TL in combination with TDoA and RSS and TL in combination with ADoA, RSS and TDoA. We observe that the error of estimation decreases when the combination approach is applied compared to the error obtained with the standalone positioning techniques, TL and ADoA.

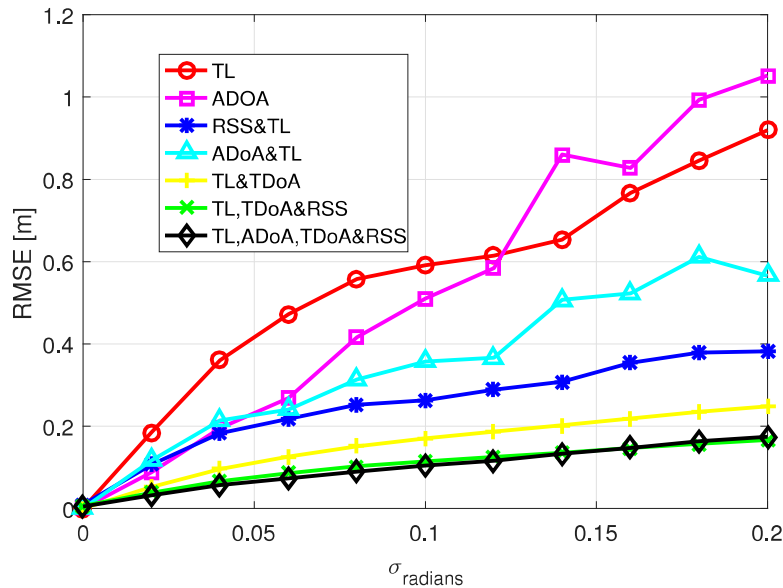


Figure 2.10: RMSE for receiver localization using TL, ADoA, TDoA and RSS

## 2.4 Conclusion

We presented in this chapter the concept of VANs used for localizing a single receiver in an indoor scenario of single access point with MMW propagation characteristics. We introduced TL, ADoA, RSS and TDoA for receiver localization using the LS, WLS and ML estimators. The performance of the techniques with different estimators is tested through simulations in terms of RMSE and CDF of the location estimation error. Localization accuracy for each of the four techniques has been compared with the CRLB. Moreover, the concept of hybridization in localization improved the localization accuracy of the receiver when compared to accuracy attained from standalone positioning techniques. After tackling localization in known environment with single transmitter, we will tackle in the next chapter localization and mapping in environment without a-priori knowledge.

# Chapter 3

## Simultaneous Localization and Environment Mapping without a-priori Knowledge

### 3.1 Introduction

Originally, the concept of Simultaneous Localization and Mapping (SLAM) was achieved (in robotics) by moving a robot in an unknown environment to be recognized [204]. The process is based on steering a laser beam across a dense number of test directions. Then, the round-trip time (RTT) of the signal reflected by the obstacles is estimated in each direction. Hence, the distance to obstacles, inferred from the RTT, was used to build the indoor map. Accurate ranging and high angle resolution are the two main inputs for an accurate SLAM. Such aspects were usually achieved through laser technology. Despite the interest of the technology and the approach adopted therein, the system has to be as the technology has to be equipped with laser and mechanical steering devices; hence, it is complex and high-cost integration in mobile devices [205][206].

At mmWave frequencies, very few works have dealt with SLAM approaches. We particularly mention the works of [204] and [207] where the authors proposed a radar-based system operating at mmWaves to overcome the shortcomings of laser. They provided high ranging accuracy using wideband signals and high directional antenna with mechanical steering. Technically, the reflected signal from the obstacle is scanned in front of the radar transceiver to estimate the distance from the obstacle. Thanks to the large system bandwidth and high temporal resolution of the paths, the proposed approaches therein have shown high accuracy. However, the system has to be in radar-like configuration, i.e. perpendicular to the obstacle, in order to have highly accurate mapping. We should mention that this radar-like system was possible in mmWaves as the latter promotes the implementation of massive antenna arrays at the ANs [208]-[211]. This is indeed

possible due to the reduced size of antenna arrays. For instance, the works in [212]-[215] proposed new designs of personal radar with SLAM features using massive antenna arrays placed in a smart-phone or tablet. Likewise, the authors of [216] adopted mmWave technology with multi-antenna radar system to scan the environment even if the smart-phone is kept in the user pocket. The concept of SLAM is expected to be widely spread in the future, especially in the domain of IoT [217].

In this chapter, our approach for SLAM in mmWave technologies is totally different. The proposed work does not impose any constraint on the receiver orientation and configuration; rather, it exploits the rays characteristics and the separation capabilities of these rays at the receiver to propose an innovative framework (called MOSAIC) for localization and mapping purposes. More precisely, the chapter exploits one or more of the localization metrics, i.e. AoA, TDoA, and RSS, to achieve the obstacle detection, mapping and dimensioning. The latter are assumed to have different shapes and randomly distributed in the indoor environment. Throughout the chapter, the system model is firstly derived for one AN and one receiver and then extended to multiple ANs. The number of ANs has been optimized through Cramer-Rao Lower Bounds (CRLB) derivations. The CRLBs outcomes are then used in the simulations to assess the proposed localization and mapping approaches.

Technically speaking, we will briefly introduce a first approach available in literature on the localization of a receiver (Rx) in a known environment using the concept of virtual anchor nodes (VANs). Then, as shown in Fig. 3.1, the concept of Rx localization is extended to unknown environment. In this case, MOSAIC proposes to exploit the information obtained by at least two channel metrics (TDoA, AoA, RSS) to estimate the Rx position. To implement a joint localization and mapping, MOSAIC is based on the estimation of the VANs positions, followed by the estimation of the obstacles sides directions and positions. Moreover, MOSAIC proposes two approaches for the obstacles dimensions (i.e. sides). This chapter extends our previous work in [218] in which the room geometry has been identified using the AoA metric only. The contributions of this chapter could be summarized as follows:

- Exploitation of the map-based mmWave channel characteristics to provide localization and mapping in indoor scenarios.
- Extension of our previous work in [218] based on AoA metrics to other metrics (RSS and TDoA): this extension is needed since in real scenarios these channel metrics are available and could be exploited to improve the localization and mapping accuracy
- Exploitation of the VANs principle widely used in literature to realize the obstacle positioning, dimensioning and mapping. In this chapter, MOSAIC proposes two different approaches for mapping. The first one is based on

estimating the cloud of reflection points (CoRP) belonging to the obstacle borders. The CoRP will be used to estimate the obstacles limits, positions and dimensions. The second is based on determining the obstacles vertices.

- Derivation and exploitation of the CRLB to optimize the number of ANs needed to achieve a target accuracy.
- Validation of proposed approaches through extensive simulation results. A professional mmWave ray tracing tool has been also used for the simulation results.

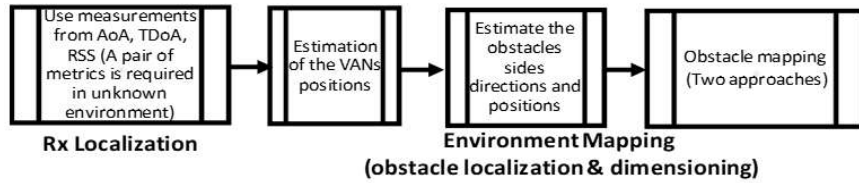


Figure 3.1: Steps needed in MOSAIC

For the sake of clarification, the following notations will be adopted in the chapter. A point in the environment starts with letter  $\mathbf{p}$ . For instance,  $\mathbf{pT}$ ,  $\mathbf{pR}$  and  $\mathbf{pV}$  stand for the transmitter, receiver and VAN positions. The index  $k$  stands for time while  $i$  stands for the  $i^{\text{th}}$  received ray component (RRC) respectively. Also, the subscript notation  $(i, j)$  is used to indicate the difference in measurement between the element  $i$  and element  $j$  while the subscript  $m$  refers to an AN. Throughout the chapter, the time index  $k$  is mentioned only when necessary for the sake of simplification of the model.

The rest of this chapter is organized as follows. In Section 2, we develop the system model and the localization methodology of the receiver using mmWave. In Section 3, we introduce localization approaches in mmWave with an extension to unknown environment. In section 4, new approaches for context inference by estimating obstacles positions and dimensions are presented. In Section 5, the effect of the number of ANs is discussed using the CRLB. Then, the simulation results for an indoor environment are provided in section 6, while conclusions are drawn in Section 7.

## 3.2 MOSAIC: System Model and Environment

### 3.2.1 System Environment

We consider in this chapter a 2D indoor environment consisting of a room bounded by 4 walls for the sake of simplicity. The extension to 3D environment is left for

further work. The room geometry is assumed to be known with single transmitter and single receiver. This assumption does not change any step in the proposed approaches neither in the conclusions but makes the model simpler to argue. The room boundaries and radio-reflective obstacles in the reflective objects are grouped in a set  $\mathcal{O}$ . Obstacles are described as two-dimensional flat polygonal faces with sharp vertices and straight edges. Each oriented obstacle  $S$  is denoted by its perpendicular line, described by:

$$y = yp + \alpha \cdot (x - xp) \quad (3.1)$$

where  $\mathbf{p} = (xp, yp)$  is a point of intersection between the obstacle and its perpendicular and  $\alpha$  is the slope of the line orthogonal to the obstacle  $S$ . By assumption, a single mmWave transmitter (Tx) is deployed in the room at a location  $\mathbf{pT}$ . Additionally, the transmitter is assumed to broadcast its position to the node(s) targeted for localization.

Throughout the chapter, AoA will be the main metric for localization and mapping. It is very robust against power loss and absorption at mmWave [219]. The AoA spectrum has been widely used in literature [187][188]. It gives the power received at each angle of arrival hence it is usually modeled as a  $2 \times L$  matrix,  $\mathbf{SP}(\theta)$ , that records the amplitude of each RRC as a function of the azimuth  $\theta$  at a given location  $\mathbf{p}$ , where  $L$  is the number of RRCs. Each RRC can be either due to a LoS link between the transmitter and the receiver or due to NLoS link caused by reflections of one or more surfaces in the obstacle set  $\mathcal{O}$ . Localization in this case is achieved by observing NLoS paths as virtual LoS rays coming through virtual LoS links from VANs, whereby the concept of VAN is elaborated in 2.3.1. A sorting in decreasing order of  $\mathbf{SP}(\theta)$  according to the first row, i.e. to ray power, allows to characterize the received signal in which the first column has the highest power. In practice, if the receiver and transmitter are in LoS, this column represents  $\theta_0$ , the AoA of the LoS ray, and its corresponding power. The columns  $2 : L$  represent the NLoS paths.

### 3.3 Localization using mmWaves

In this section, we consider a harsh environment with one Tx and one Rx only. We tackle the problem of localization in mmWave while mainly based on AoA measurements due its robustness against power loss in mmWave [219]. Other measurement metrics such as TDoA and RSS are needed if the environment map is unknown.



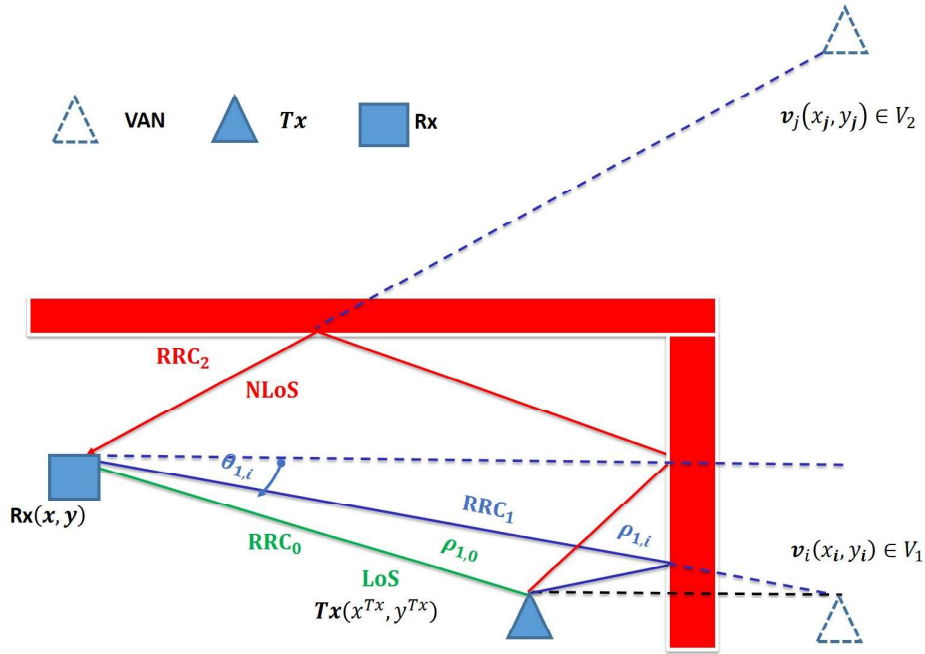


Figure 3.2: VANs related to first ( $RRC_1$ ) and second order ( $RRC_2$ ) of reflections

### 3.3.1 The Triangulation (TL) Algorithm in Known Environment: an AoA based Approach

This algorithm is based on estimating the location of a receiver at position  $\mathbf{pR}$  using a set of triangulation steps followed by a verification of the estimated positions [198][218]. In this section and for the sake of clarification, we assume that the location orientation and dimensions of the obstacle are known at the receiver.

The TL provides good accuracy with low complexity versus the conventional maximum likelihood (ML) algorithm<sup>1</sup>. TL steps are based on forming a triangle between the unknown receiver and each VAN. As shown in Figure 3.2, the following relations are constructed using trigonometric relations in the right triangle formed between the receiver  $\mathbf{pR}_k$  at time  $k$  and VAN  $\mathbf{pV}_i$  as follows:

$$xV_i - xR_k = \rho_{k,i} \cdot \cos \theta_{k,i} \quad (3.2)$$

$$yV_i - yR_k = \rho_{k,i} \cdot \sin \theta_{k,i} \quad (3.3)$$

where  $\mathbf{pV}_i = (xV_i, yV_i)$  and  $\mathbf{pR}_k = (xR_k, yR_k)$  are the VANs and the unknown receiver respectively.  $\theta_{k,i}$  and  $\rho_{k,i}$  are the AoA and the distance of the RRC "transmitted virtually" from the VAN  $\mathbf{pV}_i$  to the receiver at position  $\mathbf{pR}_k$ , respectively. In this section, we aim at estimating the position of the receiver, i.e.

<sup>1</sup>For a fair comparison, ML results will be provided in the simulations results section.

$xR_k$  and  $yR_k$  in equation (3.2) and equation (3.3). Hence, using  $\theta_{k,i}$  and  $\mathbf{pV}_i$  (assumed known in this section), the problem turns out to find  $\rho_{k,i}$ . The latter could be easily estimated by simply differentiating between the signal originated from different VANs. Hence, for each pair of VANs  $\mathbf{pV}_i$  and  $\mathbf{pV}_j$ , the following equation holds:

$$\mathbf{V} = \mathbf{\Gamma} \cdot \mathbf{\Xi} \quad (3.4)$$

where  $\mathbf{V}$ ,  $\mathbf{\Gamma}$ , and  $\mathbf{\Xi}$  are defined as follows:

$$\mathbf{V} = \begin{bmatrix} xV_i - xV_j \\ yV_i - yV_j \end{bmatrix}$$

$$\mathbf{\Gamma} = \begin{bmatrix} \cos \theta_{k,i} & -\cos \theta_{k,j} \\ \sin \theta_{k,i} & -\sin \theta_{k,j} \end{bmatrix}$$

$$\mathbf{\Xi} = \begin{bmatrix} \rho_{k,i} \\ \rho_{k,j} \end{bmatrix}$$

Solving equation (3.4), we obtain:

$$\mathbf{\Xi} = \mathbf{\Gamma}^{-1} \cdot \mathbf{V}_{i,j} \quad (3.5)$$

Knowing  $\mathbf{\Xi}$ , the estimation of the position  $\mathbf{pR}_k$  of the receiver can be done by inserting  $\rho_{k,i}$  in equation (3.2) and equation (3.3). The TL steps are repeated  $I$  times, that is the total number of all possible pairs of  $(\mathbf{pV}_i, \mathbf{pV}_j)$ ,  $i \neq j$  in the set  $V_1$ .

### 3.3.2 Rx Localization in unknown environment

When the environment is unknown (i.e. there is no information on the obstacles in the room), the first step of the TL approach could not be applied as the VANs positions are unknown. To solve this problem, additional localization metrics such as TDoA and RSS<sup>2</sup> are considered. Indeed, if for instance both AoA and TDoA measurements are available, the rays of both metrics are sorted in a decreasing order in terms of power. The first ray will be denoted as the LoS and the rest are the NLoS rays. The receiver position will be then deduced as the intersection point which verifies both the AoA and TDoA based distance equations. The algorithm for Rx localization is defined as follows.

- Find the distance between  $\mathbf{pT}$  and  $\mathbf{pR}_k$  using TDoA measurements of the first path. Theoretically, the distance of travel for the first ray is calculated from the TDoA as follows:

$$\rho_{k,0} = c \cdot t_{k,0} \quad (3.6)$$

where  $c$  is the speed of light,  $\rho_{k,0}$  is the distance traveled by the first ray (LoS ray) and  $t_{k,0}$  is the TDoA of the first ray, assumed to be in LoS.

---

<sup>2</sup>These measurements are primordial for channel estimation at mmWaves

- Find  $\theta'_{k,0}$ , the triangulated angle of  $\theta_{k,0}$  i.e. the AoA of the first ray (LoS ray), as follows:

$$\begin{cases} \theta'_{k,0} = \pi/2 - \theta_{k,0}, 0 \leq \theta_{k,0} \leq \pi/2 \\ \theta'_{k,0} = \theta_{k,0} - \pi/2, \pi/2 \leq \theta_{k,0} \leq \pi \\ \theta'_{k,0} = 3\pi/2 - \theta_{k,0}, \pi \leq \theta_{k,0} \leq 3\pi/2 \\ \theta'_{k,0} = \theta_{k,0} - 3\pi/2, 3\pi/2 \leq \theta_{k,0} \leq 2\pi \end{cases} \quad (3.7)$$

- Using equation (3.6) and equation (3.7), estimate the position of the receiver as follows:

$$\mathbf{pR}_k = \mathbf{pT} + \rho_{k,0} \cdot \boldsymbol{\Omega} \cdot \begin{bmatrix} \sin \theta'_{k,0} \\ \cos \theta'_{k,0} \end{bmatrix} \quad (3.8)$$

where  $\mathbf{pR}_k = [xR_k \ yR_k]^T$ ,  $\mathbf{pT} = [xT \ yT]^T$  and  $\boldsymbol{\Omega}$  is defined as follows:

$$\begin{cases} \boldsymbol{\Omega} = [-1 \ -1]^T, 0 \leq \theta_{k,0} \leq \pi/2 \\ \boldsymbol{\Omega} = [1 \ -1]^T, \pi/2 \leq \theta_{k,0} \leq \pi \\ \boldsymbol{\Omega} = [1 \ 1]^T, \pi \leq \theta_{k,0} \leq 3\pi/2 \\ \boldsymbol{\Omega} = [-1 \ 1]^T, 3\pi/2 \leq \theta_{k,0} \leq 2\pi \end{cases} \quad (3.9)$$

It is very clear from these derivations that localization in mmWave can be easily done with or without environment knowledge as long as there is sufficient measurements. Moreover, it is straightforward to mention that the availability of the LoS components highly improves the accuracy of the localization approaches. In case the LoS ray is not available, the estimation of the Rx position will be biased. However, as shown in [220], the estimation error could be very small if appropriate algorithms are implemented. In this chapter, we are not proposing any approach for separation between LoS and NLoS yet the approach in [220] is easily adopted.

### 3.4 Context Inference and Obstacle Mapping in MOSAIC

The main target of this section is to estimate obstacles locations and their dimensions using the received signal at Rx. MOSAIC implements obstacle detection in two steps: (1) estimating the position of the VANs using TL (i.e. using AoA), RSS and TDoA; (2) estimating the obstacle direction, points of reflection and obstacle dimensions<sup>3</sup>.

---

<sup>3</sup>All the calculations hereafter are presented in ideal conditions, i.e. without measurements errors, for the sake of simplification. However, in simulations, a bias due to measurements errors is added to different models

### 3.4.1 Estimation of VANs positions

Here, three different algorithms are proposed depending on the available measurement metrics. The first algorithm is based on the TL discussed earlier, the second one is based on the TDoA while the third is based on RSS.

#### 3.4.1.1 Algorithm 1- TL for Estimating VANs

As stated above, the first step for mapping consists in estimating the positions of the VANs. However, these depend on the obstacles whose positions and dimensions are assumed unknown. Mathematically speaking, this requires estimating the different parameters  $(xV_i, yV_i, \rho_{k,i})$  which represent the coordinates of the VANs and their distances with respect to the receiver.

The scenario is developed under harsh conditions, i.e. one transmitter and one receiver are only available for both localization and context inference. Hence, to deal with these conditions, we propose to move the receiver step-by-step while collecting new estimation. Technically, the estimation of  $(xV_i, yV_i, \rho_{k,i})$  depends on the relative position of the receiver with respect to the VANs, as shown in Fig. 3.3. For instance, assuming that the AoA for the LoS path between the transmitter and receiver and the AoA for the NLoS path (LoS virtually) between the transmitter and receiver (VAN and receiver) fall in the first quadrant, the system of equations describing the relation between the different parameters in  $(xV_i, yV_i, \rho_{k,i})$  defined in equation (3.2) and equation (3.3) is as follows:

$$\begin{cases} xV_i - xR_k = \rho_{k,i} \cdot \cos \theta_{k,i} \\ xR_k - xT = \rho_{k,0} \cdot \sin \theta_{k,0} \end{cases} \quad (3.10)$$

$$\begin{cases} yV_i - yR_k = \rho_{k,i} \cdot \sin \theta_{k,i} \\ yR_k - yT = \rho_{k,0} \cdot \cos \theta_{k,0} \end{cases} \quad (3.11)$$

where  $\rho_{k,0}$  is the distance between the receiver position at time  $k$  and the transmitter,  $\theta_{k,0}$  is the AoA for the LoS link between the transmitter and the receiver,  $\rho_{k,i}$  is the distance between the VAN to be localized and the original receiver position and  $\theta_{k,i}$  is the AoA for the NLoS link corresponding to  $\mathbf{pV}_i$ . By solving the above two systems of equations, we obtain:

$$\begin{cases} xV_i - xT = \rho_{k,0} \cdot \sin \theta_{k,0} + \rho_{k,i} \cdot \cos \theta_{k,i} \\ yV_i - yT = \rho_{k,0} \cdot \cos \theta_{k,0} + \rho_{k,i} \cdot \sin \theta_{k,i} \end{cases} \quad (3.12)$$

The receiver now is moved to a new position  $\mathbf{pR}_{k+1}$  as shown in Fig. 3.3 so that we can solve the new system of equations where the unknown variables become the positions of the VANs. The latter defines the relation between the parameters in  $(xV_i, yV_i, \rho_{k,i})$  corresponding to the new receiver position is:

$$\begin{cases} xV_i - xT = \rho_{k+1,0} \cdot \sin \theta_{k+1,0} + \rho_{k+1,i} \cdot \cos \theta_{k+1,i} \\ yV_i - yT = \rho_{k+1,0} \cdot \cos \theta_{k+1,0} + \rho_{k+1,i} \cdot \sin \theta_{k+1,i} \end{cases} \quad (3.13)$$

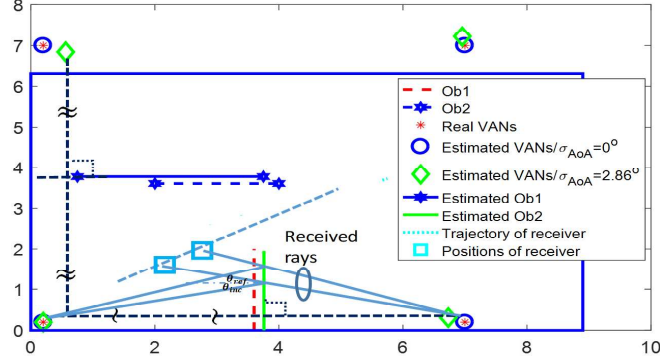


Figure 3.3: Estimated VANs by moving the receiver from  $\mathbf{pR}_k$  to  $\mathbf{pR}_{k+1}$

where  $\rho_{k+1,i}$  and  $\theta_{k+1,i}$  are the distance and the AoA, respectively, corresponding to the link between the VAN  $\mathbf{pV}_i$  and the new receiver position  $\mathbf{pR}_{k+1}$ . Then, the estimation of the VANs is done by combining the two systems of equations in equation (3.12) and equation (3.13). This leads to the following:

$$\begin{bmatrix} \cos \theta_{k,i} & -\cos \theta_{k+1,i} \\ \sin \theta_{k,i} & -\sin \theta_{k+1,i} \end{bmatrix} \begin{bmatrix} \rho_{k,i} \\ \rho_{k+1,i} \end{bmatrix} = \begin{bmatrix} -\sin \theta_{k,0} & \sin \theta_{k+1,0} \\ -\cos \theta_{k,0} & \cos \theta_{k+1,0} \end{bmatrix} \begin{bmatrix} \rho_{k,0} \\ \rho_{k+1,0} \end{bmatrix} \quad (3.14)$$

The two unknowns,  $\rho_{k,i}$  and  $\rho_{k+1,i}$ , are calculated as follows:

$$\begin{bmatrix} \rho_{k,i} \\ \rho_{k+1,i} \end{bmatrix} = \Sigma^{-1} \begin{bmatrix} -\sin \theta_{k,0} & \sin \theta_{k+1,0} \\ -\cos \theta_{k,0} & \cos \theta_{k+1,0} \end{bmatrix} \begin{bmatrix} \rho_{k,0} \\ \rho_{k+1,0} \end{bmatrix} \quad (3.15)$$

where  $\Sigma = \begin{bmatrix} \cos \theta_{k,i} & -\cos \theta_{k+1,i} \\ \sin \theta_{k,i} & -\sin \theta_{k+1,i} \end{bmatrix}$ .

$\rho_{k,i}$  and  $\rho_{k+1,i}$  are then replaced in equation (3.12) or equation (3.13) to estimate  $xV_i$  and  $yV_i$ . Knowing that RRCs come from the transmitter via a LoS link and from VANs via NLoS links, this process is iterated over all entries of the AoA power spectrum  $SP_{\mathbf{p}}(\theta)$ , a  $(2 \times L)$  matrix, to estimate the positions of all VANs. The calculations are repeated at every receiver position.

### 3.4.1.2 Algorithm 2- TDoA for Estimating VANs

TDoA can be also used for the estimation of the VANs. The distances between the receiver and the VAN  $\mathbf{pV}_i$  in absence of noise is represented as follows:

$$\rho_{(0,i)} = c \cdot t_{(0,i)} = \rho_i - \rho_0, i = 1, \dots, L - 1 \quad (3.16)$$

where  $t_{(0,i)}$  is the TDoA of the received signal at the pair of the VAN  $\mathbf{pV}_i$  and the transmitter respectively, and  $c$  is the speed of the signal propagation. As

shown in equation (3.16), the estimated TDoAs are converted to range difference of arrival (RDoA) measurements creating a set of nonlinear equations describing the hyperbolic range difference. The receiver position can be estimated from the intersection of the resultant hyperboloids. In realistic scenarios, RDoA measurements  $\tilde{\rho}_{(0,i)}$  are obtained with noise as modeled in the following equation:

$$\tilde{\rho}_{(0,i)} = \rho_{(0,i)} + \epsilon_{(0,i)} = \rho_i - \rho_0 + \epsilon_{(0,i)}, i = 1, \dots, L-1 \quad (3.17)$$

where  $\epsilon_{(0,i)}$  is the zero mean Gaussian random noise vector of the RDoA measurement. equation (3.17) can be written as  $\tilde{\rho}_{(0,i)} + \rho_0 = \rho_i + \epsilon_{(0,i)}$ . Hence, squaring and substituting with equation (3.28), we obtain:

$$\begin{aligned} xR(xV_i - xT) + yR(yV_i - yT) + \rho_0\tilde{\rho}_{(0,i)} = \\ \frac{1}{2} [(xV_i^2 - xT^2) + (yV_i^2 - yT^2) - \tilde{\rho}_{(0,i)}^2] + \frac{1}{2} \epsilon_{(0,i)}^2 + \rho_i\epsilon_{(0,i)} \end{aligned} \quad (3.18)$$

Hence, the model is given by:

$$\mathbf{G} \cdot \mathbf{pR} = \mathbf{H} \quad (3.19)$$

where  $\mathbf{G}$ , and  $\mathbf{H}$  are defined as follows:

$$\mathbf{G} = \begin{bmatrix} x_1 - xT & y_1 - yT \\ \vdots & \vdots \\ x_{L-1} - xT & y_{L-1} - yT \end{bmatrix}$$

$$\mathbf{H} = \begin{bmatrix} \frac{1}{2} (q_{(0,1)} - \tilde{\rho}_{(0,1)}^2) - \rho_0\tilde{\rho}_{(0,1)} \\ \vdots \\ \frac{1}{2} (q_{(0,L-1)} - \tilde{\rho}_{(0,L-1)}^2) - \rho_0\tilde{\rho}_{(0,L-1)} \end{bmatrix}$$

where  $q_{(0,i)} = \mathbf{pV}_i^T \mathbf{pV}_i - \mathbf{pT}^T \mathbf{pT}$ . Three TDoA measurements are observed at three different positions of the receiver  $\mathbf{pR}_k$ ,  $\mathbf{pR}_{k+1}$  and  $\mathbf{pR}_{k+2}$  respectively. The following system of equations is constructed based on the difference between the measurements taken at  $\mathbf{pR}_k$  and  $\mathbf{pR}_{k+1}$  and those taken at  $\mathbf{pR}_k$  and  $\mathbf{pR}_{k+2}$ , respectively:

$$\begin{aligned} \mathbf{G} (\mathbf{pR}_k - \mathbf{pR}_{k+1}) &= \mathbf{H}_k - \mathbf{H}_{k+1} \\ = \begin{bmatrix} \frac{1}{2} (\tilde{\rho}_{k+1,(0,1)}^2 - \tilde{\rho}_{k,(0,1)}^2) + \rho_{k+1,0}\tilde{\rho}_{k+1,(0,1)} - \rho_{k,0}\tilde{\rho}_{k,(0,1)} \\ \vdots \\ \frac{1}{2} (\tilde{\rho}_{k+1,(0,L-1)}^2 - \tilde{\rho}_{k,(0,L-1)}^2) + \rho_{k+1,0}\tilde{\rho}_{k+1,(0,L-1)} - \rho_{k,0}\tilde{\rho}_{k,(0,L-1)} \end{bmatrix} \end{aligned} \quad (3.20)$$

$$\begin{aligned} \mathbf{G} (\mathbf{pR}_k - \mathbf{pR}_{k+2}) &= \mathbf{H}_k - \mathbf{H}_{k+2} \\ = \begin{bmatrix} \frac{1}{2} (\tilde{\rho}_{k+2,(0,1)}^2 - \tilde{\rho}_{k,(0,1)}^2) + \rho_{k+2,0}\tilde{\rho}_{k+2,(0,1)} - \rho_{k,0}\tilde{\rho}_{k,(0,1)} \\ \vdots \\ \frac{1}{2} (\tilde{\rho}_{k+2,(0,L-1)}^2 - \tilde{\rho}_{k,(0,L-1)}^2) + \rho_{k+2,0}\tilde{\rho}_{k+2,(0,L-1)} - \rho_{k,0}\tilde{\rho}_{k,(0,L-1)} \end{bmatrix} \end{aligned} \quad (3.21)$$

equation (3.20) and equation (3.21) can be written in matrix notations as:

$$\mathbf{G} \cdot \mathbf{P}_d = \mathbf{H}_d \quad (3.22)$$

where  $\mathbf{P}_d$  and  $\mathbf{H}_d$  are defined as follows:

$$\mathbf{P}_d = \begin{bmatrix} \mathbf{pR}_k - \mathbf{pR}_{k+1} & \mathbf{pR}_k - \mathbf{pR}_{k+2} \end{bmatrix} \quad (3.23)$$

$$\mathbf{H}_d = \begin{bmatrix} \mathbf{H}_k - \mathbf{H}_{k+1} & \mathbf{H}_k - \mathbf{H}_{k+2} \end{bmatrix} \quad (3.24)$$

The Least Square (LS) solution of  $\mathbf{G}$  yields:

$$\hat{\mathbf{G}} = \mathbf{H}_d \cdot \mathbf{P}_d^{-1} \quad (3.25)$$

As a result, the positions of the VANs are estimated as follows:

$$\begin{bmatrix} x_1 & y_1 \\ \vdots & \vdots \\ x_{L-1} & y_{L-1} \end{bmatrix} = \hat{\mathbf{G}} + \begin{bmatrix} x^T & y^T \\ \vdots & \vdots \\ x^T & y^T \end{bmatrix} \quad (3.26)$$

### 3.4.1.3 RSS for Estimating VANs using LS Solution

The RSS approach can be also used to estimate the positions of VANs required for obstacle detection. The received power at these anchor nodes follows a log-normal shadowing pathloss model in mmwave channels [196][197]. The received power,  $P_i$ , is calculated using the following equation:

$$P_i [dBm] = P_0 - 10\eta \log_{10} \rho_i + \epsilon_i, i = 1, \dots, L-1 \quad (3.27)$$

where  $P_0$  is the power at the reference distance  $\rho_0$ ,  $\eta$  is the pathloss exponent (PLE),  $\rho_i$  is the Euclidean distance between Rx and the VAN  $\mathbf{pV}_i$ , and  $\epsilon_i$  is the zero mean Gaussian random variable measured in dB scale with shadowing fading effect described by the standard deviation  $\sigma_\rho$ . The square of the distance  $\rho_i$  between the VAN  $\mathbf{pV}_i$  and the receiver  $\mathbf{pR}$  is represented as follows:

$$\rho_i^2 = \|\mathbf{pV}_i - \mathbf{pR}\|_2^2 = (xV_i - xR)^2 + (yV_i - yR)^2 \quad (3.28)$$

Without loss of generality, we assume the transmitter to be the reference. Hence, for  $i \geq 1$ , we define the following:

$$xR \cdot \rho_i^2 - \rho_0^2 = xV_i^2 - 2xR \cdot xV_i + yV_i^2 - 2yR \cdot yV_i \quad (3.29)$$

Expressing equation (3.29) in matrix form, we obtain the following equation:

$$\begin{bmatrix} 2xV_1 & 2yV_1 \\ \vdots & \vdots \\ 2xV_{L-1} & 2yV_{L-1} \end{bmatrix} \cdot \begin{bmatrix} xR \\ yR \end{bmatrix} = \begin{bmatrix} xV_1^2 - xT^2 + yV_1^2 - yT^2 + \rho_0^2 - \rho_1^2 \\ \vdots \\ xV_{L-1}^2 - xT^2 + yV_{L-1}^2 - yT^2 + \rho_0^2 - \rho_{L-1}^2 \end{bmatrix} \quad (3.30)$$

The real distance  $\rho_i$  is not known in RSS localization; hence, noisy estimations of the distance,  $\tilde{\rho}_i$ , obtained from equation (3.27), are related with the unknown position of the receiver  $\mathbf{pR} = [xR, yR]^T$  as follows:

$$\mathbf{R} \cdot \mathbf{pR} = \mathbf{T} \quad (3.31)$$

where  $\mathbf{R}$  and  $\mathbf{T}$  are defined as follows:

$$\mathbf{R} = \begin{bmatrix} 2(xV_1 - xT) & 2(yV_1 - yT) \\ \vdots & \vdots \\ 2(xV_{L-1} - xT) & 2(yV_{L-1} - yT) \end{bmatrix}$$

$$\mathbf{T} = \begin{bmatrix} xV_1^2 - xT^2 + yV_1^2 - yT^2 + \rho_0^2 - \rho_1^2 \\ \vdots \\ xV_{L-1}^2 - xT^2 + yV_{L-1}^2 - yT^2 + \rho_0^2 - \rho_{L-1}^2 \end{bmatrix}$$

Equation (3.31) can be extended to  $N$  different positions  $\{\mathbf{pR}_k, \mathbf{pR}_{k+1}, \dots, \mathbf{pR}_N\}$ . Hence, the following system of equations is generated based on the difference between the measurements taken at  $\mathbf{pR}_k$  and  $\mathbf{pR}_n$ ,  $n = k+1, \dots, k+N$ , respectively:

$$\begin{aligned} \mathbf{R}(\mathbf{pR}_k - \mathbf{pR}_n) &= \mathbf{T}_1 - \mathbf{T}_n \\ &= \begin{bmatrix} \tilde{\rho}_{k,0}^2 - \tilde{\rho}_{k,1}^2 - \tilde{\rho}_{n,0}^2 + \tilde{\rho}_{n,1}^2 \\ \vdots \\ \tilde{\rho}_{k,0}^2 - \tilde{\rho}_{k,L-1}^2 - \tilde{\rho}_{n,0}^2 + \tilde{\rho}_{n,L-1}^2 \end{bmatrix} \end{aligned} \quad (3.32)$$

where  $\tilde{\rho}_{n,i}^2$  is the estimated distance between VAN  $\mathbf{pV}_i$  and the receiver at position  $\mathbf{pR}_n$ , knowing that  $\rho_{n,i}^2$  is defined as follows:

$$\rho_{n,i}^2 = \|\mathbf{pV}_i - \mathbf{pR}_n\|_2^2 = (xV_i - xR_n)^2 + (yV_i - yR_n)^2 \quad (3.33)$$

The target is to estimate  $\mathbf{R}$  in order to estimate the positions of the VANs. A simple Least Square (LS) estimator gives:

$$\hat{\mathbf{R}} = \mathbf{T}_d \cdot \mathbf{P}_d^T (\mathbf{P}_d \mathbf{P}_d^T)^{-1} \quad (3.34)$$

where  $\mathbf{T}_d$  and  $\mathbf{P}_d$  are now defined as follows:

$$\mathbf{P}_d = [ \mathbf{pR}_k - \mathbf{pR}_{k+1} \quad \mathbf{pR}_k - \mathbf{pR}_{k+2} \quad \dots \quad \mathbf{pR}_k - \mathbf{pR}_N ] \quad (3.35)$$

$$\mathbf{T}_d = [ \mathbf{T}_1 - \mathbf{T}_2 \quad \mathbf{T}_1 - \mathbf{T}_3 \quad \dots \quad \mathbf{T}_1 - \mathbf{T}_N ] \quad (3.36)$$

As a result, the positions of the VANs are estimated as follows:

$$\begin{bmatrix} xV_1 & yV_1 \\ \vdots & \vdots \\ xV_{L-1} & yV_{L-1} \end{bmatrix} = \frac{1}{2} \hat{\mathbf{R}} + \begin{bmatrix} xT & yT \\ \vdots & \vdots \\ xT & yT \end{bmatrix} \quad (3.37)$$



### 3.4.1.4 Estimating VANs using RSS-WLS solution

The aim here is to enhance the estimation taking into account the noise variance. We start with an example of 3 measurements and then the equations are updated accordingly. Equation (3.32) can be written as:

$$\mathbf{P}_{WLS} \cdot \mathbf{R}_{WLS} = \mathbf{T}_{WLS} \quad (3.38)$$

where  $\mathbf{P}_{WLS}$ ,  $\mathbf{R}_{WLS}$  and  $\mathbf{T}_{WLS}$  are defined as follows:

$$\mathbf{P}_{WLS} = \begin{bmatrix} \mathbf{P}_{12}(1) & \mathbf{P}_{13}(1) & 0 & \dots & 0 \\ \mathbf{P}_{12}(2) & \mathbf{P}_{13}(2) & & & \\ & 0 & \ddots & \vdots & \vdots \\ & \vdots & \dots & \mathbf{P}_{12}(1) & \mathbf{P}_{13}(1) \\ & 0 & \dots & \mathbf{P}_{12}(2) & \mathbf{P}_{13}(2) \end{bmatrix}$$

$$\mathbf{R}_{WLS} = \begin{bmatrix} 2(xV_2 - xV_1) \\ 2(yV_2 - yV_1) \\ \vdots \\ 2(xV_L - xV_1) \\ 2(yV_L - yV_1) \end{bmatrix}$$

$$\mathbf{T}_{WLS} = \begin{bmatrix} \mathbf{T}_d(1,1) \\ \mathbf{T}_d(1,2) \\ \vdots \\ \mathbf{T}_d(L-1,1) \\ \mathbf{T}_d(L-1,2) \end{bmatrix}$$

where  $\mathbf{P}_{12} = \mathbf{pR}_k - \mathbf{pR}_{k+1}$  and  $\mathbf{P}_{13} = \mathbf{pR}_k - \mathbf{pR}_{k+2}$ . Additionally, knowing that the dimensions of  $\mathbf{R}_{WLS}$  and  $\mathbf{T}_{WLS}$  are  $2 \cdot (L-1) \times 1$  and the dimension of  $\mathbf{P}_{WLS}$  is  $2 \cdot (L-1) \times 2 \cdot (L-1)$ . Hence,  $\mathbf{P}_{WLS}$  can be written as follows:

$$\mathbf{P}_{WLS} = \mathbf{I} \otimes \begin{bmatrix} \mathbf{P}_{12}(1) & \mathbf{P}_{13}(1) \\ \mathbf{P}_{12}(2) & \mathbf{P}_{13}(2) \end{bmatrix} \quad (3.39)$$

where  $\mathbf{I}$  is the identity matrix of dimension  $(L-1) \times (L-1)$ . Consequently,  $\mathbf{R}_{WLS}$  of the VANs can be estimated by:

$$\hat{\mathbf{R}}_{WLS} = \frac{1}{2} (\mathbf{W}_{WLS} \cdot \mathbf{P}_{WLS})^{-1} \mathbf{W}_{WLS} \cdot \mathbf{T}_{WLS} \quad (3.40)$$

where the weighting matrix  $\mathbf{W}_{WLS}$  is equal to the inverse of the covariance matrix  $\mathbf{\Sigma}_{WLS}$  of the vector  $\mathbf{T}_{WLS}$ .

### 3.4.2 Obstacle Detection

After the estimation of the VANs, the target is to detect the obstacles in the room. Referring to Fig. 3.3, obstacle detection is achieved using either RSS and AoA or TDoA and AoA. The obstacle detection is done by the following steps at each Rx position  $k$ :

- The VANs positions are firstly estimated as detailed in the previous section.
- Since the VANs are the mirrors of the transmitter with respect to all surfaces of the obstacles in the room, the obstacles are then the perpendicular to the line connecting the transmitter to each estimated VAN respectively. The perpendicular line passes through the midpoint of the segment  $[\mathbf{pV}_i\mathbf{pT}]$ . The latter is calculated as follows:

$$\mathbf{pM}_i = \frac{\mathbf{pT} + \mathbf{pV}_i}{2} \quad (3.41)$$

where  $\mathbf{pM}_i = (xM_i, yM_i)$ . Then, the normal to the point of reflection (PoR)  $\mathbf{pS}_i$  corresponding to VAN  $\mathbf{pV}_i$  is calculated as follows:

$$\mathbf{n}_i = \mathbf{pT} - \mathbf{pV}_i \quad (3.42)$$

where  $\mathbf{n}_i = (xn_i, yn_i)$ .

- equation (3.1) is used to write the obstacle surface, where  $\alpha$  and  $\mathbf{pM}_i = (xM_i, yM_i)$  are the slope and midpoint of segment  $[\mathbf{pV}_i\mathbf{pT}]$ , respectively. Fig. 3.3 shows the estimated obstacles by firstly estimating its location (the midpoint between Tx and VAN) and direction.
- Using the AoA and the estimated positions of the receiver, VAN and obstacle, the point of reflection at the obstacle can be easily deduced. It is simply the point of intersection between the line  $[\mathbf{pV}_i, \mathbf{pR}]$  and the obstacle line. Then, the vector crossing the PoR  $\mathbf{S}_{k,i}$  from the receiver to the transmitter is represented as follows:

$$\mathbf{w}_i = \mathbf{pV}_i - \mathbf{pR} \quad (3.43)$$

where  $\mathbf{w}_i = (xW_i, yW_i)$ . Then, we solve for the points of intersection between VANs and the receiver to estimate the PoRs as follows:

$$\mathbf{pS}_i = \mathbf{pR} + \left( \text{inv}(\text{diag}(\mathbf{n}_i \cdot \mathbf{w}_i)) \cdot ((\mathbf{pM}_i - \mathbf{pR}) \cdot \mathbf{n}_i)^T \right)^T \cdot \mathbf{w}_i \quad (3.44)$$

- At each receiver measurement, this procedure is iterated over all pairs of  $(\mathbf{pV}_i, \mathbf{pT})$ ,  $i = 1, 2, \dots, L$ , where  $L$  is the number of VANs. At each iteration, an estimated point of reflection belonging to the obstacle side is created. Using all these measurements, a cloud (set) of reflection points is generated.

- Using the CoRP, an interpolation between these points is applied. It is followed by a simple smoothing operation.

In summary, obstacle surfaces are detected and estimated using a set of connected reflection points. Using the concept of mirroring, we iterate over all pairs of  $(\mathbf{pV}_i, \mathbf{pT})$  at each Rx position to detect an obstacle surface. Then, the problem turns down to estimate the obstacle limits.

### 3.4.3 Obstacle Dimensioning: Finding the Obstacle Limits

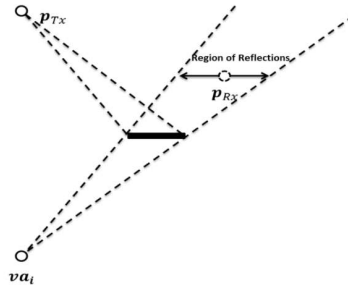


Figure 3.4: Region of possible reflections

After detecting the direction of the obstacles in the room and the corresponding CoRP, the boundaries of the obstacle are left to be set. Here two approaches are proposed (jointly or separately):

**Approach 1: Estimate the vertices by power measurements** As shown in Fig. 3.4, a point of reflection is obtained at the obstacle if the receiver moves within the region of all possible reflections determined by the obstacle limits, the position of the transmitter, and the related VAN. Hence, the AoA/TDoA/RSS spectrum generated at all receiver positions will dramatically change when the receiver leaves the region of reflection. Indeed, mmWave signals suffer from absorption loss by each obstacle. Hence, a change in the reflection environment will change when Rx changes from a region of reflection to another. Without loss of generality, when the receiver moves to the right or to the left outside the region of reflection shown in Fig. 3.4, the power of the received signal at the corresponding AoA will dramatically change raising the existence of the object limit. So the latter could be estimated by a simple border detection through power measurements, i.e separating the power of an obstacle ray from noise or walls rays. In this chapter, the detection is based on a simple energy detector algorithm whose threshold is set to maximize the probability of detection.

**Approach 2: Estimate the vertices as intersections of the obstacle sides:** This approach could be applied if the obstacle is of 2D shape (not 1D). As shown

in the previous section, each side of the obstacle is firstly determined via its direction and the CoRP. Hence, the limits (i.e. the vertices) of the obstacles are simply determined by the intersections of these sides.

To show the effectiveness of the proposed approaches, a simulation is executed in an indoor environment with a rectangular obstacle, a moving receiver across several positions and 4 transmitters as shown in Fig. 3.5. In this figure, it is very clear that the estimated points of reflection reproduce well the obstacle shape.

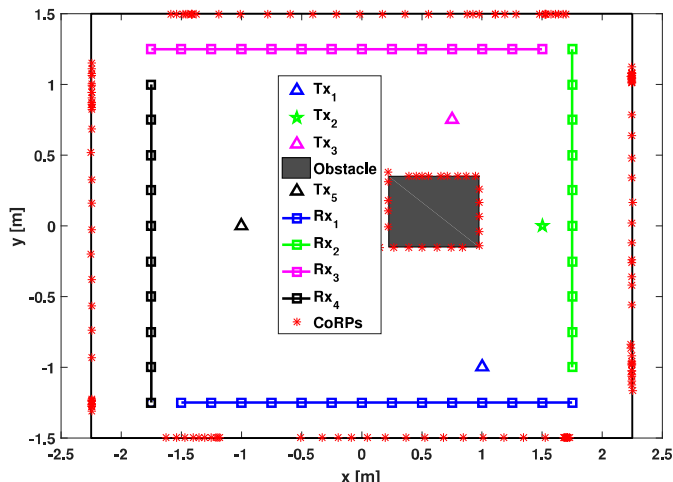


Figure 3.5: Indoor scenario for CoRPs' Estimation using AoA with static transmitter and moving Receiver

### 3.4.4 Clustering the Cloud of Vertices Points

Each measurement at each Rx position provides an estimation of the point of reflection first and then, through obstacle limits calculations, provides an estimation of the vertices constituting the obstacle. However, as these measurements are biased due to noise, a clustering of all measurements is required. Without loss of generality, the K-means algorithm [221] has been used to cluster the set of estimates of the obstacle vertices. Then, the sum of absolute differences approach is implemented to specify the centroids of the clusters. The latter represent the component-wise median of a set of estimations for an obstacle vertex.

### 3.4.5 Discussion on MOSAIC

One AN was used so far for receiver localization and obstacle detection. If the obstacle is known then the estimation of the receiver position follows from the VANs positions. However, when the obstacle information is not available, the estimation of both the receiver and the VANs positions can be done if enough

measurement metrics (TDoA and AoA, RSS and AoA) are available.

The estimation accuracy depends on the availability of LoS path. When it is not available, the measurements (mainly the AoA) will be biased since in our approach, the first path is considered to be the LoS. To overcome this problem and reduce the bias, it is very important to increase the number of ANs leading to an increase in the LoS measurements which implies a large number of points of reflection that could be used to determine the obstacle limits. On the other side, the limits of the obstacle are estimated if and only if the receiver is within the range of reflection. Nevertheless, this is not always the case with a single receiver at a given position and single AN as shown in Fig. 3.5. Consequently, having large number of ANs will also enhance the mapping accuracy. So, one question arise: how many ANs do we need in MOSAIC at a receiver position, i.e. without tracking?

## 3.5 Optimal Number of ANs

The target in this section is to explore the effect of increasing the number of ANs in terms of localization accuracy and mapping capabilities. Indeed, it has been shown in the previous section that the environment mapping depends on the estimation of the VANs which depends on the localization accuracy of the receiver. However, increasing the number of ANs indefinitely leads to additional measurements to be processed from one side and might not provide the best accuracy from the other side. To answer this question, we derive the CRLB of each algorithm proposed in Section 4 at each position of the Rx.

### 3.5.1 CRLB Derivations with $N$ ANs

The optimal number of ANs needed is analyzed via CRLB optimization for each metric.

#### 3.5.1.1 CRLB for Algorithm 1 (The TL Approach)

Here, we assume that the AoA measurements taken at the receiver coming from all ANs are independent. Assuming a wideband multipath model, we estimate the receiver position using the TL technique based on a Gaussian AoA model. This model represents scenarios where there is a strong LoS component that could be resolved by the receiver separately from multiple NLoS components due to local scattering. For a single transmitter  $\mathbf{pT}$  with an AoA  $\theta(\mathbf{pT})$  at the receiver, we consider a Gaussian LoS model with local scattering defined as:

$$p_{LoS}(\hat{\theta}/\mathbf{pT}) = \frac{1}{\sqrt{2\pi}\sigma(1-2Q(\frac{\pi}{2\sigma}))} \exp\left(-\frac{(\hat{\theta}-\theta(\mathbf{pT}))^2}{2\sigma^2}\right) \quad (3.45)$$

where  $\hat{\theta} \in [0, \pi]$ ,  $Q(t) = \int_t^\infty \exp(-t^2/2)/\sqrt{2\pi} dt$  and  $\sigma^2$  is the estimation error variance, representing the spatial extent of scattering. Additionally, the remaining AoA measurements due to reflected and scattered NLoS paths are assumed to be virtually in LoS with VANs. Hence, the distribution of these NLoS paths is defined as follows:

$$p_{NLoS}(\hat{\theta}_i/\mathbf{pV}_i) = \frac{1}{\sqrt{2\pi}\sigma(1-2Q(\frac{\pi}{2\sigma}))} \exp\left(-\frac{(\hat{\theta}_i - \theta_i(\mathbf{pV}_i))^2}{2\sigma^2}\right) \quad (3.46)$$

where  $\theta_i(\mathbf{pV}_i)$  is the true AoA coming from the VAN  $\mathbf{pV}_i$  to the receiver knowing that  $\mathbf{pV}_0 = \mathbf{pT}$ . Hence, the AoA estimates are generated for a wideband multipath model based on the following distribution:

$$p_{wideband}(\hat{\theta}_0, \hat{\theta}_1, \dots, \hat{\theta}_{L-1}/\mathbf{pT}) = p_{LoS}(\hat{\theta}_0/\mathbf{pT}) p_{NLoS}(\hat{\theta}_1/\mathbf{pV}_1) \dots p_{NLoS}(\hat{\theta}_{L-1}/\mathbf{pV}_{L-1}) \quad (3.47)$$

where  $L$  is the number of RRCs. Accordingly, the log-likelihood function for the estimates of the AoA for all RRCs is as follows:

$$L(\hat{\theta}_0, \hat{\theta}_1, \dots, \hat{\theta}_{L-1}/\mathbf{pT}, \mathbf{pV}) = -\sum_{i=0}^{L-1} \frac{(\hat{\theta}_i - \theta_i(\mathbf{pV}_i))^2}{\sigma^2} \quad (3.48)$$

Based on what has been derived for single transmitter in terms of the probability density function (pdf) of the wideband multipath model in equation (3.47), the log-likelihood function for the estimates of the AoA for all RRCs corresponding to multiple transmitters (i.e. ANs) is as follows:

$$L(\hat{\theta}_1, \hat{\theta}_2, \dots, \hat{\theta}_{L-1}/\mathbf{pT}, \mathbf{pV}) = -\sum_{m=1}^M \sum_{i=1}^{L-1} \frac{(\hat{\theta}_i - \theta_i(\mathbf{pV}_{m,i}))^2}{\sigma^2} \quad (3.49)$$

where  $\theta_i(\mathbf{pV}_{m,i})$  is the true AoA coming from the VAN  $\mathbf{pV}_{m,i}$  corresponding to the transmitter  $\mathbf{pT}_m$  reaching the receiver  $\mathbf{pR}$  and  $\mathbf{pV}_{m,0} = \mathbf{pT}_m$ . Then, we construct the Fisher information matrix (FIM)  $\mathbf{F}(\{\mathbf{pT}, V\})$  in order to calculate the CRLB, which is  $\mathbf{F}^{-1}(\{\mathbf{pT}, \mathbf{pV}\})$ . For the Gaussian model in equation (3.47),  $\mathbf{F}(\{\mathbf{pT}, V\})$  is defined as follows:

$$\mathbf{F}(\{\mathbf{pT}, \mathbf{pV}\}) = \begin{pmatrix} \sum_{m=1}^M \sum_{i=1}^{L-1} \frac{\sin^2(\theta_i)}{\sigma^2 \rho_{m,i}^2} & -\sum_{m=1}^M \sum_{i=1}^{L-1} \frac{\cos(\theta_i) \sin(\theta_i)}{\sigma^2 \rho_{m,i}^2} \\ -\sum_{m=1}^M \sum_{i=1}^{L-1} \frac{\cos(\theta_i) \sin(\theta_i)}{\sigma^2 \rho_{m,i}^2} & \sum_{m=1}^M \sum_{i=1}^{L-1} \frac{\cos^2(\theta_i)}{\sigma^2 \rho_{m,i}^2} \end{pmatrix} \quad (3.50)$$

where  $\rho_{m,i}$  is the distance between  $\mathbf{pV}_{m,i}$  corresponding to the transmitter  $\mathbf{pT}_m$  and the receiver  $\mathbf{pR}$ . Knowing that the total error of localizing the receiver is

the sum of variances along  $x$  and  $y$ , we define the CRLB for localization under NLoS environment using the TL technique as follows:

$$\begin{aligned} CRLB_{\theta|NLoS} &= Tr(\mathbf{F}^{-1}(\{\mathbf{p}\mathbf{T}, V\})) \\ &= \frac{\sigma^2 \sum_{m=1}^M \sum_{i=1}^{L-1} \frac{1}{\rho_{m,i}^2}}{\sum_{m=1}^M \sum_{i=1}^{L-1} \sum_{k=1, k \neq i}^{L-1} \frac{\sin^2(\theta_i - \theta_k)}{\rho_{m,i}^2 \rho_{m,k}^2}} \end{aligned} \quad (3.51)$$

In case of LoS environment, the CRLB for localization using TL technique based on AoA approach is as follows:

$$CRLB_{\theta|LoS} = \frac{\sigma^2 \sum_{m=1}^M \frac{1}{\rho_{m,LoS}^2}}{\sum_{m=1}^M \sum_{k=1, k \neq m}^M \frac{\sin^2(\theta_m - \theta_k)}{\rho_{m,LoS}^2 \rho_{k,LoS}^2}} \quad (3.52)$$

### 3.5.1.2 CRLB for Algorithm 2 (TDoA Metric)

The TDoA measurements taken at the receiver from multiple ANs are assumed to be independent. The distances between the receiver and the VAN  $\mathbf{p}\mathbf{V}_{m,i}$  corresponding to the transmitter  $\mathbf{p}\mathbf{T}_m$  in absence of noise is represented as follows:

$$\rho_{m,(i,0)} = c \cdot t_{m,(i,0)} = \rho_{m,i} - \rho_{m,0}, m = 1, \dots, M \& i = 1, \dots, L - 1 \quad (3.53)$$

where  $t_{m,i1}$  is the TDoA of the received signal at the pair of the VAN  $\mathbf{p}\mathbf{V}_{m,i}$  and the transmitter  $\mathbf{p}\mathbf{T}_m$  respectively, and  $c$  is the speed of light. As shown in equation (3.53), the estimated TDoAs are converted to RDoA measurements creating a set of nonlinear equations describing the hyperbolic range difference. In realistic scenarios, RDoA measurements  $\tilde{\rho}_{m,i0}$  are obtained with noise and modeled as:

$$\tilde{\rho}_{m,(i,0)} = \rho_{m,(i,0)} + \epsilon_{m,(i,0)} = \rho_{m,i} - \rho_{m,0} + \epsilon_{m,(i,0)}, m = 1, \dots, M \quad (3.54)$$

where  $i = 1, \dots, L - 1$  and  $\epsilon_{m,(i,0)}$  is the zero mean Gaussian random noise vector of the RDoA measurement with a  $(L - 1) \cdot (L - 1)$  covariance matrix  $\mathbf{\Sigma}_d$ . Thus, the pdf of  $\tilde{\rho}_{m,(i,0)}$  defined in equation (3.54) is as follows:

$$\begin{aligned} Pr(\tilde{\boldsymbol{\rho}}; \boldsymbol{\rho}) &= \prod_{m=1}^M \prod_{i=1}^{L-1} \frac{1}{\sqrt{2\pi c^2 \sigma_T^2}} \exp \left[ -\frac{(\tilde{\rho}_{m,(i,0)} - \rho_{m,(i,0)})^2}{2c^2 \sigma_T^2} \right] \\ &= \frac{1}{(2\pi c^2 \sigma_T^2)^{\frac{M \cdot (L-1)}{2}}} \exp \left[ -\frac{\sum_{m=1}^M \sum_{i=1}^{L-1} (\tilde{\rho}_{m,(i,0)} - \rho_{m,(i,0)})^2}{2c^2 \sigma_T^2} \right] \end{aligned} \quad (3.55)$$

Using the second partial derivative of the LLF for the pdf defined in equation (3.55), we obtain:

$$\frac{\partial^2 (\log(Pr(\tilde{\boldsymbol{\rho}}; \boldsymbol{\rho})))}{\partial \boldsymbol{\rho}^2} = -\frac{M \cdot (L - 1)}{c^2 \sigma_T^2} \quad (3.56)$$

Consequently, the optimal number of ANs required to achieve a TDoA localization accuracy defined by the CRLB is as follows:

$$M_{optimal} = \frac{c^2 \sigma_T^2}{(L-1) \cdot CRLB_t} \quad (3.57)$$

### 3.5.1.3 CRLB for Algorithm 3 (RSS Approach)

In RSS based approach, the log likelihood function (LLF) of the pdf of  $P_i$  is expressed as follows:

$$\begin{aligned} \log(Pr(\mathbf{P}\mathbf{T}; \boldsymbol{\rho})) &= \\ \log \left( \prod_{m=1}^M \prod_{i=1}^{L-1} \frac{10/\log 10}{\sqrt{2\pi\sigma_\rho^2}} \frac{1}{P_{m,i}} \exp \left[ -\frac{\left(\frac{10\eta}{\sigma_\rho \log 10}\right)^2}{8} \left( \log \frac{\rho_{m,i}^2}{\tilde{\rho}_{m,i}^2} \right)^2 \right] \right) & \\ = M \cdot (L-1) \cdot \log \left( \frac{10}{\log(10) \sqrt{2\pi\sigma_\rho^2}} \right) + & \quad (3.58) \\ \sum_{m=1}^M \sum_{i=1}^{L-1} \left( \log \left( \frac{1}{P_{m,i}} \right) - \frac{\left(\frac{10\eta}{\sigma_\rho \log 10}\right)^2}{2} \left( \log \left( \frac{\rho_{m,i}}{\tilde{\rho}_{m,i}} \right) \right)^2 \right) & \end{aligned}$$

where  $\rho_{m,i}$  is the distance between the VAN  $\mathbf{pV}_{m,i}$  corresponding to the transmitter  $\mathbf{pT}_m$  and the receiver  $\mathbf{pR}$  and  $\tilde{\rho}_{m,i}$  is its estimate. Then, the second partial derivative is defined as follows:

$$\frac{\partial^2 (\log(Pr(\mathbf{P}; \boldsymbol{\rho})))}{\partial \rho^2} = -\frac{\left(\frac{10\eta}{\sigma_\rho \log 10}\right)^2}{\ln 10} \sum_{m=1}^M \sum_{i=1}^{L-1} \frac{1}{\rho_{m,i}^2} \left( \frac{1}{\ln 10} - \log \left( \frac{\rho_{m,i}}{\tilde{\rho}_{m,i}} \right) \right) \quad (3.59)$$

Hence, the optimal number of ANs is obtained by optimizing the following CRLB for a target localization accuracy:

$$\begin{aligned} CRLB_{RSS} &= \frac{-1}{\frac{\partial^2 (\log(Pr(\mathbf{P}; \boldsymbol{\rho})))}{\partial \rho^2}} \\ &= \frac{\ln 10}{\left(\frac{10\eta}{\sigma_\rho \log 10}\right)^2} \frac{1}{\sum_{m=1}^M \sum_{i=1}^{L-1} \frac{1}{\rho_{m,i}^2} \left( \frac{1}{\ln 10} - \log \left( \frac{\rho_{m,i}}{\tilde{\rho}_{m,i}} \right) \right)} \quad (3.60) \end{aligned}$$

## 3.5.2 Discussion

The CRLB of the different metrics decreases with the number of ANs, except for AoA, in which a further discussion should be provided. Indeed, when the AoA metric is used for localization and mapping, it is very important to separate between the LoS and NLoS cases. In the former, an additional number of ANs



increases the resolvability of the Rx location as it will be shown in next section. However, in the case of NLoS, the increase in the ANs will increase the number of ambiguities hence it deteriorates the estimation. This is not the case in RSS or TDoA since they are used to support the TL approach. Another conclusion can be derived from the calculations of the CRLBs. equation (3.60) and equation (3.57) show that the number  $M$  of ANs and the number  $L$  of RRCs can be exchanged without changing in the CRLB. This means that both RSS and TDoA present similar results if the number of anchor nodes is increased or the number of reflections is increased.

## 3.6 Simulation Results

### 3.6.1 Parameters and Environment Settings

The room geometry is of rectangular shape of size  $(10 \times 10)m^2$ . The south-western corner of the room is assumed to be the reference of the Cartesian coordinate system. The angles are measured with respect to the positive part of the x-axis. The transmitter is set at position  $\mathbf{p}_T = (0.2, 0.2)$  m. The antenna at the transmitter is assumed to be omnidirectional; hence, the transmitted power  $\mathbf{SP}(\theta)$  is constant for all  $\theta$ . An antenna array is considered at the receiver with a reception beam pattern described as  $\mathbf{SP}(\theta) = \exp\left(-\frac{\theta^2}{2s^2}\right)$ ,  $s = 0.1$ . The value of parameter  $s$  and the Gaussian shape have been devised empirically. Additionally, all results are simulated for 10000 realizations.

### 3.6.2 Performance of the Rx Localization Algorithm in unknown Environment

In this section, we provide the simulation results of the localization accuracy in an unknown environment. We remind the reader that an unknown environment refers to the case where there is no information about the obstacles in the room. We implemented different combinations of the basic standalone positioning techniques (TL, RSS, and TDoA) to achieve additional enhancement in the localization accuracy. Fig. 3.6 shows the RMSE of estimating the receiver's position using TL, TL in combination with TDoA, TL in combination with RSS and TL in combination with RSS and TDoA. It is very clear that the hybrid approach presents the best results. Particularly, the combination of the TL and TDoA has a good accuracy and presents comparable results with those obtained with all metrics. In terms of localizing VANs, Fig. 3.7 shows that the estimation error can be greatly reduced, reaching few centimeters, if the number of Rx measurements is high enough. For instance, the error is shown to be less than 0.075 m at  $\sigma_{TDOA} = 0.2$  ns and less than 0.04 m at  $\sigma_{TDOA} = 0.1$  ns with 100 Rx positions.

This means that a mobile receiver can perfectly estimate the positions of the VANs.

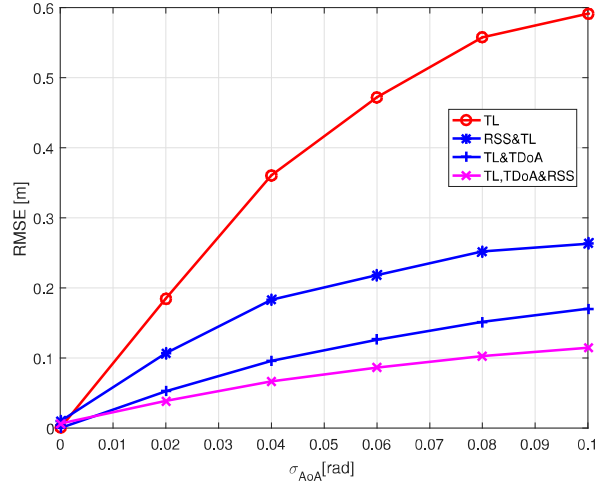


Figure 3.6: Simulation Results of the Hybrid Approach

### 3.6.3 Optimal Number of ANs

Increasing the number of ANs is proposed for the sake of enhancing localization and obstacle mapping accuracy. This enhancement is expected to increase the probability of LoS links and the number of estimations for the obstacle vertices. Thus, the optimal number of ANs is recognized as a compromise between the number that achieves the best localization accuracy and the number that achieves full detection of an obstacle. As shown in Fig. 3.8, the localization accuracy for TL becomes worse with the growing number of ANs. The decrease of the CRLB level using TL as the number of ANs grows is due to the NLoS environment. The AoA localization based technique is highly sensitive to errors under NLoS scenario since the rays coming from NLoS paths will deteriorate the localization accuracy. This is indeed expected as AoA is very sensitive to errors as shown in literature. For instance, an error of  $5^\circ$  might lead to high direction error which is translated by high position error.

However, in LoS conditions, higher number of ANs decreases the CRLB level of the localization accuracy as shown in Fig. 3.8. In such scenario, the AoA of the LoS ray is less biased to error compared to that of the NLoS ray; hence, the localization accuracy is enhanced with higher number of ANs. Moreover, the increase in the number of ANs is shown in Fig. 3.9 to decrease the CRLB using RSS and TDoA. Finally, as expected, the rise in the number of ANs is shown to enhance the mapping ability. It is very clear that at least 30 ANs are needed to

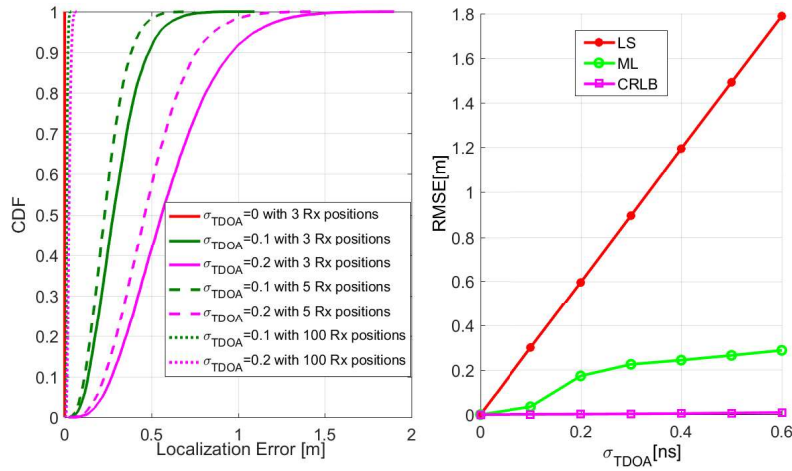


Figure 3.7: Estimation error of localizing VANs based on TDoA approach using LS and ML versus  $\sigma_{TDOA}$

have a good estimation of the VANs hence the obstacle vertices.

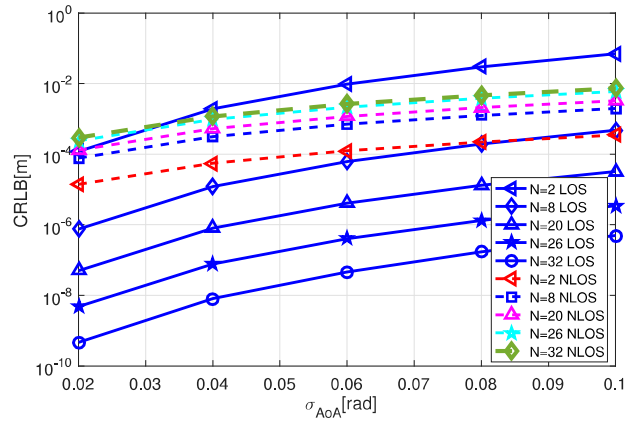


Figure 3.8: CRLB of localization accuracy using AoA under LoS/NLoS conditions for various number of ANs

### 3.6.4 Obstacle Mapping

After localizing the VANs, the obstacles in the room are to be mapped in terms of their positions, dimensions and limits. Three types of obstacles have been considered: a square, a triangle and a hexagon. Fig. 3.11 shows the estimated vertices of a triangular obstacle in the room with  $M = 12$  and  $M = 42$  ANs, respectively, using the TL with  $\sigma_{AoA} = 0.09rad$  (almost  $5^\circ$ ) and the K-means algorithm to cluster the set of estimated obstacle vertices. It is very clear that

the TL approach presents very good accuracy if the number of ANs is large enough. Moreover, the results are in line with CRLB derived in the previous section which specifies at least 30 ANs for good accuracy. Fig. 3.12 presents the mapping results of a square and hexagonal obstacles using TDoA approaches, provided in Section IV with  $\sigma_{TDoA} = 0.05ns$  and  $\sigma_{TDoA} = 0.1ns$ , respectively. Here, the cloud of vertices points at each measurement is shown as well as the resulting estimated vertices using K-means algorithm.

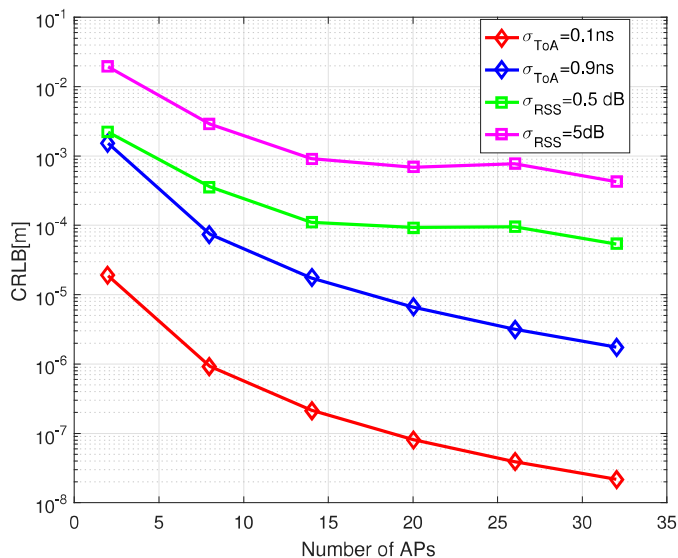


Figure 3.9: CRLB of localization accuracy versus number of ANs using TDoA and RSS

### 3.6.5 Analysis and Conclusions on the Simulations Results

As shown in Fig. 3.10, the CRLB level of the TL (AoA- based approach) decreases with the growing number of ANs under LoS environment. Nevertheless, this is not the case with NLoS environment. However, as the obstacle mapping highly depends on the localization accuracy from one side and needs the reflection paths from the other side, it becomes very important to select the optimal number of ANs which is able to realize both localization and mapping. Another important point resides in the AoA measurement errors as they highly affect the accuracy of the obstacle mapping. However, thanks to the large number of antennas implemented in mmWave technology, these errors are very small [220]. Similarly, TDoA is shown to achieve high accuracy in terms of localizing VANs with respect to the noise variance of the TDoA measurements. In practice, the

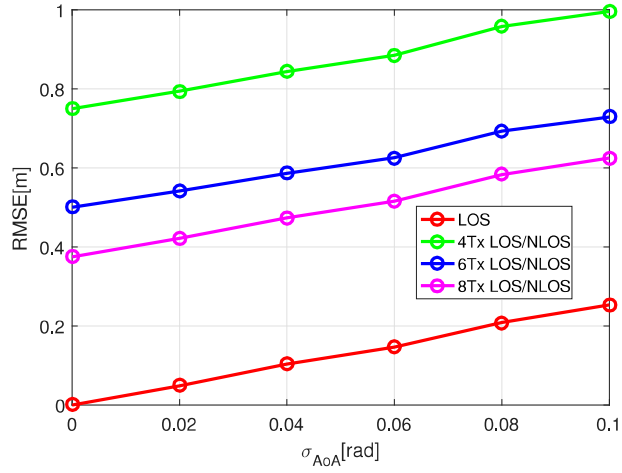


Figure 3.10: RMSE versus  $\sigma_{AoA}$  for estimating receiver under LoS/NLoS channel

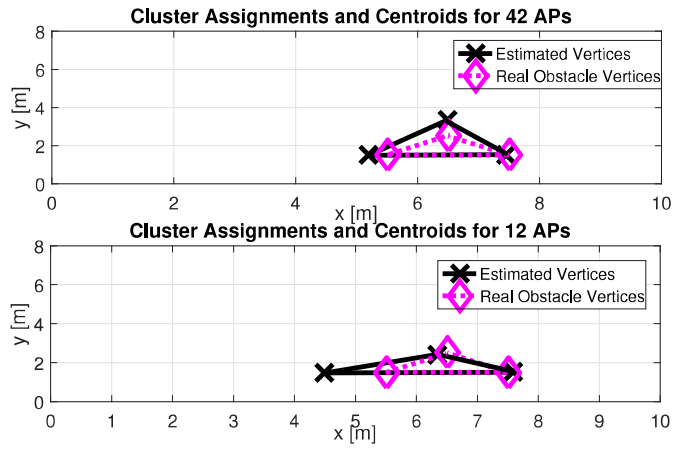


Figure 3.11: Obstacle (triangle) mapping using the TL approach to estimate the VANs

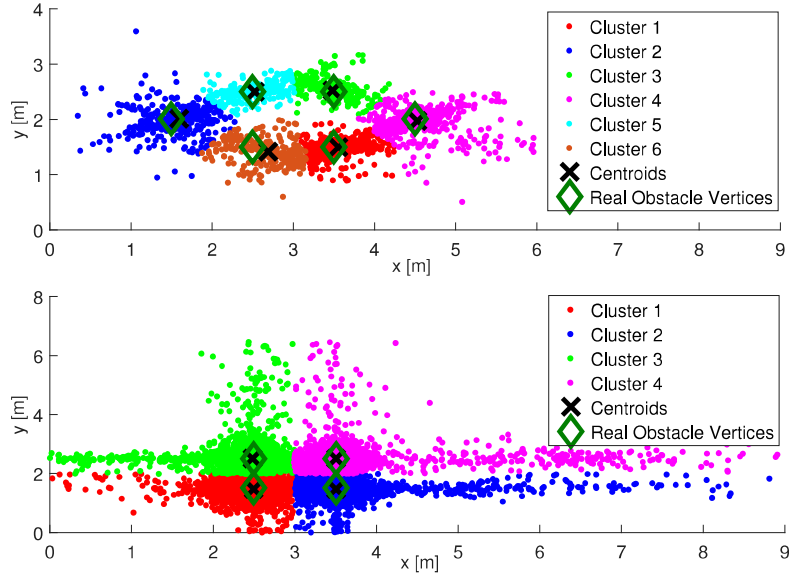


Figure 3.12: Obstacle (hexagon and Square) mapping using TDoA

TDoA based approach provides a negligible estimation error in the localization approach. However, the mapping needs an estimation of the AoA which again needs to be very accurate. In terms of raw accuracy, 10 GHz bandwidth is required to achieve accurate estimation using TDoA with an error in the order of 0.1 ns in terms of  $\sigma_t$ . This is indeed one advantage of using mmWave whose band can reach few GHz.

RSS based approach is the worst in terms of estimating the VANs positions due to an increased error in the Rx localization as shown in the CRLB given in Fig. 3.10. Moreover, this bias is increased in practice due to the absorption loss by the obstacles on the NLoS rays powers. Finally, it is worth mentioning that the simulation results have shown that the localization and mapping within the MOSAIC framework present an excellent accuracy reaching few centimeters if appropriate algorithms and parameters are selected.

### 3.7 Conclusion

In this chapter, we presented MOSAIC a framework for joint localization and mapping. The concept is based on few steps based on localization of the receiver, followed by the estimation of the VANs using TL, TDoA and RSS and then obstacle detection and dimensioning. Obstacle detection is achieved via an estimation of CoRP and then obstacle dimensioning is achieved by two different approaches which estimate the vertices of the obstacle either by power measurements or by

following the geometric definition of these vertices as intersections of the obstacle sides if and only if the obstacle is of 2D shape.

The performance of the localization techniques is tested through simulations in terms of RMSE and CDF of the location estimation error. In terms of obstacle detection, the chapter proposed a new approach based on VANs and mirroring. A thorough analysis of the proposed approaches has been made in the chapter from theoretical and algorithmic point of view. Simulations have shown that finding the optimal number of ANs using the CRLB is a compromise between localization and obstacle mapping accuracy.

In summary, this chapter consists a first of its kind in mapping an indoor environment based on the channel measurements. Definitely, much work could be achieved in the future. Among others, the localization and detection of multiple objects is a possible future direction. Also, an extension to 3D localization and mapping for this work tackling not only single bounce but also double bounce will be proposed in the next chapter.

# Chapter 4

## Extension to 3D Localization and Mapping

### 4.1 Introduction

This chapter raises an important question on the opportunities offered by millimeter Waves (mmWaves) signals for 3D localization and mapping (3D-LOCMAP) in vehicular and indoor environments. More precisely, this chapter presents a technical framework for 3DLOCMAP using the mmWave channel response and mmWave propagation characteristics. To do so, we firstly introduces a combination between Triangulation (TL) and Received Signal Strength (RSS) or Time of Arrival (ToA) measurements for 3DLOCMAP. In the case of a channel model with single bounce, the environment mapping (such as obstacles) is achieved by estimating the positions of virtual anchor nodes (VANs), known as mirrors of the real anchors with respect to obstacle. Then, the obstacle position and dimensions are found via the estimation of the reflector points on the obstacle. In case of double-bounce, the scenario is observed from single-bounce perspective by estimating Virtual Receiver (VRx), VAN, and two Points of Reflection (PoR). Simulation results have shown the accuracy of the proposed framework which can be extended for further investigations. The work here will open the door for multiple applications in vehicular, robotics, health, radar-like systems, and Internet of Things (IoT). In this chapter, we tackle the joint problem of 3D localization and mapping (3DLOCMAP). The high-level proposed approach is shown in Figure 4.1. It allows us developing context inference and mapping of the environment with high accuracy reaching sub meters (few centimeters in some cases). In this work, we are tackling two different environments: the vehicular and indoor and we propose a framework for 3DLOCMAP using a professional mmWave channel simulator. The contribution of this chapter can be summarized in the following aspects:

- Exploitation of the map-based mmWave channel criteria to provide 3D



localization and mapping. MmWave signals have no scattering effect and they realize high penetration loss through obstacles. This fact triggers the use of Snell's law for obstacle detection and classification.

- We use the concept of Virtual Anchor Nodes (VANs) to estimate the location of each mmWave receiver (Rx) using the combination between the proposed Triangulation (TL) technique and RSS or ToA.
- Introduction of the virtual receiver (VRx) to develop environment mapping in the case of double-bounce channel propagation
- Validation of proposed approaches through extensive simulation results.

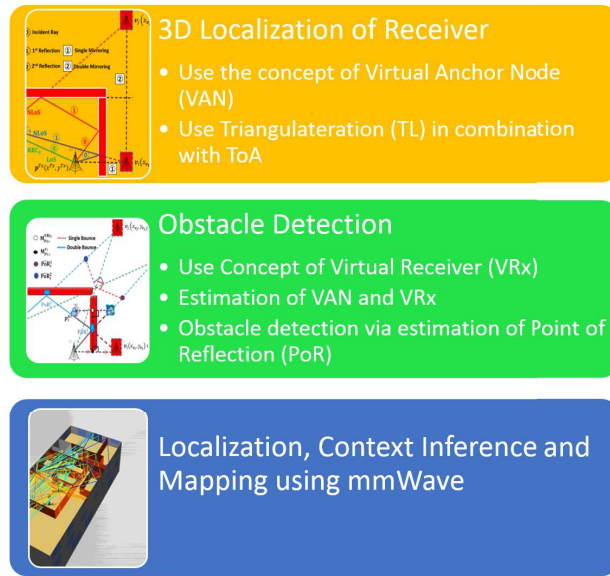


Figure 4.1: The process of localization, context inference and mapping using geometric approach

The rest of this chapter is organized as follows. In Section 2, we develop the system model and the 3D localization methodology of the receiver using mmWave. In Section 3, we perform 3D localization for a receiver in an unknown environment. Then, obstacle mapping for single bounce and double bounce scenarios in 3D environment is tackled in section 4 and section 5 respectively. In Section 6, we provide simulation results while conclusions are drawn in Section 7.

## 4.2 System Model using Millimeter Wave

### 4.2.1 Environment Settings

The proposed mmWave localization techniques are tested in a 3D environment. The boundaries and radio-reflective obstacles in the reflective objects are grouped in a set  $\mathcal{O}$ . Obstacles are described as three-dimensional flat polygonal faces with sharp vertices and straight edges. Each oriented surface  $S$  of 3D obstacle is denoted by its perpendicular line, written as:

$$a(x - p_x) + b(y - p_y) + c(z - p_z) + d = 0 \quad (4.1)$$

where  $\mathbf{p} = (p_x, p_y, p_z)$  is a point of intersection between the surface and its perpendicular and  $\vec{n} = (a, b, c)$  is the vector orthogonal to the surface  $S$ . By assumption, a single mmWave AP is deployed at a location  $\mathbf{p}^{Tx}$ . Additionally, the AP is assumed to broadcast its position and the specifications of the objects in  $\mathcal{O}$  to the node(s) targeted for localization. In this chapter, the AoA will be firstly prioritized and investigated since the AoA metric is not sensitive to the absorption loss at mmWave. It will be then complemented by other metrics, such as RSS and ToA, when necessary. The AoA spectrum,  $P_p(\theta)$ , is a  $3 \times N_p$  matrix that records the amplitude of each received ray component (RRC) as a function of the azimuth  $\theta$  and elevation  $\phi$  at a given location  $\mathbf{p}$ , where  $N_p$  is the number of RRCs. Each RRC can be either due to a LoS link between the transmitter and the receiver or due to NLoS link induced by reflections of one or more surfaces in the obstacle set  $\mathcal{O}$ . Then,  $SP_p(\theta)$  is a  $3 \times N_p$  matrix, which contains in its first row the amplitude of each RRC sorted in decreasing order, in its second row the azimuth  $\theta$  with respect to reference angle  $\theta_0$ , and in its third row the elevation  $\phi$  with respect to reference angle  $\phi_0$ . Moreover, the boundaries of the testing environment are assumed to be known for the node(s) to be localized.

### 4.2.2 Virtual Anchors

As the environment is unknown, the NLoS rays are recognized as virtual LoS rays transmitted from VANs to fulfill the condition on the number of anchor nodes needed for localization. The first column vector of  $SP_p(\theta, \phi)$  represents the LoS path between the transmitter and the receiver to be localized, and the columns  $2 : N_p$  represent the NLoS paths. So, we have  $N_p - 1$  RRCs that correspond to NLoS paths. Each of these paths can be modeled as emitted by a VAN through a virtual LoS path reaching the receiver  $\mathbf{p}^{Rx}$ . The locations of the VANs are determined by mirroring the AP  $\mathbf{p}^{Tx}$  with respect to the surfaces in the obstacle set  $\mathcal{O}$  since it is the source of signal reflections. We denote  $V = \{v_0, v_1, \dots\}$  to be the set of the positions of all possible VANs, and we denote  $\bar{V} = \{V_0, V_1, \dots\}$  to be a partition of  $V$ . We let  $V_0 = \mathbf{p}^{Tx}$ , and each set  $V_i, i = 1, 2, \dots$  represents all VANs that have been mirrored  $i$  times due to reflections caused by any surface in

the obstacle set  $O$ . Actually, there is no limit on the number of reflections of the signal transmitted by  $\mathbf{p}^{Tx}$ . However, a mmWave signal fades quickly during its propagation as it reflects off the surfaces. So, we limited the set  $V$  by assuming a maximum reflection order  $\mu = 2$ . Hence, the set of all VANs will be represented as  $V_\mu = \bigcup_{i=0}^\mu V_i$ . As shown in Figure 4.2, the anchors  $v_i \in V_1$  represent first order of reflection and the anchors  $v_i \in V_2$  represent second order of reflection.

### 4.3 Localization of the Receiver in an unknown environment: The Proposed Algorithm

As the environment is assumed to be unknown in this section, i.e. none of the  $\mathbf{v}_i$  is known except the true TX position  $\mathbf{v}_0$ , the first step in the localization and mapping consists in finding the positions of the receiver and of the VANs and of the VRx. To solve this problem, we can easily assume that there are enough measurements about ToA/RSS/AoA<sup>1</sup>. The proposed algorithm is divided into two main steps: (1) filtering the received signal and (2) localization through hybrid approach

#### 4.3.1 Filtering the Received Rays

In a dense environment, such as indoor or dense vehicular environment, many of the rays will be received after few reflections. Hence, their powers will be beneath the noise power. In order to reduce the localization error and avoid the noise effect on the received rays' powers, the first step in the proposed algorithm is to filter out the signal keeping the strong rays. To do so, the rays are first sorted based on ToA values in ascending order where the first ray is the ray received with minimum delay. Then knowing that the noise variance is equal to  $-174 + 10 \times \log_{10}(BW)$ , the signal is filtered out to keep the strongest rays based on a received power threshold,  $\gamma_{Pr}$ , calculated as follows:

$$\gamma_{Pr} = -174 + 10 \times \log_{10}(BW) + 10 \times \log_{10} \left( \frac{1 + Q^{-1}(PFA)}{\sqrt{N_p}} \right) \quad (4.2)$$

where  $BW$  is the bandwidth,  $Q^{-1}(\cdot)$  is the inverse  $Q$  function, and  $PFA$  is the probability of false alarm to separate a ray (with a given delay) from noise.

#### 4.3.2 Estimating the Rx Position

The estimation of the Rx position is done by appropriate combination of the channel metrics. Without loss of generality, let us assume that the first received

---

<sup>1</sup>this assumption is valid and solid as these measurements are needed for channel estimation at mmWave

path corresponds to a LoS. Hence, we can easily write (see Fig. 4.2):

$$\begin{cases} x^{Rx} = x^{Tx} + \rho_0 \sin(\phi_0^{AoA}) \cos(\theta_0^{AoA}) \\ y^{Rx} = y^{Tx} + \rho_0 \sin(\phi_0^{AoA}) \sin(\theta_0^{AoA}) \\ z^{Rx} = z^{Tx} + \rho_0 \cos(\phi_0^{AoA}) \end{cases} \quad (4.3)$$

where  $\mathbf{p}^{Tx} = (x^{Tx}, y^{Tx}, z^{Tx})$ ,  $\mathbf{p}^{Rx} = (x^{Rx}, y^{Rx}, z^{Rx})$ ,  $\rho_0$  is the distance traveled by the first ray, and  $\phi_0^{AoA}$  and  $\theta_0^{AoA}$  are the elevation and the azimuth of the AoA for the ray assumed to be in LoS. Consequently, the estimated receiver position  $\hat{\mathbf{p}}^{Rx}$  is calculated as follows:

$$\widehat{\mathbf{pR}} = \mathbf{pT} + \rho_0 \begin{bmatrix} \sin(\phi_0^{AoA}) \cos(\theta_0^{AoA}) \\ \sin(\phi_0^{AoA}) \sin(\theta_0^{AoA}) \\ \cos(\phi_0^{AoA}) \end{bmatrix} \quad (4.4)$$

It is very clear from equation (4.4) that the estimation of the Rx position requires the knowledge of the distance  $\rho_0$  traveled by the LoS path. The latter could be easily estimated using either RSS or ToA metric as follows.

#### 4.3.2.1 RSS

RSS is used to estimate the distance traveled by each ray using the free space pathloss model. The pathloss for each ray is calculated first as follows:

$$PL_i = P^t - P_i^r - 20 \times \log_{10}\left(\frac{4 \times \pi \times f_c}{c}\right) \quad (4.5)$$

where  $PL_i$  is the pathloss for the  $i$ th path,  $c$  is the speed of light,  $P^t$  is the transmitted power in dB,  $P_i^r$  is the received power for the  $i$ th path in dB and  $f_c$  is the carrier frequency. Thus, the distance traveled by the  $i$ th ray is then estimated as follows:

$$\rho_i = 10^{PL_i/20} \quad (4.6)$$

#### 4.3.2.2 ToA

ToA can also be used to estimate the distance traveled by each ray as follows:

$$\rho_i = c \times toa_i \quad (4.7)$$

where  $toa_i$  is the ToA for the  $i$ th ray.

Hence, using  $\rho_0$  from equation (4.6) or equation (4.7) in equation (4.4), the estimation of the Rx position in an unknown environment can be directly obtained.

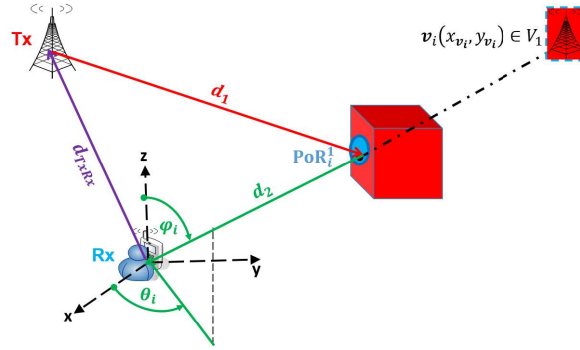


Figure 4.2: VANs related to first order of reflection

## 4.4 Obstacle Mapping in Single Bounce Scenario

The main target of this section is to estimate obstacles locations and their dimensions using the received signal. We introduce obstacle detection in three steps; (1) estimate the position of the VANs, (2) estimate the positions of VRx, and (3) estimate the obstacle direction and dimensions by finding the points of reflection on the obstacles, as shown in 4.3. The VANs and the receiver are estimated using the TL algorithm for NLoS environments. Then, we will use the concept of mirroring to detect the obstacle in between the transmitter and the VANs.

### 4.4.1 Estimation of the VAN Positions

The model in equation (4.6) can be easily extended to NLoS rays for obstacle mapping. Here, two different scenarios can be targeted: single bounce and double bounce.

#### 4.4.1.1 Single Bounce Scenario

After estimating the Rx position, we need to estimate the VANs for rays coming from NLoS paths. In case of single bounce scenario, the paths are considered to be transmitted from virtual transmitters denoted by VANs. In other words, the received ray coming through NLoS path is considered to be a virtual LoS path coming from the VAN. The VANs are estimated for the 3D geometric model shown in Figure 4.2 as follows:

$$\begin{cases} x_i^v = x^{Rx} + \rho_i \sin(\phi_i^{AoA}) \cos(\theta_i^{AoA}) \\ y_i^v = y^{Rx} + \rho_i \sin(\phi_i^{AoA}) \sin(\theta_i^{AoA}) \\ z_i^v = z^{Rx} + \rho_i \cos(\phi_i^{AoA}) \end{cases} \quad (4.8)$$

where  $\mathbf{v}_i = (x_i^v, y_i^v, z_i^v)$  is the VAN corresponding to the  $i$ -th NLoS ray where  $i = 1, \dots, N_p - 1$  and  $\rho_i$  is the distance traveled by the corresponding path.

#### 4.4.2 Obstacle Detection through Points of Reflection

After estimating the VANs, we need to categorize them into two sets: The first one is the set of VANs that are obtained due to walls, floor and ceiling reflections, and the second one is the set of VANs that are obtained due to obstacle reflections. This classification can be done by applying the concept of mirroring over the transmitter with respect to the room boundaries in order to find the VANs of the first set. Hence, we will be able to identify the VANs that are due to obstacle reflections. The obstacle is detected by estimating the points of reflection, gathered as cloud of reflection points (CoRP) of the rays induced by the obstacle. If the size of this CoRP is large enough, a good estimation by interpolation and extrapolation of the obstacle sides (hence obstacle shape) is possible. However, for a given receiver position and a single transmitter, the set of VANs and hence the size of the CoRP is limited leading to a biased estimation of the obstacle shape. Hence, we need to increase the number of APs in order to estimate all the VANs required to do perfect estimation of the obstacle.

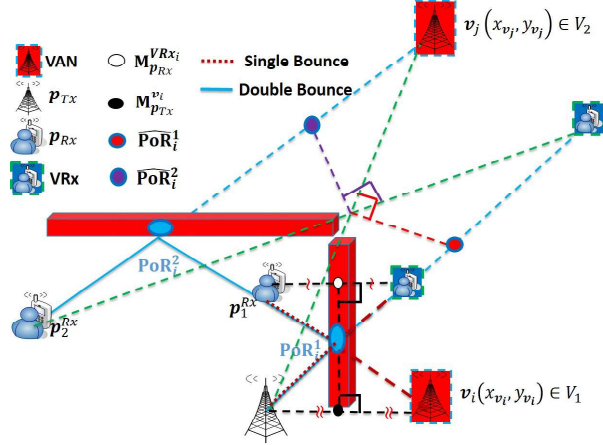


Figure 4.3: VAN and VRx related to first and second order of reflection

The estimation of the reflection point could be done in different ways, depending on the available measurements. It is mainly based on the geometry of reflected rays, obstacle orientation and the positions of VANs and Rx. In the sequel, we assume that the angle of departure (AoD) for each ray is known<sup>2</sup>. First, the midpoint between the transmitter and VAN  $\mathbf{v}_i$  is calculated as follows:

$$\mathbf{M}_i = \frac{\mathbf{pT} + \mathbf{pV}_i}{2} \quad (4.9)$$

where  $\mathbf{M}_{\mathbf{p}T_x}^{\mathbf{V}_i} = \left( x^{\mathbf{M}_{\mathbf{p}T_x}^{\mathbf{V}_i}}, y^{\mathbf{M}_{\mathbf{p}T_x}^{\mathbf{V}_i}}, z^{\mathbf{M}_{\mathbf{p}T_x}^{\mathbf{V}_i}} \right)$ . Then, the normal to the point of reflection

<sup>2</sup>this assumption is considered here for the ease of derivations. if this information is not available the estimation can still be done at the expense of additional calculation complexity

tion (PoR)  $\mathbf{PoR}_1^i$  corresponding to VAN  $\mathbf{v}_i$  is calculated as follows:

$$\mathbf{n}_i^{PoR1} = \mathbf{p}^{Tx} - \mathbf{v}_i \quad (4.10)$$

where  $\mathbf{n}_i^{PoR1} = \left( x_{n_i^{PoR1}}, y_{n_i^{PoR1}}, z_{n_i^{PoR1}} \right)$ . Then, the vector crossing the PoR  $\mathbf{PoR}_i^1$  from the receiver to the transmitter is represented as follows:

$$\mathbf{w}_i = \mathbf{v}_i - \mathbf{p}^{Rx} \quad (4.11)$$

where  $\mathbf{w}_i = (x^{w_i}, y^{w_i}, z^{w_i})$ . Then, we solve for the points of intersection between VANs and the receiver to estimate the PoRs as follows:

$$\mathbf{S}_i = \mathbf{pR} + \left( \text{inv}(\text{diag}(\mathbf{n}_i \cdot \mathbf{w}_i)) \times ((\mathbf{M}_i - \mathbf{pR}) \times \mathbf{n}_i)^T \right)^T \cdot \mathbf{w}_i \quad (4.12)$$

Then, the distance traveled by each ray coming from NLoS path passing from the transmitter to the receiver through the PoR is estimated as follows:

$$\rho_i^{Tx-PoR-Rx} = \frac{\sqrt{(x^{Tx} - x_i^{PoR})^2 + (y^{Tx} - y_i^{PoR})^2 + (z^{Tx} - z_i^{PoR})^2} + \sqrt{(x^{Rx} - x_i^{PoR})^2 + (y^{Rx} - y_i^{PoR})^2 + (z^{Rx} - z_i^{PoR})^2}}{\quad} \quad (4.13)$$

### 4.4.3 Estimation of the Reflection Coefficient

The reflection coefficient that corresponds to the absorption loss induced by the reflection of the obstacle can be determined for each NLoS path. It is calculated using the RSS value as follows:

$$\Gamma_i = PL_i - \left( P^t - 20 \times \log_{10}(d_i^{travel}) - 20 \times \log_{10} \left( \frac{4 \times \pi \times f_c}{c} \right) + 4.3 \right) \quad (4.14)$$

## 4.5 Obstacle Detection for double-bounce scenario

### 4.5.1 Estimation of the VAN and VRx Positions

As shown in Fig. 4.3, the double bounce scenario is observed as two stages of single bounce scenario. Here, two points of reflection are to be considered. Moreover, we introduce the virtual receiver (VRx) defined by mirroring Rx on each obstacle. In practice, VRx position is unknown and has to be estimated. It is very useful in this scenario in order to estimate the two points of reflection, as it will be detailed later. Similar to the single bounce scenario, the distance traveled by

each ray is estimated using either the ToA or RSS measurements. Assuming the ray with the strongest RSS value and minimum ToA to be the LoS path, the receiver position is estimated using equation (4.4). As the Angle of Departure (AoD) of each ray is in general known through channel estimation, then VRx position is estimated as follows:

$$\begin{cases} x_i^{VRx} = x^{Tx} + \rho_i \sin(\phi_i^{AoD}) \cos(\theta_i^{AoD}) \\ y_i^{VRx} = y^{Tx} + \rho_i \sin(\phi_i^{AoD}) \sin(\theta_i^{AoD}) \\ z_i^{VRx} = z^{Tx} + \rho_i \cos(\phi_i^{AoD}) \end{cases} \quad (4.15)$$

where  $\mathbf{p}^{VRx} = (x^{VRx}, y^{VRx}, z^{VRx})$ , and  $\phi_i^{AoD}$  and  $\theta_i^{AoD}$  are the elevation and the azimuth of the AoD for the  $i$ th ray sent by transmitter.

It is worth mentioning that, in the case of double bounce scenario, the positions of the VANs can be easily estimated through equation (4.8). Similar to the single-bounce scenario, the set of VANs induced by obstacle reflection is determined using equation (4.15). Double-bounce scenario is observed as two steps of single bounce scenario where the first PoR is the VRx that is estimated as  $\mathbf{PoR}_i^1$  is estimated in a single bounce scenario. After estimating the VRx, the second step of single-bounce is between the VRx and the transmitter in order to estimate the second PoR  $\mathbf{PoR}_i^2$  shown in Figure 4.3.

## 4.5.2 Estimation of the Reflection Points

The estimation of the reflection point could be done in different ways, depending on the available measurements. It is mainly based on the geometry of reflected rays, obstacle orientation and the positions of VANs and Rx. In the sequel, we assume that the angle of departure (AoD) for each ray is known<sup>3</sup>. First, the midpoint between the receiver and VRx is calculated as follows:

$$\mathbf{M}_{\mathbf{p}^{Rx}}^{\mathbf{VRx}_i} = \frac{\mathbf{p}^{Rx} + \mathbf{VRx}_i}{2} \quad (4.16)$$

where  $\mathbf{M}_{\mathbf{p}^{Rx}}^{\mathbf{VRx}_i} = \left( x_{\mathbf{p}^{Rx}}^{\mathbf{VRx}_i}, y_{\mathbf{p}^{Rx}}^{\mathbf{VRx}_i}, z_{\mathbf{p}^{Rx}}^{\mathbf{VRx}_i} \right)$ . Then, the normal to the second PoR  $\mathbf{PoR}_i^2$  corresponding to VRx  $\mathbf{VRx}_i$  is calculated as follows:

$$\mathbf{n}_i^{PoR2} = \mathbf{p}^{Rx} - \mathbf{VRx}_i \quad (4.17)$$

where  $\mathbf{n}_i^{PoR2} = \left( x_{n_i^{PoR2}}, y_{n_i^{PoR2}}, z_{n_i^{PoR2}} \right)$ . Then, the vector crossing the PoR  $\mathbf{PoR}_i^2$  from the transmitter to the VRx is represented as follows:

$$\mathbf{w}_i = \mathbf{VRx}_i - \mathbf{p}^{Tx} \quad (4.18)$$

---

<sup>3</sup>this assumption is considered here for the ease of derivations. if this information is not available the estimation can still be done at the expense of additional calculation complexity



where  $\mathbf{w}_i = (x_i^w, y_i^w, z_i^w)$ . Then, we solve for the points of intersection between VRxs and the transmitter to estimate the PoRs as follows:

$$\begin{aligned} \mathbf{PoR}_i^2 &= \mathbf{p}^{Tx} + \\ &\left( \text{inv}(\text{diag}(\mathbf{n}_i^{PoR2} \cdot \mathbf{w}_i)) \times \left( \left( \mathbf{M}_{\mathbf{p}^{Rx}}^{\mathbf{VRx}_i} - \mathbf{p}^{Tx} \right) \times \mathbf{n}_i^{PoR2} \right)^T \right)^T \cdot \mathbf{w}_i \end{aligned} \quad (4.19)$$

Then, the distance traveled by each ray coming from NLoS path passing from the transmitter to the receiver through the PoR is estimated using equation (4.13). The reflection coefficient is then estimated using equation (4.14).

### 4.5.3 Correction of the Estimated Positions of PoR

After estimating the PoR, the target is to estimate the AoD and AoA so that we compare with exact results. The estimated elevation angle of AoD,  $\hat{\phi}_i^{AoD}$ , is estimated as follows:

$$\hat{\phi}_i^{AoD} = -\sin^{-1} \left( \frac{z_i^{PoR1} - z^{Tx}}{d_i^{Tx-PoR1}} \right) \quad (4.20)$$

where

$$d_i^{Tx-PoR1} = \sqrt{(x^{Tx} - x_i^{PoR1})^2 + (y^{Tx} - y_i^{PoR1})^2 + (z^{Tx} - z_i^{PoR1})^2}$$

is the distance between the estimated first PoR  $\mathbf{PoR}_1^i$  and the transmitter  $\mathbf{p}^{Tx}$ . On the other hand, the estimated elevation angle of AoA,  $\hat{\phi}_i^{AoA}$ , is estimated as follows:

$$\hat{\phi}_i^{AoA} = -\sin^{-1} \left( \frac{z_i^{PoR2} - z^{Rx}}{d_i^{Rx-PoR2}} \right) \quad (4.21)$$

where

$d_i^{Rx-PoR2} = \sqrt{(x^{Rx} - x_i^{PoR2})^2 + (y^{Rx} - y_i^{PoR2})^2 + (z^{Rx} - z_i^{PoR2})^2}$  is the distance between the estimated second PoR  $\mathbf{PoR}_2^i$  and the receiver  $\mathbf{p}^{Rx}$ . Similarly, the estimated azimuthal angles of AoA and AoD are estimated as follows respectively:

$$\hat{\theta}_i^{AoD} = \cos^{-1} \left( \frac{y_i^{PoR1} - y^{Tx}}{d_i^{Tx-PoR1}} \right) \quad (4.22)$$

$$\hat{\theta}_i^{AoA} = \cos^{-1} \left( \frac{y_i^{PoR2} - y^{Rx}}{d_i^{Rx-PoR2}} \right) \quad (4.23)$$

Then, we calculate the error between the real and estimated values of azimuthal AoD, elevation AoD, azimuthal AoA and elevation AoA, respectively, as follows:

$$\begin{cases} \epsilon_i^{HAoD} = w2\pi i \left( \hat{\theta}_i^{AoD} - \theta_i^{AoD} \right) \\ \epsilon_i^{VAoD} = w2\pi i \left( 360 - \hat{\phi}_i^{AoD} - \phi_i^{AoD} \right) \\ \epsilon_i^{HAoA} = w2\pi i \left( 360 - \hat{\theta}_i^{AoA} - \theta_i^{AoA} \right) \\ \epsilon_i^{VAoA} = w2\pi i \left( 360 - \hat{\phi}_i^{AoA} - \phi_i^{AoA} \right) \end{cases} \quad (4.24)$$

where  $w2\pi$  is a wrapping function to  $180^\circ$ . Then, the estimated first PoR  $\mathbf{PoR}_1^i$  is corrected by rotation as follows:

$$\begin{cases} \hat{x}_i^{PoR1} = \left( x_i^{PoR1} + \left( x_i^{PoR1} - x_i^{M_{PoR1}^{PoR2}} \right) \times \cos \epsilon_i^{HAoD} - \left( y_i^{PoR1} - y_i^{M_{PoR1}^{PoR2}} \right) \times \sin \epsilon_i^{HAoD} \right) \times \cos \epsilon_i^{VAoD} \\ \hat{y}_i^{PoR1} = \left( y_i^{PoR1} + \left( x_i^{PoR1} - x_i^{M_{PoR1}^{PoR2}} \right) \times \sin \epsilon_i^{HAoD} + \left( y_i^{PoR1} - y_i^{M_{PoR1}^{PoR2}} \right) \times \cos \epsilon_i^{HAoD} \right) \times \cos \epsilon_i^{VAoD} \\ \hat{z}_i^{PoR1} = z_i^{PoR1} \times \cos \epsilon_i^{VAoD} \end{cases} \quad (4.25)$$

where  $M_{PoR1}^{PoR2} = \left( x_i^{M_{PoR1}^{PoR2}}, y_i^{M_{PoR1}^{PoR2}}, z_i^{M_{PoR1}^{PoR2}} \right)$  is the midpoint between  $\mathbf{PoR}_1^i$  and  $\mathbf{PoR}_2^i$ . Similarly, the estimated second PoR  $\mathbf{PoR}_2^i$  is corrected by rotation as follows:

$$\begin{cases} \hat{x}_i^{PoR2} = \left( x_i^{PoR2} + \left( x_i^{PoR2} - x_i^{M_{PoR1}^{PoR2}} \right) \times \cos \epsilon_i^{HAoA} - \left( y_i^{PoR2} - y_i^{M_{PoR1}^{PoR2}} \right) \times \sin \epsilon_i^{HAoA} \right) \times \cos \epsilon_i^{VAoD} \\ \hat{y}_i^{PoR2} = \left( y_i^{PoR2} + \left( x_i^{PoR2} - x_i^{M_{PoR1}^{PoR2}} \right) \times \sin \epsilon_i^{HAoA} + \left( y_i^{PoR2} - y_i^{M_{PoR1}^{PoR2}} \right) \times \cos \epsilon_i^{HAoA} \right) \times \cos \epsilon_i^{VAoD} \\ \hat{z}_i^{PoR2} = z_i^{PoR2} \times \cos \epsilon_i^{VAoD} \end{cases} \quad (4.26)$$

It is worth mentioning that the reflection coefficient equivalent to the absorption loss can be estimated in the same way as in the single bounce scenario. However, it will correspond to the absorption due to two reflections.

## 4.6 Simulation Results

### 4.6.1 Simulation Environment

We define the position, orientation and antenna characteristics of the transmitter and the receiver placed in a 3D environment with reflecting and blocking obstacles. Scattering, diffraction and vertical propagation are neglected at mmWave. We use image-based ray-tracing method to trace the paths between transmitter and receiver surrounded by obstacles in a 3D environment. The carrier frequency used in  $f_c = 60GHz$  with a bandwidth of  $BW = 250MHz$ . The scenario under test consists of  $N$  transmitters and a receiver. The LoS path does not always exist. Additionally, each path is characterized by a complex amplitude gain and a delay based on environmental properties. The complex amplitude gain of a path is obtained from the transmitter and receiver antenna gain, reflection coefficient and the path attenuation. Antenna gain is related to the radiation patterns. We assume constant complex permittivity for each object.

Reflections are then computed using Fresnel's equations as a function of this permittivity and angle-of-incidence. The reflection coefficient is the product of the phase shifts and attenuations. Moreover, path attenuation is modeled by the free-space path loss (FSPL) that defines the gain of the received signal based on the propagating distance  $d$  and wavelength  $\lambda$ . The phase shift is represented as a rotation by  $d/\lambda$  in the complex plane. The antennas are assumed to have radiation pattern with  $60^\circ$  half power beam width (HPBW). In this chapter,

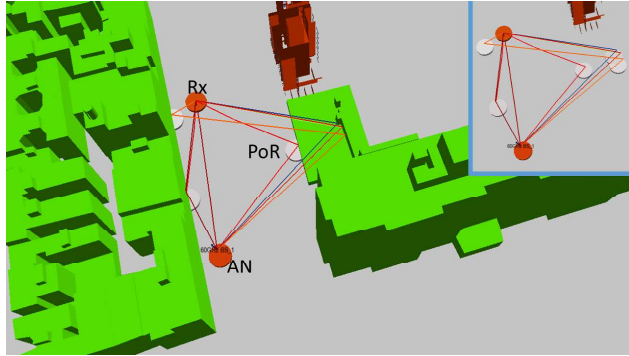


Figure 4.4: Vehicular Outdoor Environment, with PoR. The right top corner shows the PoRs without the environment

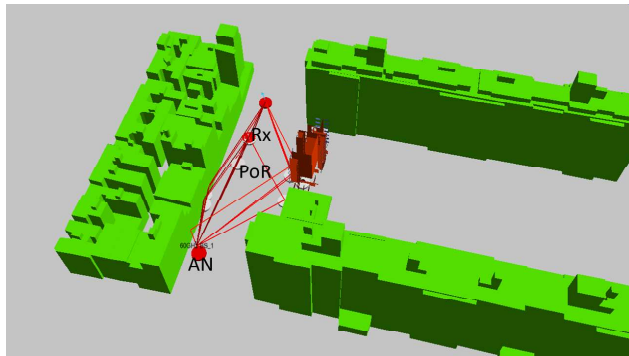


Figure 4.5: Another Vehicular Outdoor Environment showing estimated PoR

we consider two particular environments: an outdoor vehicular environment and indoor environment. Each of these environments has been recently of great research interest. Indeed, the framework of 3DLOCMAP can be directly applied in autonomous vehicles to sense and map the obstacles around and in vehicular networks for multiple purposes (detect human crossing the road, sensing the environment, traffic measurement, etc). 3DLOCMAP can be also used for robotics in indoor environment to map objects. In both applications, 3DLOCMAP acts as a radar-like system. All the simulations have been ran using the commercial S\_5G Channel Simulator<sup>©</sup> developed by Siradel.

### 4.6.2 Outdoor Vehicular Environment

The outdoor vehicular environment shown in Fig. 4.4 consists of a single AN and multiple Rx each considered as a single receiver. Only single and double bounce reflections are considered. As shown in the right top corner of Fig. 4.4, we are able to estimate the different PoRs including two PoRs for the ray induced by double bounce reflection and two PoRs for the ray induced by single bounce reflection. The result shows accurate detections of PoRs. Similarly, the results in Fig. 4.5 show the estimation of the PoR for another vehicular outdoor environment. In case of single bounce, the PoR is shown to be estimated accurately. On the other hand, the two PoRs for the double bounce case are estimated with small error. Nevertheless, the achieved information is that the received ray in this case is induced by double reflections. The estimation error is shown in Fig. 4.6 in terms root mean square error (RMSE) of estimating the PoR (given in terms of its coordinates), distance between the AN and the estimated PoR, and the distance between the AN and the estimated receiver passing through the estimated PoR. The error is shown to increase with the increase of the noise  $\sigma_{AoA}^o$  in AoA measurements. Moreover, the distance between the AN and PoR is estimated with higher error due to the estimation error of the PoR which is due to the error in the AoA. However, the distance traveled by the transmitted ray from the AN to the Rx passing through the PoR is shown to be estimated with higher accuracy since it is based on the ToA measurements and not related to the exact position of the PoR.

### 4.6.3 Indoor Environment

3DLOCMAP was also implemented in indoor environment. As shown in Fig. 4.7, the power scale shows the variation of transmitted rays in terms of RSS. The transmitted rays are first filtered based on RSS threshold value  $\gamma_{Pr}$  determined by equation (4.2), in which PFA=0.05. Hence, the rays with RSS higher than  $\gamma_{Pr}$ , shown in right top corner in Fig. 4.7, are used for estimating the Rx and PoR. Similarly, the estimation error shown in Fig. 4.8 shows higher accuracy in terms of distance traveled from AN to Rx passing through the PoR compared

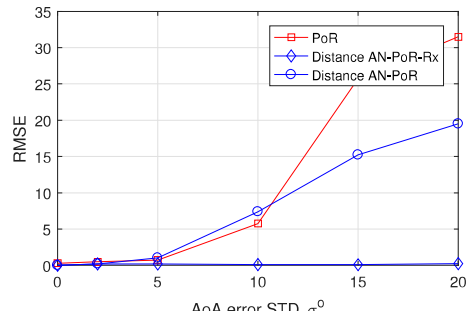


Figure 4.6: RMSE measurements for the PoR, Distance AN-PoR-Rx, Distance AN-PoR, Outdoor Vehicular Environment

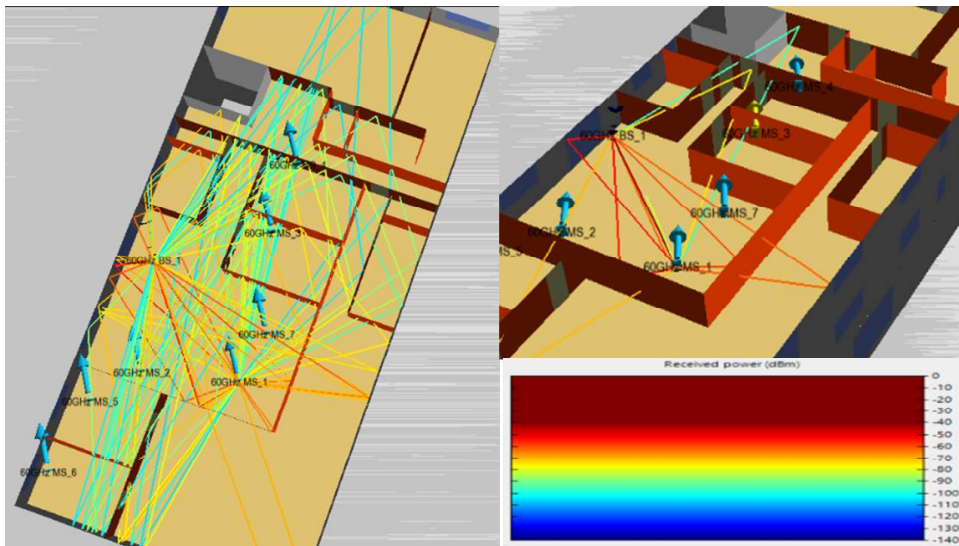


Figure 4.7: Indoor Environment

to the estimation of the distance between the AN to PoR that is estimated with additional errors. Nevertheless, indoor environment shows a higher accuracy of estimation compared to outdoor vehicular environment.

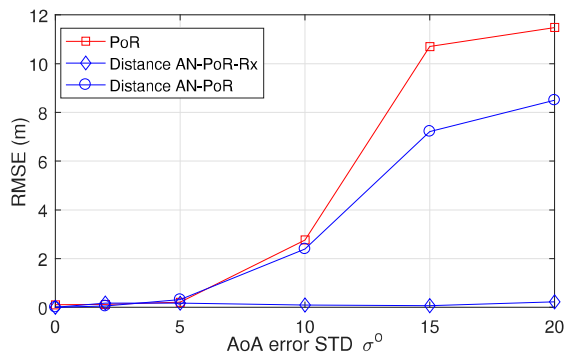


Figure 4.8: RMSE measurements for the PoR, Distance AN-PoR-Rx, Distance AN-PoR, Indoor Environment

## 4.7 Conclusion

We presented in this chapter 3DLOCMAP and its potential application in vehicular and indoor environments. We proposed a general framework to estimate the Rx position and estimate the environment through obstacle mapping. The concept of VANs has been introduced from literature to propose a first estimation of the points of reflection. Our work introduced then the concept of virtual receiver highly important in the case of double bounce reflection. The results of this chapter were provided in real scenarios using the commercial 5G Channel Simulator<sup>©</sup> developed by Siradel. The simulation results have perfectly shown that 3DLOCMAP can perfectly estimate the environment as long as the error in the AoA estimation is less than  $5^{\circ}$ . Definitely, much work could be achieved in the future. Among others, the localization, detection and classification (object, human, etc) of moving objects will be of order in the future research directions [222].

# Chapter 5

## Localization and Mapping in Mobile Environment

### 5.1 Introduction

Recently, new approaches have been considered in SLAM using mmWave frequencies due to their unique channel characteristics. Actually, it was shown that the channel at mmWave behaves as quasi-optical channel. The Line of Sight (LoS) ray is the dominant, while in None Line of Sight (NLoS), most of the power is carried by a single bounce. Furthermore, the reflections don't generate significant amount of scattering [223] and consequently Snell's law applies.

In this chapter, we consider localization and mapping in mobile environment. In this regard, tracking filters are used in order to achieve high localization and mapping accuracy. In literature, different tracking filters have been proposed and applied to handle the mobility of the mobile terminals. Kalman Filter (KF) [224] is an adaptive recursive solution for the estimation of linear Gaussian process based on Least Square Error (LSE). Nevertheless, non-linear processes are not handled with the standard KF solutions. Extended Kalman Filter (EKF), Second-order extended Kalman Filter (SEKF) [225], and Unscented Kalman Filter (UKF) are examples from the family of Kalman filters. EKF is the first extension of the KF; it performs a first order linearization of the nonlinear system and then applies the conventional KF estimation. SEKF preserves the second-order terms via the Taylor series development of the transition and measurement equations. UKF is based on selecting a set of sigma points and performing unscented transform. The conditional mean and variance are computed by UKF with third order of accuracy for Gaussian noise. Recently, cubature Kalman filter (CKF) [226] was introduced based on the utilization of a spherical radial cubature rule for estimation of the Gaussian filter. The Monte Carlo based filtering, called also particle filters, handles complex nonlinear systems [227]. Particle filters utilize a large number of independent random variables defined as particles in order to update

the posterior probability. The location, weights, and propagation of the particles are adjusted according to the Bayesian rule. Recently, nonlinear filters based on probability density function (PDF) have gained some attention since PDF captures all the statistical characteristics of a random variable. Mainly, two kinds of criteria are generally used in PDF filtering: PDF shaping and entropy minimization. PDF shaping is based on picking filtering parameters so that the PDF of the residual follows a narrow distributed zero mean Gaussian PDF [228]. On the other hand, entropy minimization techniques aim at minimizing the entropy of the filtering residual [229]-[231].

In this chapter, EKF and UKF based PDF are adopted by deriving the appropriate analytical framework of the CoRP model within a mobile context. It has been shown that our approach can reach centimeter accuracy in terms of environment mapping.

For clarification, the following notations will be used throughout this chapter:  $\mathbf{p}$  stands for positions, for example,  $\mathbf{pT}$ ,  $\mathbf{pR}$ ,  $\mathbf{pV}$  and  $\mathbf{pM}$  are respectively the positions of transmitter, receiver, Virtual Anchor Node (VAN) and midpoint between VAN and transmitter. The index  $k$  stands for time, and  $i$  stands for the  $i^{th}$  received ray.

The chapter is organized as follows. In Section 2, the framework is briefly re-described and we summarize the derivations for the geometric approach proposed in Chapter 3. The model is then extended in Section 3 to include ToA and AoA biased measurements. In Section 5, EKF is detailed and neural network is introduced in Section 6 using UKF based PDF filter. Finally, Section 6 provides simulation results and conclusion is drawn in Section 7.

## 5.2 Enhancing the Geometric SLAM Approach using EKF

As stated in Chapter 3, the steps considered in the geometric SLAM approach are summarized as follows:

- Localization of the receiver position at every time  $k$
- Estimation of the VANs
- Estimation of the PoR for every RRC  $i$

A mobile environment is considered in this chapter. Hence, we introduce in this section the use of EKF to enhance the accuracy of estimating the PoRs.

### 5.2.1 Localization of the Receiver

As stated earlier, localization of the receiver is based on simple steps derived from the relation between the geometric environment and the channel measurements.



Consider that the first received path corresponds to a LoS, the position of the receiver can be written as follows :

$$\mathbf{pR} = \mathbf{pT} + \rho_0 \begin{bmatrix} \cos(\theta_0) \\ \sin(\theta_0) \end{bmatrix} \quad (5.1)$$

where  $\mathbf{pT} = (xT, yT)$ ,  $\mathbf{pR} = (xR, yR)$ ,  $\theta_0$  is the angle of arrival corresponding to LoS path and  $\rho_0$  is the distance traveled between Tx and Rx. This latter could be easily estimated using ToA metric as follows:

$$\rho_i = c \cdot T_i \quad (5.2)$$

where  $c=3 \cdot 10^8$ m/s is the speed of light, and  $T_i$  is the ToA for  $i^{th}$  ray, where  $i = 0$  corresponds to the LoS.

### 5.2.2 Estimation of the VANs positions

The VANs are the mirrors of real anchors (transmitter) with respect to obstacles, such as room boundaries. Using Fig. 5.1, the estimation of the VAN position is given by:

$$\begin{cases} xV_i = xR + \rho_i \cdot \cos(\theta_i) \\ yV_i = yR + \rho_i \cdot \sin(\theta_i) \end{cases} \quad (5.3)$$

or equivalently,

$$\mathbf{pV}_i = \mathbf{pR} + \rho_i \begin{bmatrix} \cos(\theta_i) \\ \sin(\theta_i) \end{bmatrix} \quad (5.4)$$

where  $\mathbf{pV}_i = (xV_i, yV_i)$  is the VAN corresponding to the  $i^{th}$  NLoS ray and  $\rho_i$  is the distance between Tx and Rx for NLoS.

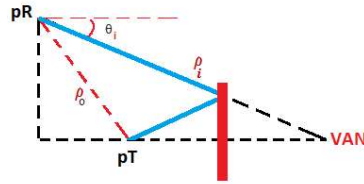


Figure 5.1: Virtual Anchor Node as a mirror to Tx

### 5.2.3 Obstacle Mapping through the CoRP

Once the VANs positions are estimated, the problem turns out then to find the PoRs on the environment boundaries (and maybe the obstacles in the environment). As estimated in Chapter 3 section 3.4.2, the PoRs are simply points of intersection between the perpendicular bisector of the line connecting the transmitter and each estimated VAN and, the line connecting the VANs and the receiver at each time  $k$ .

Fig. 5.2 shows the calculated PoRs positions,  $\mathbf{pS}_i$ , in ideal channel measurements (i.e. without any bias). It can be clearly seen that the proposed algorithm is able to exactly retrieve these positions.

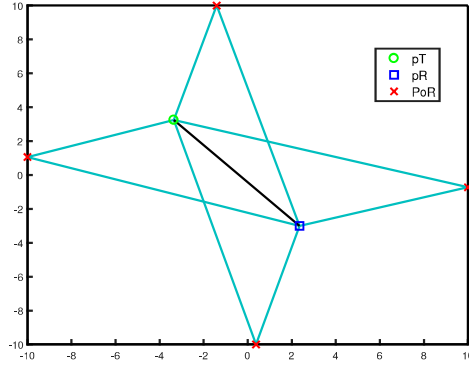


Figure 5.2: Exact positions of PoRs

### 5.2.4 Points of Reflection in Presence of Metric Estimation Bias

Starting with equation (3.44), the estimated  $\mathbf{pS}_i$  in the presence of measurement noise (e.g. AoA error), can be written as follows:

$$\widehat{\mathbf{pS}}_i = \mathbf{pS}_i + \Delta\mathbf{pS}_i \quad (5.5)$$

where

$$\Delta\mathbf{pS}_i = \Delta\mathbf{pR} + \text{inv}(\text{diag}(\mathbf{n}_i \cdot \mathbf{w}_i)) \cdot \left( \left( - \left( \frac{\Delta\mathbf{pR} - \Delta\mathbf{w}_i}{2} \right) \cdot \mathbf{n}_i - \Delta\mathbf{pV}_i \cdot \mathbf{q}_i \right) \mathbf{w}_i + (\mathbf{q}_i \cdot \mathbf{n}_i) \Delta\mathbf{w}_i \right) \quad (5.6)$$

where  $\mathbf{q}_i$ , the vector passing through  $\mathbf{pR}$  and the midpoint between  $\mathbf{pT}$  and  $\mathbf{pV}_i$ ;  $\mathbf{n}_i$ , the normal to the point of reflection  $\mathbf{S}_i$ ;  $\mathbf{w}_i$ , the vector crossing the point of

reflection  $\mathbf{pS}_i$  to the virtual receiver defined as the mirroring point of the receiver with respect to the obstacle, are defined as follows:

$$\mathbf{q}_i = \begin{bmatrix} \frac{xT+xV_i}{2} - xR \\ \frac{yT+yV_i}{2} - yR \end{bmatrix} \quad (5.7)$$

$$\mathbf{n}_i = \mathbf{pT} - \mathbf{pV}_i \quad (5.8)$$

$$\mathbf{w}_i = \mathbf{pV}_i - \mathbf{pR} \quad (5.9)$$

The errors of estimation  $\Delta\mathbf{pR}$ ,  $\Delta\mathbf{pV}_i$  and  $\Delta\mathbf{w}_i$  for estimating  $\mathbf{pR}$ ,  $\mathbf{pV}_i$  and  $\mathbf{w}_i$  are calculated based on the error on either the AoA measurements or TDoA measurements.

#### 5.2.4.1 PoR Estimation in Presence of AoA Bias

Assuming a biased estimation of the AoA, the error  $\Delta\mathbf{pR}$  of estimating the receiver is given as follows :

$$\Delta\mathbf{pR} = \epsilon_\theta \cdot \rho_0 \begin{bmatrix} -\sin \theta_0 \\ \cos \theta_0 \end{bmatrix} \quad (5.10)$$

where  $\epsilon_\theta$  is the AoA error in radians. Hence,  $\Delta\mathbf{pR}$  imposes an error  $\Delta\mathbf{pV}_i$ , the error of estimating the VAN  $\mathbf{pV}_i$  as:

$$\Delta\mathbf{pV}_i = \epsilon_\theta \left( \rho_0 \begin{bmatrix} -\sin \theta_0 \\ \cos \theta_0 \end{bmatrix} + \rho_i \begin{bmatrix} -\sin \theta_i \\ \cos \theta_i \end{bmatrix} \right) \quad (5.11)$$

Moreover, the error in AoA measurements impose an error of  $\Delta\mathbf{w}_i$  for estimating  $\mathbf{w}_i$  calculated as:

$$\Delta\mathbf{w}_i = \epsilon_\theta \cdot \rho_i \begin{bmatrix} -\sin \theta_i \\ \cos \theta_i \end{bmatrix} \quad (5.12)$$

Thus, the PoRs are estimated with error as shown in Figure 5.3:

#### 5.2.4.2 PoR Estimation in Presence of TDoA Error

On the other hand, assuming error in TDoA,  $\Delta\mathbf{pR}$  is given by:

$$\Delta\mathbf{pR} = c \cdot \epsilon_t \cdot \begin{bmatrix} \sin \theta_0 \\ \cos \theta_0 \end{bmatrix} \quad (5.13)$$

where  $c$  is the speed of light,  $\epsilon_t$  is the TDoA error in radians. Similarly,  $\Delta\mathbf{pR}$  imposes an error  $\Delta\mathbf{pV}_i$  that is:

$$\Delta\mathbf{pV}_i = c \cdot \epsilon_t \cdot \left( \begin{bmatrix} \sin \theta_0 \\ \cos \theta_0 \end{bmatrix} + \begin{bmatrix} \sin \theta_i \\ \cos \theta_i \end{bmatrix} \right) \quad (5.14)$$

Finally, the error in TDoA measurements impose an error of  $\Delta\mathbf{w}_i$  for estimating  $\mathbf{w}_i$  calculated as:

$$\Delta\mathbf{w}_i = c \cdot \epsilon_t \cdot \begin{bmatrix} \sin \theta_i \\ \cos \theta_i \end{bmatrix} \quad (5.15)$$

Hence, the PoRs are estimated with error as shown in Figure 5.4:

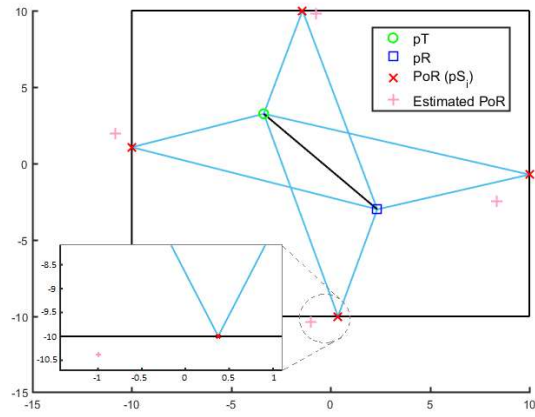


Figure 5.3: Estimated positions of PoR with AoA bias at  $\sigma = 5^\circ$

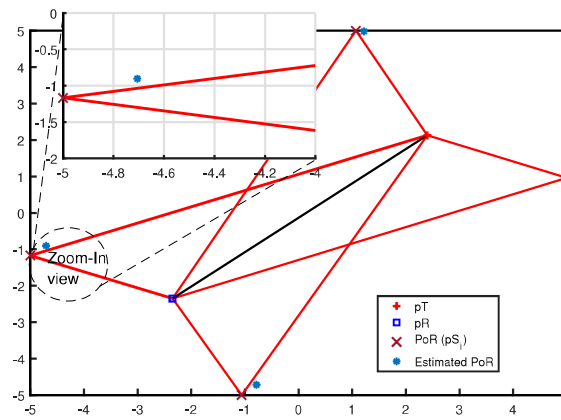


Figure 5.4: Estimated positions of PoR with ToA bias at  $\sigma = 1$  ns

### 5.2.5 Extended Kalman Filter in Tracking the PoRs

Accurate mapping is quite a challenging task in biased measurements. As seen in Fig. 5.6 and 5.11, a biased ToA or AoA leads to high error in the environment mapping. Hence, it is very important to improve the estimation accuracy from one side and adapt the mapping to mobile conditions.

To solve this problem and extend our work to a SLAM approach, the EKF has been developed. Indeed, EKF can efficiently work in non-linear systems, it has very low memory requirement and computation complexity compared to other Bayesian positioning and tracking algorithms such as Particle Filter (PF).

In order to perform the EKF filter, it is very important to derive both the hidden and observational processes due to bias. The main challenge therein is to have a model of the PoR  $\mathbf{pS}_i$  with respect to the mobile receiver position. The processes of the EKF filter are described as:

$$\begin{aligned}\mathbf{pR}_k &= f(\mathbf{pR}_{k-1}) + \mathbf{Q}_{k-1} \\ \mathbf{pS}_{i_k} &= h(\mathbf{pR}_k) + \mathbf{R}_{k-1}\end{aligned}\quad (5.16)$$

where  $f$  and  $h$  are the hidden and the observational processes of PoR respectively, and they are defined as follows:

$$\begin{aligned}f &= \begin{bmatrix} xR \\ yR \end{bmatrix} \\ h &= \begin{bmatrix} xR \\ yR \end{bmatrix} + d_{(\mathbf{pS}_i, \mathbf{pR})} \begin{bmatrix} 1 \\ \tan\theta_i \end{bmatrix}\end{aligned}\quad (5.17)$$

$\mathbf{Q}$  and  $\mathbf{R}$  represent the covariance matrices of the two processes.

#### Proof of equation (5.17)

The problem turns out in finding a relation between  $\mathbf{pS}_i$  and  $\mathbf{pR}$ . Starting with equations equation (5.1), we can write:

$$\begin{cases} \widehat{xS}_i = \widehat{xR} + d_{(\mathbf{pS}_i, \mathbf{pR})} \\ \widehat{yS}_i = \widehat{yR} + d_{(\mathbf{pS}_i, \mathbf{pR})} \cdot \tan\theta_i \end{cases}\quad (5.18)$$

where the difference between  $\mathbf{pS}_i$  and  $\mathbf{pR}$  is given by :

$$d_{(\mathbf{pS}_i, \mathbf{pR})} = \frac{(\rho_i^2 - \rho_0^2)}{2(\rho_0 \cos\theta_0 + \rho_i \cos\theta_i) + \tan\theta_i(\rho_0 \sin\theta_0 + \rho_i \sin\theta_i)}\quad (5.19)$$

Hence, the estimated position of the receiver is given by:

$$\widehat{\mathbf{pR}} = \mathbf{pR} + \mathbf{d}_{pR}\quad (5.20)$$

### For ToA

where  $\mathbf{d}_{pR} = c\varepsilon_0 \cdot \begin{bmatrix} \cos(\theta_0) \\ \sin(\theta_0) \end{bmatrix}$  is the error of estimating  $\mathbf{pR}$ .

### For AoA

where  $\mathbf{d}_{pR} = \rho_0\mu_0 \cdot \begin{bmatrix} -\sin(\theta_0) \\ \cos(\theta_0) \end{bmatrix}$  is the error of estimating  $\mathbf{pR}$ .

By substituting equation (5.20) in equation (5.18), the estimated positions of  $\mathbf{pS}_i$  in terms of  $\mathbf{pR}$  yields:

$$\widehat{\mathbf{pS}}_i = \mathbf{pR} + d_{(\mathbf{pS}_i, \mathbf{pR})} \cdot \begin{bmatrix} 1 \\ \tan\theta_i \end{bmatrix} + \mu \cdot \begin{bmatrix} e_{xS} \\ e_{yS} \end{bmatrix} \quad (5.21)$$

or equivalently:

$$\widehat{\mathbf{pS}}_i = \mathbf{pR} + d_{(\mathbf{pS}_i, \mathbf{pR})} \begin{bmatrix} 1 \\ \tan\theta_i \end{bmatrix} + \mathbf{dS}_i \quad (5.22)$$

where  $\mathbf{dS}_i = \mu \cdot \begin{bmatrix} e_{xS} \\ e_{yS} \end{bmatrix}$  is the error for estimating  $\mathbf{pS}_i$ .

## 5.3 Improvement by Neural Network: UKF filter with MEC

EKF was not sufficient to enhance the results for highly non-linear systems. For that was the Unscented Kalman Filter (UKF), it takes a bunch of points called sigma points and approximate it with a fact that more the number of points, more precise our approximation will be. The conditional mean and variance are computed by UKF with third order of accuracy of Gaussian noises and at least second order for non-Gaussian.

On the other hand, Monte Carlo based filtering (also called particle filters), handles complex nonlinear systems. It is based on using huge number of independent random variables, that are the particles, to represent and update posterior probability by adjusting there location, weight and propagation according to Bayesian rule. Unfortunately, there are no basic rules to know how to design a proposal distribution. In addition to that, a large number of particles is required to achieve satisfying results, which also means highly complex computations.

A sampling method, known by Unscented transformation (UT) method, is used by UKF to define the considered wighted sigma points because when a Gaussian is passed through a non linear function, it does not remains a Gaussian anymore but we will use UT to approximate the Gaussian from the resulting figure . Steps

of UT transformation method are summarized as follows :

1. Compute Set of Sigma Points
2. Assign Weights to each sigma point
3. Transform the points through non linear function
4. Compute Gaussian from weighted and transformed points
5. Compute Mean and Variance of the new Gaussian.

Recently, nonlinear filters based on probability density functions (PDF) attracted the attention of researches since they capture all statistical characteristics of a random variable. PDF shaping and entropy minimization are two kinds of criteria that can be used in PDF filtering. PDF shaping depend on selecting filtering parameters so that the PDF of the residual follows a narrow distributed zero mean Gaussian PDF. Whereas, entropy minimization minimizes the entropy of the filtering residual (Figure 5.5). Despite its advantage, PDF filter can only guarantee local optimum. Convergence of global optimum can be guaranteed by combining both UKF and PDF filtering, as we will discuss later. Despite

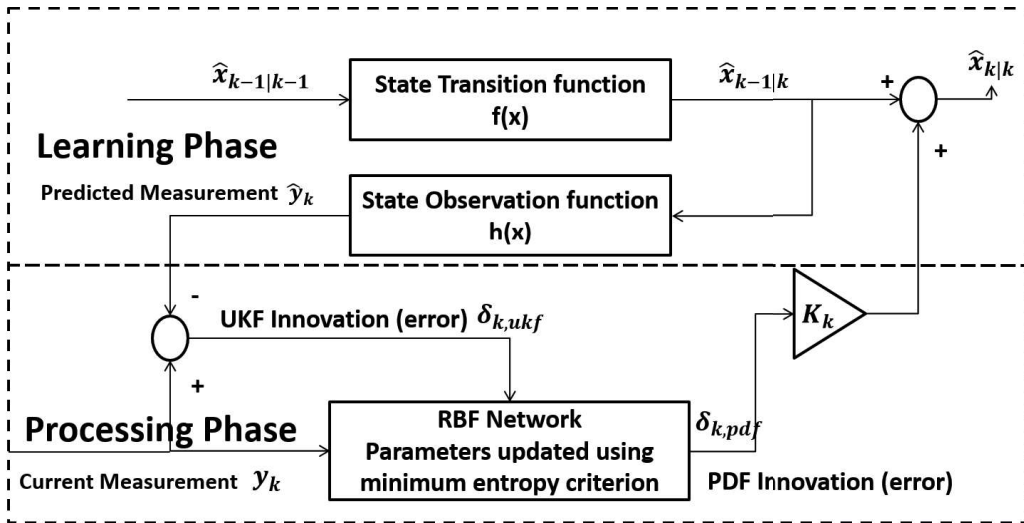


Figure 5.5: schematic of UKF based PDF filter

its good performance under Gaussian noises, UKF fail to perform under non-Gaussian noises. It is already known that UKF ensures a third order accuracy, but to improve its performance, an additional term should be added based on the higher order moment of approximation error. At the same time, highly complex computations are required for particle filters (PF) [29] to deal with non-Gaussian

non-linear systems. PF use a large number of independent particle variables to update the posterior probability.

The aim of our work is to reduce the shortcoming of the UKF and PDF getting an optimal estimation based on minimum entropy criterion. For that a UKF based on PDF filter is proposed to ensure convergence to global optimum. This combination is divided into two parts : prediction of error in UKF represented by  $v^{ukf}$  and output of an RBF-network whose weights are tuned by the entropy of innovation itself represented by  $v^{pdf}$ .

### 5.3.1 Basic Concepts

We consider the PDF of random vector  $\mathbf{x}$  in Lebesgue measure is represented by  $p(x)$ .  $x_k$  represents the true state in time step  $k$ ; while  $\hat{x}_k$  (or  $x_{k|k}$ ) and  $x_{k|(\hat{k}-1)}$  stands for filtered and predicted state of  $x_k$ .

#### 5.3.1.1 Probability Density Function

Probability density can be estimated by several methods. Kernel density estimation (KDE) , also known by Parzen window method, is one of these estimation methods that we will use because of its relationship with Renyi's entropy [26]. The estimation of probability density function from samples using KDE is expressed as follows:

$$f(x) = \frac{1}{N} \sum_{i=1}^N G_{\sigma}(x - x_i) \quad (5.23)$$

where  $G_{\sigma}$  is the kernel function with bandwidth  $\sigma$  and  $(x_1, \dots, x_N)$  are the samples. The kernel should be non-negative real valued integrable function preserving the following conditions:

- $\int_{-\infty}^{+\infty} G_{\sigma}(x)dx = 1$
- $G_{\sigma}(-x) = G_{\sigma}(x), \forall x$

Output of KDE is guaranteed as a probability density function by the first condition; whereas stability of the expectation of process is guaranteed by the second condition. Different kernel functions can be used; as uniform, triangular, Gaussian.. This latest, which is Gaussian kernel, is most commonly used and expressed as follows:

$$G_{\sigma}(x) = \frac{1}{\sqrt{2\pi}\sigma} \exp\left(-\frac{x^2}{2\sigma^2}\right) \quad (5.24)$$



Concerning the KDE, the bandwidth is more important than the kernel function. The mean and variance of the estimated PDF are expressed as follows:

$$\begin{aligned} Bias[\hat{p}(x)] &= E[\hat{p}(x)] - p(x) \approx \frac{\sigma^2}{2p''(x)C_1} \\ Var[\hat{p}(x)] &= E[(\hat{p}(x) - E[\hat{p}(x)])^2] \approx \frac{1}{N\sigma} C_2 p(x) \end{aligned} \quad (5.25)$$

where  $p''$  is the second order derivative of PDF, and  $C_1$  and  $C_2$  are constants related to specific kernel. According to these equations, an equalization between low bias and low variance is the best choice of the bandwidth since it influence them in opposite manners[27]. Mean integrated square error (MISE) is widely used to select the appropriate bandwidth. Its equation is given by:

$$MISE(\sigma) = arg \min_{\sigma} E \int (\hat{p}_{\sigma}(x) - p(x))^2 dx \quad (5.26)$$

Bandwidth for Gaussian Kernel is simply selected as follows:  $\sigma = 0.2\hat{\sigma}$  or  $\sigma = \hat{\sigma}(4N^{-1}(2d+1)^{-1})^{\frac{1}{d+4}}$  where  $\sigma$  is the data standard deviation,  $N$  is the number of samples, and  $d$  is the dimensionality of the data [28].

### 5.3.1.2 Renyi's Entropy and Minimum Entropy Criterion

By theory, entropy is the measure of uncertainty relative to random variables. Shannon entropy, Hartley entropy, Min-entropy and Renyi's entropy are definitions of entropy introduced for various purposes. Usually, Renyi's entropy is used to quantify randomness of random variable, and its defined as follows:

$$H_{\alpha} = \frac{1}{1-\alpha} \log \int p^{\alpha}(x) dx, \quad (5.27)$$

where order  $\alpha > 0$  and  $\alpha \neq 1$ . The most common used type of Renyi's entropy the quadratic, where  $\alpha = 2$ . It is given by:

$$H_2 = -\log \int p^2(x) dx, \quad (5.28)$$

Using KDE, probability density of  $\mathbf{x}$  is estimated as given below:

$$p(x) = \frac{1}{N} \sum_{i=1}^N G_{\Sigma}(x - x_i) \quad (5.29)$$

where  $G_{\Sigma}$  is the Gaussian function defined by the following equation:

$$G_{\Sigma}(x - x_N) = (2\pi)^{-\frac{n}{2}} (\det \Sigma)^{-\frac{1}{2}} \exp\left\{-\frac{1}{2}(x - x_i)^T \Sigma^{-1}(x - x_i)\right\} \quad (5.30)$$

Hence, Renyi's quadratic entropy is figured using KDE as shown below:

$$\begin{aligned}
H_2 &= -\log \int \left( \frac{1}{N} \sum_{i=1}^N G_{\Sigma}(x - x_i) \right)^2 dx \\
&= -\log \frac{1}{N^2} \int \left( \sum_{i=1}^N \sum_{j=1}^N G_{\Sigma}(x - x_i) G_{\Sigma}(x - x_j) \right) dx \\
&= -\log \frac{1}{N^2} \sum_{i=1}^N \sum_{j=1}^N \int G_{\Sigma}(x - x_i) G_{\Sigma}(x - x_j) dx \\
&= -\log \frac{1}{N^2} \sum_{i=1}^N \sum_{j=1}^N \int G_{\sqrt{2}\Sigma}(x_i - x_j)
\end{aligned} \tag{5.31}$$

where the last equality is based on the fact that the convolution of two Gaussian functions is also Gaussian [27].

For accuracy of estimation, the main criteria to figure the deviation between the estimation and the true value is the mean square error (MSE). Although that, it only looks after the second moment of the error. Using MSE in non-Gaussian environments cannot give the optimal solution needed. To solve this issue, it is proposed to use minimum error entropy (MEE) where it measures the dispersion of a random variable. This latest should give the sharpest error PDF since peaky error PDF are given by low entropy, however spread error PDF results from higher entropy (such as MSE).

Information potential, defined as the argument of the logarithmic in quadratic Renyi's entropy is given below:

$$\begin{aligned}
\psi(x) &= \frac{1}{N^2} \sum_{i=1}^N \sum_{j=1}^N G_{\Sigma}(x_i - x_j) \\
H_2(x) &= -\log \psi(x)
\end{aligned} \tag{5.32}$$

Note that  $\sqrt{2}$  is omitted for simplicity. Hence, to minimize the entropy we should maximize the information potential since the logarithmic function is a monotonic increasing function.

## 5.3.2 UKF based PDF Filter with MEC

### 5.3.2.1 System Model

Consider the following non-linear system:

$$\begin{aligned}
x_k &= f(x_{k-1}) + q_{k-1} \\
y_k &= h(x_k) + r_k
\end{aligned} \tag{5.33}$$

where  $x_k$  represents the state vector,  $y_k$  the measurement,  $q_{k-1}$  and  $r_k$  are respectively the process noise and measurement noise.

Difference terms in UKF, describing errors, are expressed as follows:

- $e_k^- = x_k - x_{k|k-1}$  known as prior error
- $e_k = x_k - x_{k|k}$  known as posterior error
- $v_k = y_k - \hat{y}_k$  known as innovation which describes the discrepancy between the measurement and the predicted measurement.

The UKF gain is considered in a way that posterior error covariance is minimized. Innovation term  $v_k$  is not expected to be Gaussian in non-linear and non-Gaussian systems. This work suggest adding neural network  $v_k^{pdf}$  term to the innovation knowing that the weight matrix of this term is adjusted by minimizing entropy criterion, which lead to minimization in randomness and entropy of innovation. Only innovation term is changed in this algorithm, and PDF part is added.

Tuning RBF weight was expected to be with MSE; however, MSE provide same accuracy as UKF (no better results) because it is a second order algorithm. The minimum entropy criterion (MEC) was replaced to deal with nonlinear stochastic systems.

The equation below represents the innovation term with added PDF term:

$$\begin{aligned} v_k &= v_k^{ukf} + v_k^{pdf} \\ &= y_k - \hat{y}_k + v_k^{pdf} \end{aligned} \quad (5.34)$$

Assuming that the input to the network is the UKF innovation as follows:

$$I_k = v_k^{ukf} \quad (5.35)$$

The neural network is then defined as follows:

$$v_k^{pdf} = W_k^T \Phi(I_k) \quad \text{where } W_k \in R^{p \times m} \quad (5.36)$$

which represent weight matrix of the RBF-network.

### 5.3.2.2 RBF and Weights

In order to achieve unbiased estimation, the additional term  $v_k^{pdf}$  should have zero mean. However, unlike MSE, MCE doesn't ensure to have an expectation of  $v_k^{pdf}$  equals to zero in terms of estimation error. For that, new constraints should be introduced to have expectations of  $v_k^{pdf}$  equals to zero.

Let's consider the RBF network  $y = W^T \Phi(x) R^n \rightarrow R^m$  defined as follows:

$$W = [w_1, w_2, \dots, w_{2p}]^T \quad (5.37)$$

$$\Phi(x) = [\varphi_1, \varphi_2, \dots, \varphi_{2p}]^T \quad (5.38)$$

$$\varphi_i(x) = \exp\left(-\frac{\|x - c_i\|^2}{\sigma_{rbf}^2}\right), i = 1, 2, \dots, 2p \quad (5.39)$$

If  $c_i$  and  $w_i$  are symmetrically distributed, we can say :

$$\begin{aligned} c_i &= -c_{2p-i} + 1 \\ w_i &= -w_{2p-i} + 1 \end{aligned} \quad (5.40)$$

Then for any stochastic input with symmetric PDF distribution, RBF network will have a zero-mean distribution as shown below:

$$E[y] = E[W^T \Phi(x)] = E\left[\sum_{i=1}^{2p} w_i \varphi_i(x)\right] \quad (5.41)$$

Substituting equation (5.38) and equation (5.39) in equation (5.41), the following mean is obtained:

$$E[y] = \sum_{i=1}^{2p} w_i E[\varphi_i(x) - \varphi_{2p-i+1}(x)] \quad (5.42)$$

Assume that  $p(x)$  is the PDF of  $x$ , the mean of the PDF term will be equal to zero as shown below where  $\varphi_{2p-i+1}(x)$  and  $p(x)$  are odd and even functions of  $x$  respectively.

$$\begin{aligned} E[\varphi_i(x) - \varphi_{2p-i+1}(x)] &= \int p(x) [\varphi_i(x) - \varphi_{2p-i+1}(x)] dx = 0 \\ E[y] &= \sum_{i=1}^{2p} w_i E[\varphi_i(x) - \varphi_{2p-i+1}(x)] = 0 \end{aligned} \quad (5.43)$$

In conclusion, if we have symmetrically distributed condition for the RBF network, the term  $v_k^{pdf}$  achieves a zero mean since the input to the network is sigma-point innovation with a symmetric PDF.

### 5.3.2.3 Pseudo Innovation

As mentioned previously, the innovation term changed to the following form:

$$v_k = v_k^{ukf} + W_k^T \Phi(I_k) \quad (5.44)$$

where  $W_k$  is the weight vector, that would be different for every  $k$ . However, to obtain PDF estimation a series of measurements has to be taken. Hence, to solve this problem, pseudo innovation is introduced instead of real innovation.

At time step  $k$ , the pseudo innovation is expressed as follows based on equation (5.34)

$$PI_i^k = v_i + [W_k^T - W_i^T] \Phi(I_i) = v^{ukf} + W_k^T \Phi(I_i) \quad \text{for } k - N + 1 \leq i \leq k \quad (5.45)$$

where  $N$  is the number of samples used in the estimation of PDF. Thus, we obtain the pseudo innovation term  $s_i^k$  that represents the former error time step  $k$ . Since they share the same linearly dependent term  $W_k^t$ , and due to its simple use in the estimation of PDF and the adaptive tuning process;  $s_i^k$  is introduced.

### 5.3.3 Entropy Based Non-Linear Filtering

To reduce the uncertainty from the innovation term, minimum entropy criterion is used. Ideally, PDF of the innovation has to be Gaussian with unbounded innovation or uniform with bounded term. Because of the contaminated measurements, these results are practically not achieved. To solve this problem, minimization of error entropy (MEE) should be solved as follows given a sequence of pseudo innovation data  $s_j^k$  and input  $I_k$ :

$$\min_W H(PI) \quad s.t. \quad s = v^{ukf} + W^T \Phi(I) \quad (5.46)$$

$H(\cdot)$  is the Renyi's quadratic entropy and  $W$  is the weight of the neural network. As done previously, we replace the minimization of the entropy with the maximization of the information potential, which gives:

$$\min_W H(PI) = \max_W \psi(PI) \quad (5.47)$$

The locally optimal weight is obtained by the following equation:

$$\frac{\partial \psi(PI)}{\partial W} = 0 \quad (5.48)$$

Actually, optimal solution is obtained iteratively for on-line processing; so the adaptive law is written as shown below by using gradient descent method:

$$W_{k+1} = W_k + \mu \cdot \nabla_W \psi(PI^k) \quad (5.49)$$

The potential information of the pseudo innovation at time step  $k$  is calculated by the following equation:

$$\psi(PI^k) = \frac{1}{N^2} \sum_{i=k-N+1}^k \sum_{j=k-N+1}^k G_\Sigma(PI_i^k - PI_j^k) \quad (5.50)$$

For simplicity, we represent  $\Phi(I_k)$  by  $\Phi(k)$ . Then the gradient of the information potential is expressed as follows:

$$\begin{aligned} \nabla_W \psi(PI^k) &= \frac{\partial}{\partial W} \left( \frac{1}{N^2} \sum_{i=k-N+1}^k \sum_{j=k-N+1}^k G_\Sigma(PI_i^k - PI_j^k) \right) \\ &= \frac{1}{N^2} \sum_{i,j=k-N+1}^k \frac{\partial G_\Sigma(PI_i^k - PI_j^k)}{\partial (PI_i^k - PI_j^k)} \frac{\partial (PI_i^k - PI_j^k)}{\partial W} \\ &= \left[ -\frac{1}{N^2} \sigma^{-1} \sum_{i,j=k-N+1}^k G_\Sigma(PI_i^k - PI_j^k) [\Phi(i) - \Phi(j)] (PI_i^k - PI_j^k)^T \right] \end{aligned} \quad (5.51)$$

### 5.3.4 Algorithm Summary

The algorithm can be summarized as follows:

- Select parameters for the UKF
- Choose the kernel bandwidth  $\epsilon$  (a diagonal matrix normally) and other parameters of the RBF network, the initial value of which is set to  $W1 = 0$
- Use UKF method to obtain  $x_k^{ukf}$  and equation (5.36) to obtain  $v_k$
- Modify the state estimation by  $x_k = x_k^{ukf} + K_k W_k^T \Phi(k)$
- Record  $W_k, \Phi(k)$  and  $v_k$  at each time step  $k$ .
- Construct the pseudo innovation  $PI_i^k = v_i^{ukf} + W_k^T \Phi(i)$  using the recorded information.
- Update  $W$  using equation (5.41) and equation (5.43) by the properly chosen  $\mu$
- $t + 1 \rightarrow t$  and go back to equation (5.25)

## 5.4 Simulation Results

We consider in this work a 2D indoor environment consisting of a room of known geometry (10x10), bounded by 4 walls and having one transmitter placed at  $\mathbf{pT}$ . A mmWave ray-tracing tool has been used and corresponding channel measurements were recorded at each position  $\mathbf{pR}_k$ . The simulation results are given in terms of the Mean Square Error (MSE) and provided first with and without EKF filtering, then work is extended to UKF based PDF filtering.

### 5.4.1 EKF-SLAM Results

In this section, we aim at evaluating the importance of the EKF in mapping. We do so by evaluating the estimated PoRs. For simplicity purposes, the scenario shown in Fig. 5.7 is adopted. In this figure, the estimated PoR before and after EKF are shown. Moreover, Fig. 5.8 shows the RMSE for estimating the CoRP with and without EKF adopted in the previous sections for different values of the TDoA and AoA estimation bias.

All results are recorded in terms of the ToA standard deviation  $\sigma = [0.5, 2, 4, 8]ns$  and averaged over 500 positions.

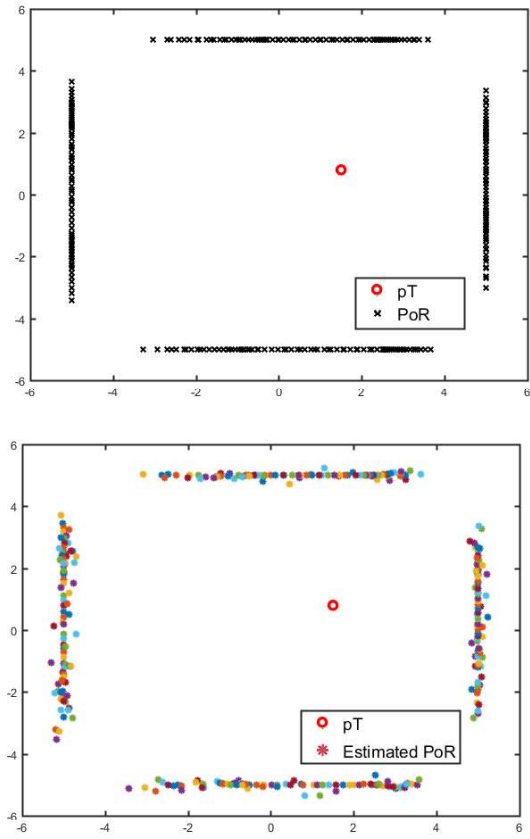


Figure 5.6: The cloud of reflection points with static transmitter and moving receiver: without ToA bias (top) and with ToA bias (bottom)

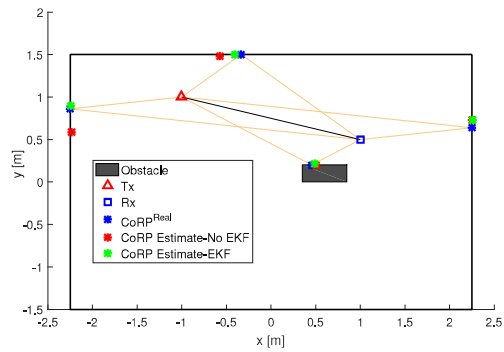


Figure 5.7: Indoor scenario for CoRPs' Estimation

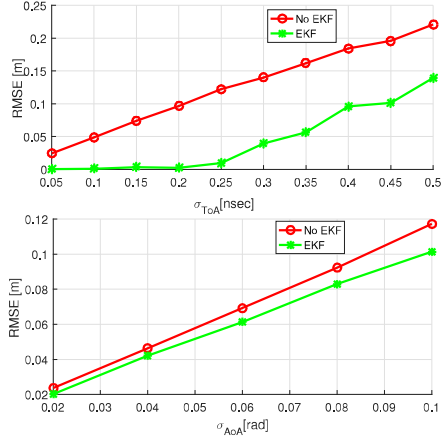


Figure 5.8: RMSE for estimating Point of Reflections versus  $\sigma_t$  and  $\sigma_\theta$

Figure 5.11 shows the CoRP with and without ToA bias when the receiver is moving in the different directions of the environment. It is very clear that a simple filtering such as K-means solution can be applied to exactly map the environment. Fig. 5.9 gives the MSE of the results without EKF and with EKF running over 1 iteration while Fig.5.10 is provided with 10 iterations. Both figures show that MORSEL framework presents a good mapping accuracy. The latter could be improved by EKF and can even reach few cm even with high ToA bias. It is worth mentioning that due to the large bandwidth available at mmWave, the paths resolvability is very high which means a reduced error in ToA measurements. All results are recorded in terms of the AoA standard deviation

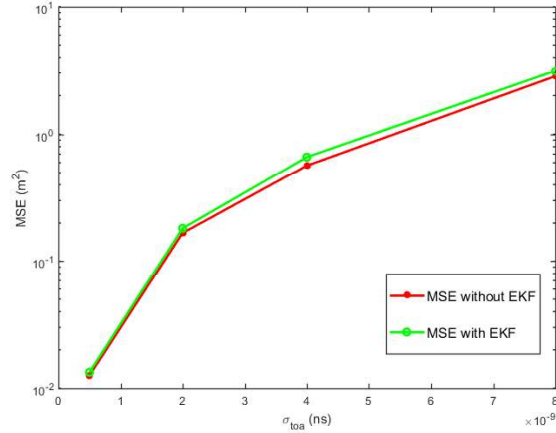


Figure 5.9: MSE ( $m^2$ ) vs  $\sigma$  of ToA ( $ns$ ), EKF with 1 iteration

$\sigma = [1, 5, 15, 25]degree$  and averaged over 100 positions.



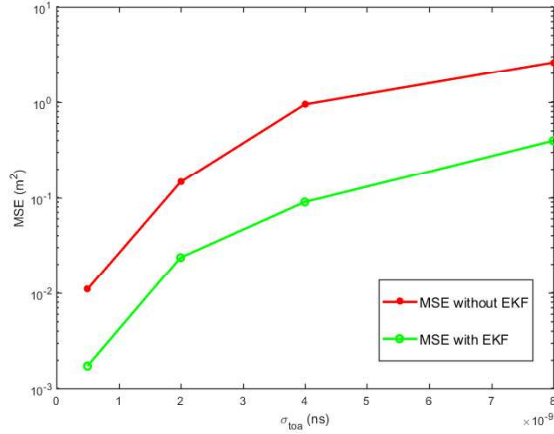


Figure 5.10: MSE ( $m^2$ ) vs  $\sigma$  of ToA ( $ns$ ), EKF with 10 iterations

Figure 5.11 shows the CoRP with and without AoA bias when the receiver is moving in the different directions of the environment. It is very clear that a simple filtering such as K-means solution can be applied to exactly map the environment. Fig. 5.12 gives the MSE of the results without EKF and with EKF running over 1 iteration while Fig.5.13 is provided with 5 iterations. Both figures show that this framework presents a good mapping accuracy. The latter could be improved by EKF and can even reach few cm even with high AoA bias. It is worth mentioning that due to the large bandwidth available at mmWave, the paths resolvability is very high which means a reduced error in AoA measurements.

### 5.4.2 UKF based PDF Results

First, we must choose the parameters of the PDF filter: We take the step size = 0.2, the number of iterations= 100, Kernel bandwidth = 0.02, and the number of the RBF =20, for 400 sample we obtain these results. Since both the process noise and the measurement noise are not Gaussian,the UKF cannot lead to satisfactory performance.PDF lter starts from 400th sample point, the time before which is used to gather data and wait for the UKF to settle down. It takes about 150 points for the PDF lter to reach its optimum, which means that Renyis entropy of the innovation is minimized. The output error term is shown in Fig.5.14. The non-Gaussianity of process and measurement noises leads to an unsatisfactory performance of the UKF.However,by introducing PDF lter, the innovation term is greatly decreased after time step 150. Fig. 5.15 depicts the PDF of the innovation term with UKF only and with proposed UKF based PDF filter. It can be seen that under the PDF lter,the probability density of the innovation is shaped into a Gaussian like one. Moreover, UKF based PDF filter enhances the accuracy of

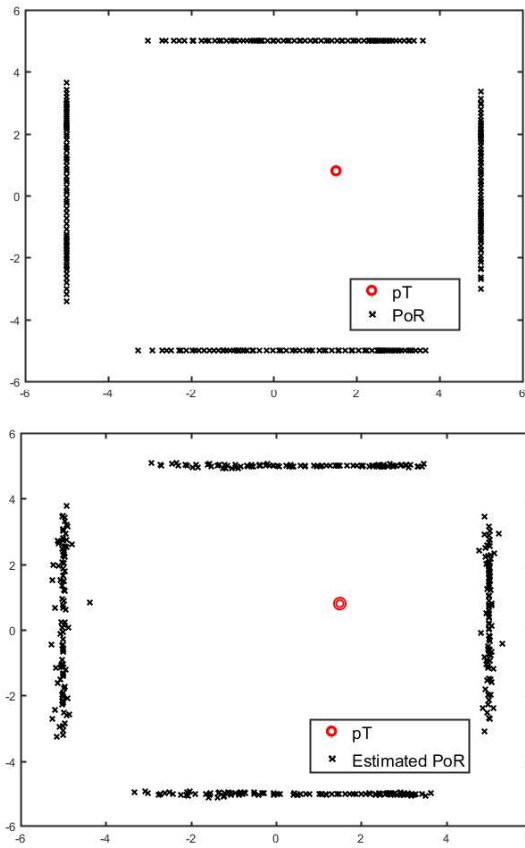


Figure 5.11: The cloud of reflection points with static transmitter and moving receiver: without AoA bias (top) and with AoA bias (bottom)

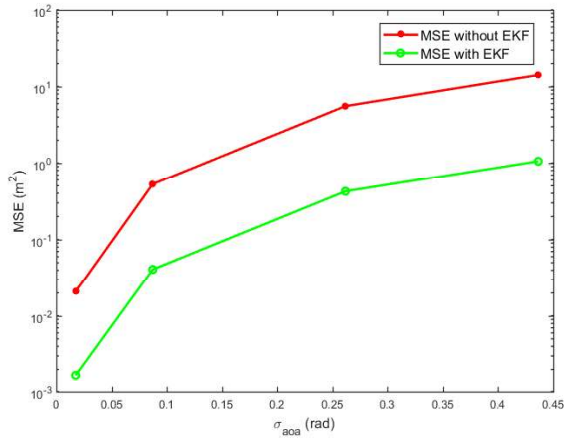


Figure 5.12: MSE ( $m^2$ ) vs  $\sigma$  of AoA ( $rad$ ), EKF with 1 iteration

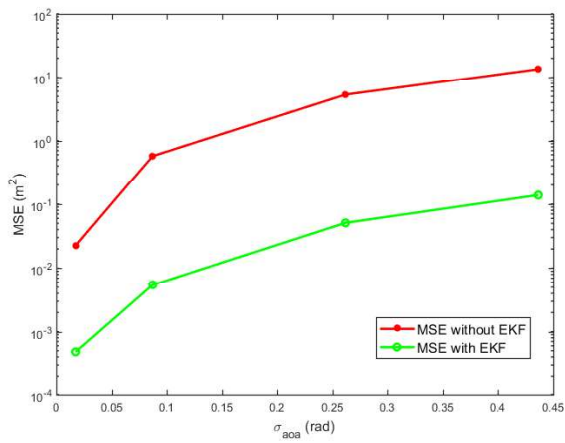


Figure 5.13: MSE ( $m^2$ ) vs  $\sigma$  of AoA ( $rad$ ), EKF with 5 iterations

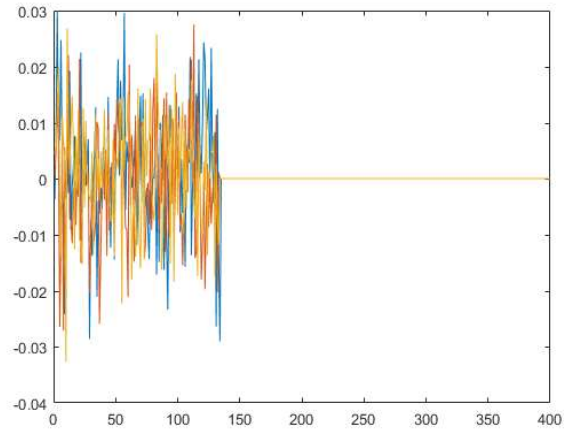


Figure 5.14: Output error(innovation) in function of k

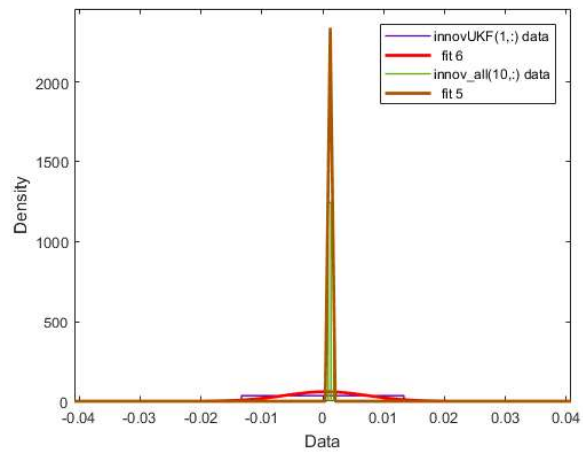


Figure 5.15: Probability density function of innovation with UKF and UKF+PDF

estimating the PoRs in comparison to EKF as shown in Figure 5.16.

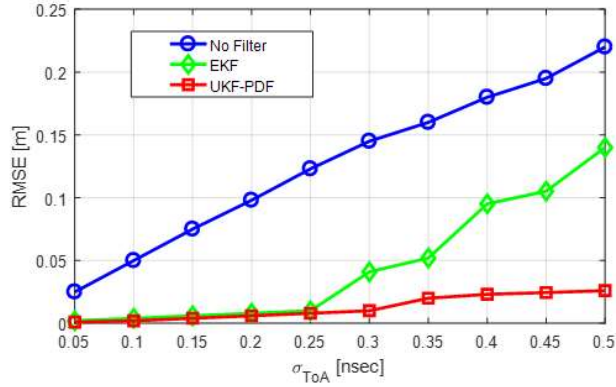


Figure 5.16: Estimation of PoR using EKF and UKF based PDF

## 5.5 Conclusion

In this chapter, we applied the proposed approaches in this dissertation for localization and mapping in mobile environment. The EKF was firstly used to enhance the proposed geometric SLAM approach. Simulations have shown that EKF provided accuracy enhancement in SLAM for environments with ToA and AoA biased measurements. Then, the learning approach introduced by the concept of neural network embedded within UKF based PDF filter under MEC has also provided further accuracy enhancement over EKF as well in SLAM.

# Chapter 6

## Conclusion and Future Work

We presented in this manuscript different techniques and approaches for localization and environment mapping using mmWave technologies in both 2D and 3D environments. Despite the different challenges of localization using mmWaves, we proposed in this manuscript a general framework to build the environment by estimating the points of reflection on the obstacles available in the environments. This has been achieved by subsequent steps that include localization of the receiver position, estimation of the VAN position and then the PoR. Then, using the cloud of reflection points, an environment mapping is possible. In this document, we have evaluated theoretically and by simulations different approaches for localization and mapping. When necessary, CRLBs have been derived. Moreover, 3D SLAM has been implemented thanks to the support of Siradel (part of ENGIE), a french company. The simulation results have perfectly shown that localization and mapping can effectively build the environment as long as the error deviation in AoA is less than 5 deg whereas in ToA it is less than  $1ns$ .

In this thesis, we have also evaluated the efficiency of the proposed algorithms in a mobile environment by implementing different versions of the Kalman filter. To do so, we derived the analytical model of the PoR in a mobile environment depending on the AoA or ToA variations and bias. While the results of the EKF filter have shown good localization and mapping accuracy, it has been shown that these results did not reach a centimeter accuracy: one of the possible targets that mmWaves can offer. This is indeed due to the possible divergence of the EKF due to large non-linearities in the mapping analytical model (it is one of the main problems in the EKF). To reach this accuracy, we adopted an Unscented Kalman filter with learning by using a minimum entropy criterion. Combined to PDF model, the UKF filter was able to obtain a coarse estimation of the analytical mode while the PDF filter makes the Renyi's entropy of the innovation as small as possible. Simulation results of the UKF with learning have shown that the accuracy of the localization and mapping can reach an unprecedented value. This will definitely open the door for different applications in both indoor and

outdoor environments such as smart homes for elderly people, IoT, smart cities, to cite a few.

As future work, different approaches can be tackled. Some might be purely technical while others are related to the evolution of the technology and its availability on the market. Here, we can cite a few possible perspectives:

- Extension of this work to a 3D mobile environment: the work in this thesis was mostly done in 2D while some results have been extended to 3D thanks to the channel measurements and the support of a French partner (Siradel). Definitely, an extension to 3D will open the door for more challenges in the reconstruction of the obstacles, in the accuracy of the mapping, and in the mobile environment that a receiver might follow.
- More learning in the processing algorithms: this is definitely interesting in an environment with some particular behaviors such as indoor smart homes. Applying advanced learning algorithms will improve the mapping accuracy hence it will open the door for more advanced applications.
- Application of the scenario to a real environment that includes different rooms, corridors, obstacles in which channel measurements are available. Unfortunately, this was not possible in this thesis due to the limitation in the computation resources that are related to the channel model (full Ray-Tracing tool) and the complexity of these environments.
- Implementation of these algorithms in a real hardware platform: this was not possible during this PhD due to the cost of the equipment.
- Extension of the proposed framework to other environments: Currently, the application of mmWaves in vehicular networks has attracted a great research interest. Hence, it would be interesting to investigate the use-cases of environment mapping in this environment.
- Development of a set of use-cases that might be of interest on the market in the next few years

# Bibliography

- [1] A. Kupper. Location-based services. Wiley, 2005
- [2] F. L. Piccolo, A new cooperative localization method for UDS cellular networks, in Proc. IEEE Global Telecommun. Conf., Dec. 2008.
- [3] C. Mensing, S. Sand, and A. Dammann, Hybrid data fusion and tracking for positioning with GNSS and 3GPP-LTE, International Journal of Navigation and Observation, vol. 2010, Aug. 2010.
- [4] C. Mensing, S. Sand, A. Dammann, and W. Utschick, Interferenceaware location estimation in cellular OFDM communications systems, in Proc. IEEE Int. Conf. Commun., Jun. 2009.
- [5] C. Mensing, S. Sand, A. Dammann and W. Utschick, "Data-Aided Location Estimation in Cellular OFDM Communications Systems," Global Telecommunications Conference, 2009. GLOBECOM 2009. IEEE, Honolulu, HI, 2009, pp. 1-7.
- [6] A. H. Sayed, A. Tarighat, and N. Khajehnouri, Network-based wireless location, IEEE Signal Process. Mag., vol. 22, no. 4, pp. 1223, Jul. 2005.
- [7] Ziming He; Yi Ma; Tafazolli, R.; , "A hybrid data fusion based cooperative localization approach for cellular networks," Wireless Communications and Mobile Computing Conference (IWCMC), 2011 7th International, pp.162-166, 4-8 July 2011, doi: 10.1109/IWCMC.2011.5982409
- [8] Ijaz, Faheem, et al. "Indoor positioning: A review of indoor ultrasonic positioning systems." Advanced Communication Technology (ICACT), 2013 15th International Conference on. IEEE, 2013.
- [9] Koyuncu, Hakan, and Shuang Hua Yang. "A survey of indoor positioning and object locating systems." IJCSNS International Journal of Computer Science and Network Security 10.5 (2010): 121-128.
- [10] Zahid Farid, Rosdiadee Nordin, and Mahamod Ismail, Recent Advances in Wireless Indoor Localization Techniques and System, Journal of Computer



Networks and Communications, vol. 2013, Article ID 185138, 12 pages, 2013.  
doi:10.1155/2013/185138

- [11] H. Liu, H. Darabi, P. Banerjee, and J. Liu. Survey of Wireless Indoor Positioning Techniques and Systems. *IEEE Transactions on Systems, Man and Cybernetics*, 37(6):10671080, 2007.
- [12] Y. Gu, A. Lo, and I. Niemegeers, A survey of indoor positioning systems for wireless personal networks, *IEEE Comm. Surveys and Tutorials*, vol. 11, no. 1, pp. 13-32, First Quarter 2009.
- [13] Disha A. A Comparative Analysis on indoor positioning Techniques and Systems. *International Journal of Engineering Research and Applications*. 2013;3:1790-6
- [14] Al-Ammar, M.A.; Alhadhrami, S.; Al-Salman, A.; Alarifi, A.; Al-Khalifa, H.S.; Alnafessah, A.; Alsaleh, M., "Comparative Survey of Indoor Positioning Technologies, Techniques, and Algorithms," in *Cyberworlds (CW), 2014 International Conference on* , vol., no., pp.245-252, 6-8 Oct. 2014
- [15] Vo Q. Duy and De P., "A Survey of Fingerprint-Based Outdoor Localization," in *IEEE Communications Surveys & Tutorials*, vol. 18, no. 1, pp. 491-506, Firstquarter 2016.
- [16] Montorsi, F.; Mazuelas, S.; Vitetta, G.M.; Win, M.Z., "On the Performance Limits of Map-Aware Localization," *Information Theory, IEEE Transactions on* , vol.59, no.8, pp.5023,5038, Aug. 2013
- [17] Chandrasekaran, G.; Ergin, M.A.; Jie Yang; Song Liu; Yingying Chen; Gruteser, M.; Martin, R.P., "Empirical Evaluation of the Limits on Localization Using Signal Strength," *Sensor, Mesh and Ad Hoc Communications and Networks, 2009. SECON '09. 6th Annual IEEE Communications Society Conference on* , pp.1,9, 22-26 June 2009
- [18] Hongbo Liu; Jie Yang; Sidhom, S.; Yan Wang; Yingying Chen; Fan Ye, "Accurate WLAN Based Localization for Smartphones Using Peer Assistance," *Mobile Computing, IEEE Transactions on* , vol.13, no.10, pp.2199,2214, Oct. 2014
- [19] Guvenc, Ismail, Sinan Gezici, and Zafer Sahinoglu. "Fundamental limits and improved algorithms for linear leastsquares wireless position estimation." *Wireless Communications and Mobile Computing* 12.12 (2012): 1037-1052
- [20] D. Dardari, A. Conti, J. Lien and M.Z. Win, The Effect of Cooperation on UWB-Based Positioning Systems Using Experimental Data, *EURASIP Journal on Advances in Signal Processing, Special Issue on Wireless Cooperative Networks*, Vol. 2008, pp.191-195, 2008

- [21] A.Conti, D. Dardari, and M. Z. Win, Experimental Results on Cooperative UWB Based Positioning Systems, in Proc. IEEE ICUWB08, vol. 1, pp. 191-195, Hannover, Sept. 2008
- [22] A. Yassine, Y. Nasser, M. Awad, B. Uguen, Hybrid positioning data fusion in heterogeneous networks with critical hearability, EURASIP Journal on Advances in Signal Processing, December 2014, pages:16, 2014:215 doi:10.1186/1687-1499-2014-215
- [23] A. Yassin, Y. Jaffal, Y. Nasser, "On the evaluation of geometric localization using Recursive Maximum Likelihood estimation," Mediterranean Electrotechnical Conference (MELECON), 2014 17th IEEE , vol., no., pp.357,361, 13-16 April 2014. doi: 10.1109/MELCON.2014.6820560
- [24] A. Yassin, M. Awad, Y. Nasser, "On the hybrid localization in heterogeneous networks with lack of hearability," Telecommunications (ICT), 2013 20th International Conference on , vol., no., pp.1,5, 6-8 May 2013. doi: 10.1109/ICTEL.2013.6632158
- [25] S. Gezici, Z. Tian, G. Giannakis, H. Kobayashi, A. Molisch, H. Poor, and Z. Sahinoglu, "Localization via ultra-wideband radios: a look at positioning aspects for future sensor networks," IEEE Signal Processing Magazine, vol. 22, no. 4, pp. 70-84, July 2005.
- [26] W. Mekonnen, E. Slottke, H. Luecken, C. Steiner, and A. Wittneben, "Constrained Maximum Likelihood Positioning for UWB Based Human Motion Tracking," International Conference on Indoor Positioning and Indoor Navigation, IPIN 2010, Zurich, Switzerland, pp. 1-10, Sept. 2010.
- [27] Z. Sahinoglu, S. Gezici, and I. Guvenc. Ultra-wideband Positioning Systems. Cambridge, 2008.
- [28] Alarifi, Abdulrahman et al. Ultra Wideband Indoor Positioning Technologies: Analysis and Recent Advances . Ed. Lyudmila Mihaylova, Byung-Gyu Kim, and Debi Prosad Dogra. Sensors (Basel, Switzerland) 16.5 (2016): 707. PMC. Web. 19 Aug. 2016.
- [29] You Zheng; Baala, O.; Caminada, A., "A new approach to design a WLAN-based positioning system," in Signal Processing and Communication Systems (ICSPCS), 2010 4th International Conference on , vol., no., pp.1-8, 13-15 Dec. 2010. doi: 10.1109/ICSPCS.2010.5709652
- [30] Long Vu-Hoang; Hung Nguyen-Manh; Chinh Phan-Duy; Dung Le-Quang; Thanh Do-Van; Vinh Tran-Quang, "A new technique to enhance accuracy of WLAN fingerprinting based indoor positioning system," in Communications

- and Electronics (ICCE), 2014 IEEE Fifth International Conference on , vol., no., pp.270-275, July 30 2014-Aug. 1 2014. doi: 10.1109/CCE.2014.6916714
- [31] R. Zhang, F. Hoeflinger, O. Gorgis, and L.M. Reindl, Indoor localization using inertial sensors and ultrasonic rangefinder, in Proc. Int. Conf. on Wireless Communications and Signal Processing (WCSP 2011), Nanjing, China, Nov. 2011, pp. 15.
- [32] A.R. Jimenez, F. Seco, J.C. Prieto, and J. Guevara, Indoor Pedestrian navigation using an INS/EKF framework for yaw drift reduction and a foot-mounted IMU, in Proc. 7th Workshop on Positioning, Navigation and Communication (WPNC 2010), Dresden, Germany, Mar. 2010, pp. 135143.
- [33] Hwan-Joo Kwak; Dong-Hun Lee; Jung-Moon Hwang; Jung-Han Kim; Chong-Kap Kim; Gwi-Tae Park, "Improvement of the inertial sensor-based localization for mobile robots using multiple estimation windows filter," in Intelligent Robots and Systems (IROS), 2012 IEEE/RSJ International Conference on , vol., no., pp.876-881, 7-12 Oct. 2012. doi: 10.1109/IROS.2012.6386032
- [34] Lei Fang, Wenliang Du and Peng Ning, "A beacon-less location discovery scheme for wireless sensor networks," Proceedings IEEE 24th Annual Joint Conference of the IEEE Computer and Communications Societies., 2005, pp. 161-171 vol. 1.
- [35] Nazir, U.; Arshad, M.A.; Shahid, N.; Raza, S.H., "Classification of localization algorithms for wireless sensor network: A survey," in Open Source Systems and Technologies (ICOSST), 2012 International Conference on , vol., no., pp.1-5, 20-22 Dec. 2012
- [36] Y.-C. Lee, Christiand, W. Yu, and J.-I. Cho, Adaptive localization for mobile robots in urban environments using low-cost sensors and enhanced topological map, in Proc. IEEE 15th International Conference on Advanced Robotics (ICAR 2011), Tallinn, Estonia, Jun. 2011, pp. 569575.
- [37] D.J. Kim, M.K. Kim, K.S. Lee, H.G. Park, and M.H. Lee, Localization system of autonomous vehicle via Kalman filtering, in Proc. Int. Conf. on Control, Automation and Systems, Gyeonggi-do, Korea, Oct. 2011, pp. 934937.
- [38] Le, T.N.; Chong, P.H.J.; Xue Jun Li; Wai Yie Leong, "A Simple Grid-Based Localization Technique in Wireless Sensor Networks for Forest Fire Detection," in Communication Software and Networks, 2010. ICCSN '10. Second International Conference on , vol., no., pp.93-98, 26-28 Feb. 2010. doi: 10.1109/ICCSN.2010.108
- [39] D. Serant, P. Thevenon, M.-L. Boucheret, O. Julien, C. Macabiau, S. Corazza, M. Dervin, and L. Ries, Development and validation of an

OFDM/DVB-T sensor for positioning, in Position Location and Navigation Symposium (PLANS), 2010 IEEE/ION, May 2010.

- [40] F. Alizadeh-shabdiz and K. Pahlavan, Estimation of position using WLAN access point radio propagation characteristics in a WLAN positioning system, Patent 7 515 578, Apr., 2009. Available: <http://www.freepatentsonline.com/7515578.html>
- [41] C. Yang, T. Nguyen, D. Venable, M. White, and R. Siegel, Cooperative position location with signals of opportunity, in Proceedings of the IEEE 2009 National Aerospace Electronics Conference (NAECON), Jul. 2009.
- [42] Enright, M.A.; Kurby, C.N., "A signals of opportunity based cooperative navigation network," Aerospace & Electronics Conference (NAECON), Proceedings of the IEEE 2009 National , vol., no., pp.213,218, 21-23 July 2009
- [43] Coluccia, A.; Ricciato, F.; Ricci, G., "Positioning Based on Signals of Opportunity," Communications Letters, IEEE , vol.18, no.2, pp.356,359, February 2014
- [44] Chun Yang; Thao Nguyen; Blasch, E., "Mobile positioning via fusion of mixed signals of opportunity," Aerospace and Electronic Systems Magazine, IEEE , vol.29, no.4, pp.34,46, April 2014
- [45] Robinson, M.; Ghrist, R., "Topological Localization Via Signals of Opportunity," Signal Processing, IEEE Transactions on , vol.60, no.5, pp.2362,2373, May 2012
- [46] A. De Angelis, M. Dionigi, R. Moschitta, A. Giglietti, and P. Carbone, "Characterization and Modeling of an Experimental UWB Pulse-Based Distance Measurement System," IEEE Transactions on Instrumentation and Measurement, vol. 58, no. 5, pp. 1479 - 1486, May 2009.
- [47] H. Wymeersch, J. Lien, and M. Win, "Cooperative localization in wireless networks," Proceedings of the IEEE, vol. 97, no. 2, pp. 427-450, Feb. 2009.
- [48] Kietlinski-Zaleski, J.; Yamazato, T.; Katayama, M., "Experimental validation of ToA UWB positioning with two receivers using known indoor features," Position Location and Navigation Symposium (PLANS), 2010 IEEE/ION , vol., no., pp.505,509, 4-6 May 2010
- [49] XU Benchong, CHEN Junjie. Localization Algorithms for Wireless Sensor Networks Based on Feasibility of Anchor Nodes Disposing, Measurement & Control Techniques,2007,8, P:46-51

- [50] Wang Jianguo; Wang Zhongsheng; Zhang Ling; Shi Fei; Song Guohua, "A New Anchor-Based Localization Algorithm for Wireless Sensor Network," in Distributed Computing and Applications to Business, Engineering and Science (DCABES), 2011 Tenth International Symposium on , vol., no., pp.239-243, 14-17 Oct. 2011. doi: 10.1109/DCABES.2011.5
- [51] A. P. Jardosh, K. Papagiannaki, E. M. Belding, K. C. Almeroth, G. Iannaccone, and B. Vinnakota, Green WLANs: on-demand WLAN infrastructures, Mobile Networks and Applications, vol. 14, no. 6, pp. 798814, Dec. 2009.
- [52] K. Chintalapudi, A. P. Iyer, and V. N. Padmanabhan, Indoor localization without the pain, in Proc. of Mobile Computing and Networking (MobiCom), 2010, pp. 173184.
- [53] J. Paek, J. Kim, and R. Govindan, Energy-Efficient Rate-Adaptive GPS-based Positioning for Smartphones, in Proc. of MobiSys, 2010.
- [54] Dhondge, K.; Hyungbae Park; Baek-Young Choi; Sejun Song, "Energy-Efficient Cooperative Opportunistic Positioning for Heterogeneous Mobile Devices," Computer Communications and Networks (ICCCN), 2012 21st International Conference on , vol., no., pp.1,6, July 30 2012-Aug. 2 2012
- [55] Zheng Sun; Farley, R.; Kaleas, T.; Ellis, J.; Chikkappa, K., "Cortina: Collaborative context-aware indoor positioning employing RSS and RToF techniques," Pervasive Computing and Communications Workshops (PERCOM Workshops), 2011 IEEE International Conference on , vol., no., pp.340,343, 21-25 March 2011
- [56] Yubin Xu; Mu Zhou; Lin Ma; Weixiao Meng, "3GPE: An energy efficient probabilistic fingerprint-assisted localization in indoor WLAN areas," Communications (ICC), 2012 IEEE International Conference on , vol., no., pp.32,36, 10-15 June 2012
- [57] Lemelson, H., Kjrgaard M. B., Hansen R., and King T. "Error estimation for indoor 802.11 location fingerprinting." in Proc. of the Fourth Int.Symposium on Location and Context Awareness (LoCA 2009), May 2009.
- [58] Lemelson, H.; Kopf, S.; King, T.; Effelsberg, W., "Improvements for 802.11-Based Location Fingerprinting Systems," in Computer Software and Applications Conference, 2009. COMPSAC '09. 33rd Annual IEEE International , vol.1, no., pp.21-28, 20-24 July 2009
- [59] <http://www.ict-where2.eu/>.
- [60] C. Pedersen, T. Pedersen, and B. H. Fleury. A variational message passing algorithm for sensor self-localization in wireless networks. In Proc. IEEE ISIT 2011, pages 21582162, Saint-Petersburg, Russia, August 2011.

- [61] V. Savic, H. Wymeersch, F. Penna, and S. Zazo. Optimized edge appearance probability for cooperative localization based on tree-reweighted nonparametric belief propagation. In Proc. IEEE ICASSP 2011, pages 30283031, Prague, Czech Republic, May 2011.
- [62] H. Nouredine, N. Gresset, D. Castelain, and R. Pyndiah. A New Variant of Nonparametric Belief Propagation for Self-Localization. In Proc. IEEE ICT 2010, pages 822827, Doha, Qatar, April 2010.
- [63] S. Hadzic, J. Bastos, and J. Rodriguez. Reference node selection for cooperative positioning using coalition formation games. In Proc. WPNC 2012, pages 105108, Dresden, Germany, March 2012.
- [64] S. Zirari and B. Denis. Comparison of links selection criteria for mobile terminal positioning in cooperative heterogeneous networks. In Proc. SoftCOM 2012, Split, Croatia, September 2012.
- [65] A. Conti, M. Guerra, D. Dardari, N. Decarli, and M.Z. Win. Network Experimentation for Cooperative Localization. IEEE JSAC, 30(2):467-475, February 2012.
- [66] Denis, B., et al. "Cooperative and heterogeneous indoor localization experiments." Communications Workshops (ICC), 2013 IEEE International Conference on. IEEE, 2013.
- [67] Sand, S.; Mensing, C.; Ma, Y.; Tafazolli, R.; Yin, X.; Figueiras, J.; Nielsen, J.; Fleury, B.H., "Hybrid Data Fusion and Cooperative Schemes for Wireless Positioning," Vehicular Technology Conference, 2008. VTC 2008-Fall. IEEE 68th , vol., no., pp.1,5, 21-24 Sept. 2008
- [68] Kemppi, P.; Rautiainen, T.; Ranki, V.; Belloni, F.; Pajunen, J., "Hybrid positioning system combining angle-based localization, pedestrian dead reckoning and map filtering," Indoor Positioning and Indoor Navigation (IPIN), 2010 International Conference on , vol., no., pp.1,7, 15-17 Sept. 2010
- [69] Tarro, Paula, Juan A. Besada, and Jos R. Casar. "Fusion of RSS and inertial measurements for calibration-free indoor pedestrian tracking." Information Fusion (FUSION), 2013 16th International Conference on. IEEE, 2013.
- [70] H. Wang, H. Lenz, A. Szabo, J. Bamberger and U. Hanebeck, WLANBased Pedestrian Tracking Using Particle Filters and Low-Cost MEMS Sensors, Proc. of the 4th Workshop on Positioning, Navigation and Communication, pp. 17, 2007.
- [71] O. Woodman and R. Harle, Pedestrian localisation for indoor environments, Proc. of the 10th Int. Conf. on Ubiquitous Computing, pp. 114123, 2008.

- [72] B. Denis, M. Maman, and L Ouvry, On the Scheduling of Ranging and Distributed Positioning Updates in Cooperative IR-UWB Networks, in Proceedings of IEEE International Conference on Ultra-Wideband (ICUWB), pp. 370-375, Sep. 2009.
- [73] D. Lieckfeldt, J. You, and D. Timmermann, An algorithm for distributed beacon selection, in IEEE International Conference on Pervasive Computing and Communications, Hong Kong, China, pp. 318-323, March 2008.
- [74] K. Das and H. Wymeersch, Censored cooperative positioning for dense wireless networks, in IEEE 21st International Symposium on Personal, Indoor and Mobile Radio Communications Workshops (PIMRC Workshops), pp.262-266, 26-30 September 2011.
- [75] J. Liu and Y. Zhang, Error control in distributed node self-localization, in EURASIP Journal on Advances in Signal Processing, January 2008.
- [76] Savic, V.; Zazo, S., "Reducing Communication Overhead for Cooperative Localization Using Nonparametric Belief Propagation," in Wireless Communications Letters, IEEE , vol.1, no.4, pp.308-311, August 2012
- [77] Hadzic, S.; Rodriguez, J., "Utility based node selection scheme for cooperative localization," Indoor Positioning and Indoor Navigation (IPIN), 2011 International Conference on , vol., no., pp.1,6, 21-23 Sept. 2011
- [78] M. B. Kjrgaard, A taxonomy for radio location fingerprinting, in Location and Context-Awareness. Springer Berlin Heidelberg, 2007, pp. 139-156.
- [79] K. El-Kafrawy, M. Youssef, A. El-Keyi, and A. Naguib, Propagation modeling for accurate indoor wlan rss-based localization, in Proc. Of the IEEE 72nd Vehicular Technology Conference Fall (VTC 2010-Fall), Ottawa, Canada, 69, September 2010, pp. 15.
- [80] T. Deyle, C. Kemp, and M. Reynolds, Probabilistic UHF RFID tag pose estimation with multiple antennas and a multipath RF propagation model, in Proc. of the 2008 IEEE/RSJ Int. Conf. on Intelligent Robots and Systems (IROS 2008), Nice, France, September 2008, pp. 1379-1384.
- [81] Z. Yang, C. Wu, and Y. Liu, Locating in fingerprint space: Wireless indoor localization with little human intervention, in Proceedings of the 18th Annual International Conference on Mobile Computing and Networking, ser. Mobicom 12, 2012, pp. 269-280.
- [82] A. Rai, K. K. Chintalapudi, V. N. Padmanabhan, and R. Sen, Zee: Zero-effort crowdsourcing for indoor localization, in Proceedings of the 18th Annual International Conference on Mobile Computing and Networking, ser. Mobicom 12, 2012, pp. 293-304.

- [83] M. Raspopoulos, C. Laoudias, L. Kanaris, A. Kokkinis, C. Panayiotou, and S. Stavrou, 3d ray tracing for device-independent fingerprint-based positioning in wlans, in 2012 9th Workshop on Positioning Navigation and Communication (WPNC 2012), March 2012, pp. 109113.
- [84] Jochen Seitz , Lucila Patino-Studencka, Bernd Schindler, Stephan Haimerl, Javier Gutierrez Boronat, Steffen Meyer, Jrn Thielecke. Sensor Data Fusion for Pedestrian Navigation Using WLAN and INS, In Symposium Gyro Technology 2007, Karlsruhe, 2007.
- [85] M. Jin, B. Koo, S. Lee, C. Park, M. Lee and S. Kim, "IMU-Assisted Nearest Neighbor Selection for Real-Time WLAN Fingerprinting Positioning," in Proc. IEEE International Conference on Indoor Positioning and Indoor Navigation (IPIN), Busan, Korea, Oct. 2014.
- [86] W. Xiao, W. Ni, and Y. K. Toh, Integrated WLAN Fingerprinting and Inertial Sensing for Indoor Positioning, International conference on Indoor Positioning and Indoor Navigation. Guimaraes, Portugal, September 2011.
- [87] Antonio J. Ruiz-Ruiz, Pedro E. Lopez-de-Teruel, Oscar Canovas. A multi-sensor LBS using SIFT-based 3D models, 2012 International Conference on Indoor Positioning and Indoor Navigation, November 13-15, 2012.
- [88] K. Hattori, R. Kimura, N. Nakajima, T. Fujii, Y. Kado, B. Zhang, T. Hazugawa, K. Takadama, Hybrid Indoor Location Estimation System Using Image Processing and WLAN Strength, in the 9th International conference on Wireless network and Information System, Shanghai China, Dec 2009:406-411.
- [89] T. Germa, F. Lerasle, N. Ouadah, V. Cadenat, Vision and RFID data fusion for tracking people in crowds by a mobile robot, Computer Vision and Image Understanding, Volume 114, Issue 6, June 2010, Pages 641-651.
- [90] Dirk Schulz, Dieter Fox, Jeffrey Hightower. People Tracking with Anonymous and ID-Sensors Using Rao-Blackwellised Particle Filters, Proc. of the International Joint Conference on Artificial Intelligence (IJCAI), 2003
- [91] Muhammad Irshan Khan and Jari Syrjarinne. Investigating Effective Methods for Integration of Buildings Map with Low cost Inertial Sensors and WLAN-based Positioning, 2013 International Conference on Indoor Positioning and Indoor Navigation, 28th-31th, October 2013.
- [92] Leung, K.Y.K.; Barfoot, T.D.; Liu, H.H.T., "Distributed and decentralized cooperative simultaneous localization and mapping for dynamic and sparse robot networks," Robotics and Automation (ICRA), 2011 IEEE International Conference on , vol., no., pp.3841,3847, 9-13 May 2011.



- [93] Heon-Cheol Lee; Seung-Hee Lee; Seung-Hwan Lee; Tae-Seok Lee; Doo-Jin Kim; Kyung-Sik Park; Kong-Woo Lee; Beom-Hee Lee, "Comparison and analysis of scan matching techniques for Cooperative-SLAM," Ubiquitous Robots and Ambient Intelligence (URAI), 2011 8th International Conference on , vol., no., pp.165,168, 23-26 Nov. 2011
- [94] Ali, A.M.; Nordin, Md Jan, "SIFT based monocular SLAM with multi-clouds features for indoor navigation," TENCON 2010 - 2010 IEEE Region 10 Conference , vol., no., pp.2326,2331, 21-24 Nov. 2010
- [95] Jiun-Fu Chen; Chieh-Chih Wang, "Simultaneous localization and mapping using a short-range passive RFID reader with sparse tags in large environments," Advanced Robotics and its Social Impacts (ARSO), 2010 IEEE Workshop on , vol., no., pp.136,141, 26-28 Oct. 2010
- [96] Kuen-Han Lin; Chieh-Chih Wang, "Stereo-based simultaneous localization, mapping and moving object tracking," Intelligent Robots and Systems (IROS), 2010 IEEE/RSJ International Conference on , vol., no., pp.3975,3980, 18-22 Oct. 2010
- [97] Kosmatopoulos, E.B.; Rovas, D.V.; Doitsidis, L.; Aboudolas, K.; Roumeliotis, S.I., "A generic framework for scalable and convergent multi-robot active simultaneous localization, mapping and target tracking," Control & Automation (MED), 2011 19th Mediterranean Conference on , vol., no., pp.151,156, 20-23 June 2011
- [98] Zhao Xinzhe; Zhang Simin, "Distributed strong tracking unscented particle filter for simultaneous localization and mapping," Control Conference (CCC), 2014 33rd Chinese , vol., no., pp.978,983, 28-30 July 2014
- [99] Brian Ferris, Dieter Fox, and Neil Lawrence. WLAN-SLAM using Gaussian process latent variable models, In Proceedings of the 20th international joint conference on Artificial intelligence (IJCAI'07), Rajeev Sangal, Harish Mehta, and R. K. Bagga (Eds.). Morgan Kaufmann Publishers Inc., San Francisco, CA, USA, 2480-2485.
- [100] Joseph Huang, David Millman, Morgan Quigley, David Stavens, Sebastian Thrun and Alok Aggarwal. Efficient, generalized indoor WLAN GraphSLAM, in 2011 IEEE International Conference on Conference: Robotics and Automation (ICRA), May 2011, Shanghai.
- [101] Piotr Mirowski, Tin Kam Ho, Saehoon Yi, Michael MacDonald. Signal-SLAM: Simultaneous localization and mapping with mixed WLAN, Bluetooth, LTE and magnetic signals, in 2013 International Conference on Indoor Positioning and Indoor Navigation (IPIN).

- [102] Z. Yang, C. Wu, and Y. Liu, Locating in Fingerprint Space: Wireless Indoor Localization with Little Human Intervention, in Proc. of ACM MobiCom , 2012.
- [103] G. Shen, Z. Chen, P. Zhang, T. Moscibroda, and Y. Zhang, Walkie- Markie: indoor pathway mapping made easy, in Proc. of USENIX NSDI, 2013.
- [104] A. Rai, K. K. Chintalapudi, V. N. Padmanabhan, and R. Sen, Zee: Zero-effort Crowdsourcing for Indoor Localization, in Proc. of ACM MobiCom , 2012
- [105] J. Yin, Q. Yang, and L. M. Ni, Learning adaptive temporal radio maps for signal-strength-based location estimation, Mobile Computing, IEEE Transactions on , vol. 7, no. 7, pp. 869883, 2008.
- [106] Z. Sun, Y. Chen, J. Qi, and J. Liu, Adaptive localization through transfer learning in indoor wi-fi environment, in Proc. of IEEE ICMLA, 2008.
- [107] H. Wang, S. Sen, A. Elgohary, M. Farid, M. Youssef, and R. R. Choudhury, No Need to War-drive: Unsupervised Indoor Localization, in Proc. of ACM MobiSys, 2012.
- [108] L. Zhang, K. Liu, Y. Jiang, X.-Y. Li, Y. Liu and P. Yang, Montage: Combine frames with movement continuity for realtime multi-user tracking, in Proc. of IEEE INFOCOM, 2014
- [109] Myerson R. B. (1997). Game theory, Analysis of conflict, Harvard University Press, ISBN: 0-674- 34115-5, Cambridge, MA, USA.
- [110] V. Srivastava et al., "Using game theory to analyze wireless ad hoc networks," in IEEE Communications Surveys & Tutorials, vol. 7, no. 4, pp. 46-56, Fourth Quarter 2005.
- [111] Ghassemi F. & Krishnamurthy V. (2008a). A Cooperative Game-Theoretic Measurement Allocation Algorithm for Localization in Unattended Ground Sensor Networks, Proceedings of 11th International Conference on Information Fusion, pp. 1-7, ISBN: 978-3-8007-3092-6, Cologne, Germany, June 2008.
- [112] B. Bejar, P. Belanovic, and S. Zazo, Cooperative localization in wireless sensor networks using coalitional game theory, in 18th European Signal Processing Conference EUSIPCO 2010, Aalborg, Denmark, August 2010.
- [113] G. A. Shah and M. Bozyigit, Exploiting Energy-aware Spatial Correlation in Wireless Sensor Networks, in Proc. of 2nd International Conference on Communication Systems Software and Middleware (COMSWARE 2007), Bangalore, India, pp. 1-6, January 2007.

- [114] Franchi, A.; Oriolo, G.; Stegagno, P., "Probabilistic mutual localization in multi-agent systems from anonymous position measures," *Decision and Control (CDC), 2010 49th IEEE Conference on*, vol., no., pp.6534,6540, 15-17 Dec. 2010
- [115] Katalenic, A.; Draganjac, I.; Mutka, A.; Bogdan, S., "Fast visual tracking and localization in multi-agent systems," *Industrial Electronics and Applications, 2009. ICIEA 2009. 4th IEEE Conference on*, vol., no., pp.1864,1870, 25-27 May 2009
- [116] ABI Research, Location Technology Research Service, Oct 2013.
- [117] Consumer Applications for Indoor Positioning, Loctronix The Insider, Vol. 1, No. 1, Available at: <http://goo.gl/PYtgwT>
- [118] D. Macagnano, G. Destino and G. Abreu Indoor Positioning: a Key Enabling Technology for IoT Applications, *IEEE World Forum on Internet of Things (WF-IoT)*, p. 117, 2014.
- [119] BUTLER FP7 project web page <http://www.iot-butler.eu/about-butler>
- [120] URUS:Ubiquitous networking Robots in Urban Settings, EU Project IST-1-045062, Web site: <http://www-iri.upc.es/groups/urus/>.
- [121] Aufrere, R.; Karam, N.; Chausse, F.; Chapuis, R., "A state exchange approach in real conditions for multi-robot cooperative localization," *Intelligent Robots and Systems (IROS), 2010 IEEE/RSJ International Conference on*, vol., no., pp.4346,4351, 18-22 Oct. 2010
- [122] P. V. Fazenda and P. U. Lima, Non-holonomic robot formations with obstacle compliant geometry, *Conference Paper, September 2007, 6th IFAC Symposium on Intelligent Autonomous Vehicles.*
- [123] S. Mastellone, D. M. Stipanovic, C. R. Graunke, K. A. Intlekofer, and M. W. Spong, Formation control and collision avoidance for multi-agent non-holonomic systems. theory and experiments, *The International Journal of Robotics Research*, vol. 27, pp. 107126, January 2008.
- [124] S. Loizou and K. Kyriakopoulos, Navigation of multiple kinematically constrained robots, *IEEE Transactions on Robotics*, vol. 24, no. 1, pp. 221231, Feb. 2008.
- [125] Ayush, K.; Agarwal, N.K., "Real time visual SLAM using cloud computing," *Computing, Communications and Networking Technologies (ICCCNT), 2013 Fourth International Conference on*, vol., no., pp.1,7, 4-6 July 2013

- [126] Heon-Cheol Lee; Seung-Hwan Lee; Tae-Seok Lee; Doo-Jin Kim; Beom-Hee Lee, "A survey of map merging techniques for cooperative-SLAM," *Ubiquitous Robots and Ambient Intelligence (URAI)*, 2012 9th International Conference on , vol., no., pp.285,287, 26-28 Nov. 2012
- [127] M. Segura, H. Hashemi, C. Sisterna, and V. Mut. Experimental demonstration of self-localized Ultra-Wideband indoor mobile robot navigation system. In *International Conference on Indoor Positioning and Indoor Navigation (IPIN)*, 2010. doi: 10.1109/IPIN.2010.5647457.
- [128] Prorok, A.; Gonon, L.; Martinoli, A., "Online model estimation of ultra-wideband TDoA measurements for mobile robot localization," in *Robotics and Automation (ICRA)*, 2012 IEEE International Conference on , vol., no., pp.807-814, 14-18 May 2012. doi: 10.1109/ICRA.2012.6224869
- [129] Bai Yan; Lu Xiaochun, "Research on UWB indoor positioning based on TDoA technique," in *Electronic Measurement & Instruments, 2009. ICEMI '09. 9th International Conference on , vol., no., pp.1-167-1-170, 16-19 Aug. 2009. doi: 10.1109/ICEMI.2009.5274900*
- [130] I. Qudah, P. Leijdekkers, and V. Gay, Using mobile phones to improve medication compliance and awareness for cardiac patients, in *Proc. Int. Conf. Pervas. Technol. Related Assisted Environ.*, 2010, pp. 17.
- [131] D. U. Khan, K. A. Siek, J. Meyers, L. M. Haverhals, S. Cali, and S. E. Ross, Designing a personal health application for older adults to manage medications, in *Proc. Int. Health Inf. Symp.*, 2010, pp. 849858.
- [132] Haibo Ye; Tao Gu; Xianping Tao; Jian Lu, "F-Loc: Floor localization via crowdsourcing," in *Parallel and Distributed Systems (ICPADS)*, 2014 20th IEEE International Conference on , vol., no., pp.47-54, 16-19 Dec. 2014
- [133] Communications Security, Reliability and Interoperability Council III WG3 E9-1-1 Location Accuracy, Report - Leveraging LBS and Emerging Location Technologies for Indoor Wireless E9-1-1, March 14, 2013. Available online at: <http://goo.gl/hwGLp7>
- [134] FCC, THIRD FURTHER NOTICE OF PROPOSED RULEMAKING, February 21, 2014.
- [135] Del Re, E., Morosi, S., Jayousi, S. Sacchi, C., "Salice-satellite-assisted localization and communication systems for emergency services," *Proc. of of the 2009 1st International Conference on Wireless Communication, Vehicular Technology, Information Theory and Aerospace and Electronic Systems Technology, IEEE Wireless VITAE conference 2009.*

- [136] Del Re E., Jayousi, S. et. al., "SALICE Project: Satellite-Assisted Localization and Communication Systems for Emergency Services," IEEE AES Magazine, Sept. 2013, pp. 4-15.
- [137] Open Mobile Alliance Location Working Group web page: <http://openmobilealliance.org/about-oma/workprogram/location/>
- [138] 3GPP TS 23.271 Functional stage 2 description of Location Services (LCS). Available at <http://goo.gl/0EZTQw>
- [139] M. Mahfouz, C. Zhang, B. Merkl, M. Kuhn, and A. Fathy, Investigation of high accuracy indoor 3-D positioning using UWB technology, IEEE Trans. Microw. Theory Tech., vol. 56, no. 6, pp. 13161330, Jun. 2008.
- [140] Di Taranto, R. ; Muppirisetty, L. ; Raulefs, R. (2014) "Location-aware Communications for 5G Networks". IEEE signal processing magazine, vol. 31(6), pp. 102-112.
- [141] D. Slock, Location aided wireless communications, in Proc. Int. Symp. on Communications Control and Signal Processing, 2012, pp. 16.
- [142] A. Dammann, G. Agapiou, J. Bastos, L. Brunel, M. Garca, J. Guillet, Y. Ma, J. Ma, J. J. Nielsen, L. Ping, R. Raulefs, J. Rodriguez, D. Slock, D. Yang, and N. Yi, WHERE2 location aided communications, in Proc. European Wireless Conf., Apr.2013, pp. 18
- [143] R. C. Daniels and R. W. Heath, Link adaptation with position/motion information in vehicle-to-vehicle networks, IEEE Trans. Wireless Commun., vol. 11, no. 2,pp. 505509, 2012.
- [144] R. Di Taranto and H. Wymeersch, Simultaneous routing and power allocation using location information, in Proc. Asilomar Conf. Signals, Systems and Computers, 2013, pp. 17001704.
- [145] Mautz, R., "The challenges of indoor environments and specification on some alternative positioning systems," in Positioning, Navigation and Communication, 2009. WPNC 2009. 6th Workshop on , vol., no., pp.29-36, 19-19 March 2009. doi: 10.1109/WPNC.2009.4907800
- [146] Halder, S. J., Park, J. G., & Kim, W. (2011). Adaptive filtering for indoor localization using Zigbee RSSI and LQI measurement.
- [147] Zhu M; Novel Positioning Algorithms for RFID-Assisted 2D MEMS INS Systems, 2008, Proceedings of the Institute of Navigation GNSS 2008 conference, Savannah, Georgia, US

- [148] Retscher, G.; Qing Fu, "Continuous indoor navigation with RFID and INS," in Position Location and Navigation Symposium (PLANS), 2010 IEEE/ION , vol., no., pp.102-112, 4-6 May 2010. doi: 10.1109/PLANS.2010.5507242
- [149] Ruiz, A.R.J.; Granja, F.S.; Honorato, J.C.P.; Rosas, J.I.G., "Pedestrian indoor navigation by aiding a foot-mounted IMU with RFID Signal Strength measurements," in Indoor Positioning and Indoor Navigation (IPIN), 2010 International Conference on , vol., no., pp.1-7, 15-17 Sept. 2010. doi: 10.1109/IPIN.2010.5646885
- [150] Fu Q, Retscher G. Using RFID and INS for indoor positioning. 2009.
- [151] Retscher, G., and Q. Fu. "An intelligent personal navigator integrating GNSS, RFID and INS for continuous position determination." *Boletim de Cincias Geodsicas* 15.5 (2009).
- [152] Zhu, M., Retscher, G., & Zhang, K. (2011). Integrated algorithms for RFID-based multi-sensor indoor/outdoor positioning solutions. *Archiwum Fotogrametrii, Kartografii i Teledetekcji*, 22.
- [153] D.Harmer; Ultra wide-band indoor positioning, Dec. 2004, online March 2008,<http://esamultimedia.esa.int/docs/NavigationProjects>
- [154] Zheng Li; Dehaene, W.; Gielen, G., "A 3-tier UWB-based indoor localization system for ultra-low-power sensor networks," in *Wireless Communications, IEEE Transactions on* , vol.8, no.6, pp.2813-2818, June 2009. doi: 10.1109/TWC.2009.080602
- [155] Stelios MA, Nick AD, Effie UD, Dimitris KM, Thomopoulos SC. An indoor localization platform for ambient assisted living using UWB. In *Proceedings of the 6th international conference on advances in mobile computing and multimedia 2008* Nov 24 (pp. 178-182).
- [156] Guoping Zhang; Krishnan, S.; Chin, F.; Chi Chung Ko, "UWB Multicell Indoor Localization Experiment System with Adaptive TDoA Combination," in *Vehicular Technology Conference, 2008. VTC 2008-Fall. IEEE 68th* , vol., no., pp.1-5, 21-24 Sept. 2008. doi: 10.1109/VETEFCF.2008.139
- [157] Retscher G,Fu Q; Using Active RFID for Positioning in Navigation Systems, *Proceedings of the 4th International Symposium on Location Based Services and Telecartography,Hong Kong, 2007*
- [158] Lionel M.NI, Yunhao Liu, Iu Cho Lau, Abhshek P. Patil; LANDMARC: Indoor Location Sensing Using Active RFID;

- [159] Bergemann, S.; Sieck, J., "Adopting the LANDMARC Positioning System for 2.4 GHz Band," in Computer Modeling and Simulation (EMS), 2011 Fifth UKSim European Symposium on , vol., no., pp.400-405, 16-18 Nov. 2011. doi: 10.1109/EMS.2011.55
- [160] S. N. Razavi and O. Moselhi, "GPS-less indoor construction location sensing," in Automation in Construction. vol. 28, 2012, pp. 128-136.
- [161] Drawil, N.M.; Amar, H.M.; Basir, O.A., "GPS Localization Accuracy Classification: A Context-Based Approach," in Intelligent Transportation Systems, IEEE Transactions on , vol.14, no.1, pp.262-273, March 2013. doi: 10.1109/TITS.2012.2213815
- [162] Paramvir Bahl, Venkata N. Padmanabhan. 2005. RADAR: An In- Building RF-based User Location and Tracking System. Microsoft Research
- [163] Yokoo, K.; Beauregard, S.; Schneider, M., "Indoor Relative Localization with Mobile Short-Range Radar," in Vehicular Technology Conference, 2009. VTC Spring 2009. IEEE 69th , vol., no., pp.1-5, 26-29 April 2009. doi: 10.1109/VETECS.2009.5073602
- [164] L. Zhao, E. T. Psota and L. C. Prez, "A comparison between UWB and TDOA systems for smart space localization," IEEE International Conference on Electro/Information Technology, Milwaukee, WI, 2014, pp. 179-183.
- [165] Hazas, M., Hopper, A; A Novel Broadband Ultrasonic Location System for Improved Indoor Positioning, IEEE Transactions on mobile Computing, Vol. 5, No. 5, May 2006.
- [166] A. Harter and A. Hopper, A distributed location system for the active office, IEEE Network, vol. 8, no.1, 1994, pp. 62-70.
- [167] Active Badge System, Web Site, 2008, <http://www.cl.cam.ac.uk/research/dtg/attarchive/ab.html>
- [168] T. King, S. Kopf, T. Haenselmann, C. Lubberger and W. Effelsberg, COMPASS: A Probabilistic Indoor Positioning System Based on 802.11 and Digital Compasses, Proc. First ACM Intl Workshop on Wireless Network Testbeds, Experimental evaluation and CHaracterization (WiN-TECH),
- [169] Hong-shik Kim; Jong-Suk Choi; Minyoung Park, "Indoor localization system using multi-modulation of ultrasonic sensors and digital compass," in Intelligent Robots and Systems, 2008. IROS 2008. IEEE/RSJ International Conference on , vol., no., pp.1359-1364, 22-26 Sept. 2008. doi: 10.1109/IROS.2008.465082.

- [170] WhereNet Web Site , 2008, [http://edu.symbol.com/docent\\_aware/WhereNet/intro/intro](http://edu.symbol.com/docent_aware/WhereNet/intro/intro), last accessed on November 2010
- [171] Zebra Technology Company Web Site, 2008, <http://www.wherenet.com/>
- [172] F. Subhan, H. Hasbullah, A. Rozyyev, and S.T. Bakhsh, Indoor positioning in Bluetooth networks using fingerprinting and lateration approach, in Proceedings of the International Conference on Information Science and Applications (ICISA 11), April 2011.
- [173] H. J. Perez Iglesias, V. Barral, and C. J. Escudero, Indoor person localization system through RSSI Bluetooth fingerprinting, in Proceedings of the 19th International Conference on Systems, Signals and Image Processing (IWSSIP 12), pp. 4043, April 2012.
- [174] Sungil Kim; Sunhwa Ha; Saad, A.; Juho Kim, "Indoor positioning system techniques and security," in e-Technologies and Networks for Development (ICeND), 2015 Forth International Conference on , vol., no., pp.1-4, 21-23 Sept. 2015
- [175] T. Rappaport et al., Millimeter Wave Wireless Communications. Pearson Education, 2014.
- [176] S. Rangan, T. Rappaport, and E. Erkip, Millimeter-wave cellular wireless networks: Potentials and challenges, Proceedings of the IEEE, vol. 102, no. 3, pp. 366385, Mar. 2014. J.
- [177] Thompson et al., 5G wireless communication systems: prospects and challenges, IEEE Commun. Mag., vol. 52, no. 2, pp. 6264, Feb. 2014.
- [178] T. Rappaport et al., Millimeter wave mobile communications for 5G cellular: It will work! IEEE Access, vol. 1, pp. 335349, 2013.
- [179] A. Kupper. Location-based services. Wiley, 2005
- [180] E. Torkildson, H. Zhang, and U. Madhow, Channel modeling for millimeter wave MIMO, in Proc. Information Theory and Applications Workshop, San Diego, CA, Jan. 2010.
- [181] A. Maltsev et al., Experimental investigations of 60 GHz WLAN systems in office environment, IEEE J. Sel. Areas Commun., vol. 27, no. 8, pp. 14881499, Oct. 2009.
- [182] M. K. Samimi and T. S. Rappaport, "Statistical Channel Model with Multi-Frequency and Arbitrary Antenna Beamwidth for Millimeter-Wave Outdoor Communications," 2015 IEEE Globecom Workshops (GC Wkshps), San Diego, CA, 2015, pp. 1-7.



- [183] L. Subrt, P. Pechac, and S. Zvanovec, New approach to modeling of diffuse reflection and scattering for millimeter-wave systems in indoor scenarios, *PIERS Online*, vol. 6, 2010.
- [184] N. Peinecke, H. Doehler, and B. Korn, Phong-like lighting for MMW radar simulation, in *Proc. SPIE*, Cardiff, UK, 2008.
- [185] G. R. MacCartney et al., Path loss models for 5G millimeter wave propagation channels in urban microcells, in *Proc. IEEE GLOBECOM*, Atlanta, GA, Dec. 2013.
- [186] T. Rappaport et al., Broadband millimeter-wave propagation measurements and models using adaptive-beam antennas for outdoor urban cellular communications, *IEEE Trans. Antennas Propag.*, vol. 61, no. 4, pp. 1850-1859, Apr. 2013.
- [187] M. Bocquet, N. Obeid, C. Loyez, C. Lethien, F. Boukour, N. Rolland, and M. Heddebaut, Comparison between 60-GHz UWB frequency modulation and UWB impulse-radio location systems, in *Radar Conference, 2008. EuRAD 2008. European*, Oct. 2008, pp. 4143.
- [188] H. R. Fang, G. P. Cao, E. A. Gharavol, K. Tom, and K. Mouthaan, 60 GHz short range planar RSS localization, in *Proceedings of Asia-Pacific Microwave Conference 2010*, 2010.
- [189] D. Bojic, E. Sasaki, N. Cvijetic, T. Wang, J. Kuno, J. Lessmann, S. Schmid, H. Ishii, and S. Nakamura, Advanced wireless and optical technologies for small-cell mobile backhaul with dynamic software defined management, *Communications Magazine, IEEE*, vol. 51, no. 9, pp. 8693, Sep. 2013.
- [190] D. Dardari, A. Conti, J. Lien and M.Z. Win, The Effect of Cooperation on UWB-Based Positioning Systems Using Experimental Data, *EURASIP Journal on Advances in Signal Processing, Special Issue on Wireless Cooperative Networks*, Vol. 2008, pp.191-195, 2008
- [191] A.Conti, D. Dardari, and M. Z. Win, Experimental Results on Cooperative UWB Based Positioning Systems, in *Proc. IEEE ICUWB08*, vol. 1, pp. 191-195, Hannover, Sept. 2008
- [192] Ziming He; Yi Ma; Tafazolli, R.; , "A hybrid data fusion based cooperative localization approach for cellular networks," *Wireless Communications and Mobile Computing Conference (IWCMC)*, 2011 7th International, pp.162-166, 4-8 July 2011, doi: 10.1109/IWCMC.2011.5982409
- [193] C. Mensing, S. Sand, A. Dammann, and W. Utschick, Interferenceaware location estimation in cellular OFDM communications systems, in *Proc. IEEE Int. Conf. Commun.*, Jun. 2009.

- [194] A. Yassine, Y. Nasser, M. Awad, B. Uguen, Hybrid positioning data fusion in heterogeneous networks with critical hearability, *EURASIP Journal on Advances in Signal Processing*, December 2014, pages:16, 2014:215 doi:10.1186/1687-1499-2014-215
- [195] S. Gezici, Z. Tian, G. Giannakis, H. Kobayashi, A. Molisch, H. Poor, and Z. Sahinoglu, "Localization via ultra-wideband radios: a look at positioning aspects for future sensor networks," *IEEE Signal Processing Magazine*, vol. 22, no. 4, pp. 70-84, July 2005.
- [196] T. Kos, M. Grgic, and G. Sisul, Mobile user positioning in gsm/umts cellular networks, in *Multimedia Signal Processing and Communications*, 48th International Symposium ELMAR-2006 focused on, Zadar, Croatia, Jun. 2006.
- [197] P. Meissner, T. Gigl, and K. Witrisal, UWB sequential monte carlo positioning using virtual anchors in *Proc. IPIN*, Zurich, Switzerland, Sep. 2010.
- [198] A. Olivier, G. Bielsa, I. Tejado, M. Zorzi, J. Widmer and P. Casari, "Lightweight Indoor Localization for 60-GHz Millimeter Wave Systems," *2016 13th Annual IEEE International Conference on Sensing, Communication, and Networking (SECON)*, London, 2016, pp. 1-9.
- [199] T. Rappaport, *Wireless Communications: Principles and Practice*. Upper Saddle River, NJ, USA: Prentice Hall PTR, 2001.
- [200] P. F. M. Smulders and L. Correia, Characterisation of propagation in 60 GHz radio channels, *Journal of Electronics Communication Engineering*, vol. 9, no. 2, pp. 7380, 1997.
- [201] P. Tarro, A. M. Bernardos, and J. R. Casar, Weighted least squares techniques for improved received signal strength based localization, *Sensors*, vol. 11, no. 9, pp. 85698592, 2011.
- [202] K. Dogancay and D. Gray, Bias compensation for least-squares multipulse TDOA localization algorithms, in *International Conference on Intelligent Sensors, Sensor Networks and Information Processing*, 2005, pp. 5156.
- [203] R. L. Freeman, *Telecommunication Transmission Handbook*, Third Edition, John Wiley & Sons Inc., 1991, pg. 494.
- [204] Dissanayake, G., Newman, P., Clark, S., Durrant-Whyte, H. F., and Csorba, M. 2001. A solution to the simultaneous localization and map building (SLAM) problem. *IEEE Transactions of Robotics and Automation* 17(3):229241.

- [205] W. Morris, I. Dryanovski, and J. Xiao, "3D indoor mapping for micro-uavs using hybrid range finders and multi-volume occupancy grids," in *Proc. RSS 2010 Workshop RGB-D: Adv. Reasoning With Depth Cameras*, 2010.
- [206] H. Durrant-Whyte and T. Bailey, Simultaneous localisation and mapping (SLAM): Part I the essential algorithms, *IEEE Robotics Autom. Mag.*, vol. 13, no. 2, pp. 99110, Jun. 2006.
- [207] A. Guerra, F. Guidi, and D. Dardari, "Position and orientation error bound for wideband massive antenna arrays," in *Proc. IEEE Int. Conf. Commun., ANLN Workshop*, 2015.
- [208] W. Hong et al., "Study and prototyping of practically Large-scale mmWave antenna systems for 5G cellular devices," *IEEE Commun. Mag.*, vol. 52, no. 9, pp. 6369, Sep. 2014.
- [209] H. Kaouach et al., "Wideband low-loss linear and circular polarization transmit-arrays in V-Band," *IEEE Trans. Antennas Propag.*, vol. 59, no. 7, pp. 25132523, Jul. 2011.
- [210] J. Hoydis, S. ten Brink, and M. Debbah, "Massive MIMO in the UL/DL of cellular networks: How many antennas do we need?" *IEEE J. Select. Areas Commun.*, vol. 31, no. 2, pp. 160171, 2013.
- [211] E. G. Larsson, F. Tufvesson, O. Edfors, and T. L. Marzetta, "Massive MIMO for next generation wireless systems," *CoRR*, vol. abs/1304.6690, 2013.
- [212] F. Guidi, A. Guerra and D. Dardari, "Millimeter-wave massive arrays for indoor SLAM," *2014 IEEE International Conference on Communications Workshops (ICC)*, Sydney, NSW, 2014, pp. 114-120.
- [213] A. Guerra, F. Guidi, and D. Dardari, "Millimeter-wave personal radars for 3D environment mapping," in *Proc. IEEE Asilomar Conf. Signals, Syst. Comput.*, Pacific Grove, USA, Nov. 2014, pp. 701705.
- [214] C. Wu, Z. Yang, and Y. Liu, "Smartphones based crowdsourcing for indoor localization," *IEEE Trans. Mobile Comput.*, vol. 14, no. 2, pp. 444457, Feb. 2015.
- [215] A. Guerra et al., "Application of transmit array antennas for indoor mapping at Millimeter-waves," in *Proc. IEEE Eur. Conf. Netw. Commun.*, 2015, pp. 7781.
- [216] F. Guidi, A. Guerra and D. Dardari, "Personal Mobile Radars with Millimeter-Wave Massive Arrays for Indoor Mapping," in *IEEE Transactions on Mobile Computing*, vol. 15, no. 6, pp. 1471-1484, June 1 2016.

- [217] Floerkemeier, C., Langheinrich, M., Fleisch, E., Mattern, F. and Sarma, S.E. eds., 2008. The Internet of Things: First International Conference, IOT 2008, Zurich, Switzerland, March 26-28, 2008, Proceedings (Vol. 4952). Springer.
- [218] A. Yassin, Y. Nasser, M. Awad and A. Al-Dubai, "Simultaneous context inference and mapping using mm-Wave for indoor scenarios," *2017 IEEE International Conference on Communications (ICC)*, Paris, 2017, pp. 1-6.
- [219] H. El-Sayed, G. Athanasiou and C. Fischione, "Evaluation of localization methods in millimeter-wave wireless systems," *2014 IEEE 19th International Workshop on Computer Aided Modeling and Design of Communication Links and Networks (CAMAD)*, Athens, 2014, pp. 345-349.
- [220] A. Shahmansoori et al., "Position and Orientation Estimation through Millimeter Wave MIMO in 5G Systems", *IEEE Trans. Wireless Commun.*, 2017, [online] Available: <https://arxiv.org/abs/1702.01605>.
- [221] L. Cheng, X. Wu and Y. Wang, "A non-line of sight localization method based on k-means clustering algorithm," *2017 7th IEEE International Conference on Electronics Information and Emergency Communication (ICEIEC)*, Macau, 2017, pp. 465-468.
- [222] A. Yassin et al., "Recent Advances in Indoor Localization: A Survey on Theoretical Approaches and Applications," *in IEEE Communications Surveys and Tutorials*, vol. 19, no. 2, pp. 1327-1346, Secondquarter 2017.
- [223] Subrt, L., Pechac, P. and Zvanovec, S., 2010. New approach to modeling of diffuse reflection and scattering for millimeter-wave systems in indoor scenarios. *PIERS Online*, 6(8), pp.719-722.
- [224] R. E. Kalman, A new approach to linear filtering and prediction problems, *Trans. ASME-J. Basic Eng.*, vol. series D, no. 82, pp. 3545, 1960.
- [225] M. Roth and F. Gustafsson, An efficient implementation of the second order extended Kalman filter, in *Proc. 14th Int. Conf. Inf. Fusion*, Chicago, IL, USA, 2011, pp. 16.
- [226] I. Arasaratnam and S. Haykin, Cubature kalman filters, *IEEE Trans. Autom. Control*, vol. 54, no. 6, pp. 12541269, 2009.
- [227] Z. Chen, Bayesian filtering: From Kalman filters to particle filters, and beyond, Adaptive Systems Lab., Univ. McMaster, Hamilton, Ontario, Canada, Tech. Rep., 2003.

- [228] J. Zhou, D. Zhou, H. Wang, L. Guo, and T. Chai, Distribution function tracking filter design using hybrid characteristic functions, *Automatica*, vol. 46, no. 1, pp. 101109, 2010.
- [229] J. Ding, C. Tianyou, and H. Wang, Offline modeling for product quality prediction of mineral processing using modeling error pdf shaping and entropy minimization, *IEEE Trans. Neural Netw.*, vol. 22, no. 3, pp. 408419, 2011.
- [230] B. Chen, Y. Zhu, J. Hu, and Z. Sun, The Institute of Control, Robotics and Systems Engineers and The Korean Institute of Electrical Engineers, Adaptive filtering under minimum information divergence criterion, *Int. J. Contr., Autom. Syst.*, vol. 7, no. 2, p. 157, 2009, co-published with Springer-Verlag GmbH.
- [231] L. Guo and H. Wang, Minimum entropy filtering for multivariate stochastic systems with non-Gaussian noises, *IEEE Trans. Autom. Control*, vol. 51, no. 4, pp. 695700, 2006.